OPEN ACCESS

African Journal of Environmental Science and Technology

November 2021
ISSN 1996-0786
DOI: 10.5897/AJEST
www.academicjournals.org

ACADEMIC JOURNALS
expand your knowledge

About AJEST

African Journal of Environmental Science and Technology (AJEST) provides rapid publication (monthly) of articles in all areas of the subject such as Biocidal activity of selected plant powders, evaluation of biomass gasifier, green energy, Food technology etc. The Journal welcomes the submission of manuscripts that meet the general criteria of significance and scientific excellence. Papers will be published shortly after acceptance. All articles are peer-reviewed

Indexing

The African Journal of Environmental Science and Technology is indexed in:
CAB Abstracts, CABI's Global Health Database, Chemical Abstracts (CAS Source Index), China National Knowledge Infrastructure (CNKI), Dimensions Database, Google Scholar, Matrix of Information for The Analysis of Journals (MIAR), Microsoft Academic

AJEST has an h5-index of 14 on Google Scholar Metrics

Open Access Policy

Open Access is a publication model that enables the dissemination of research articles to the global community without restriction through the internet. All articles published under open access can be accessed by anyone with internet connection.

The African Journal of Environmental Science and Technology is an Open Access journal. Abstracts and full texts of all articles published in this journal are freely accessible to everyone immediately after publication without any form of restriction.

Article License

Memberships and Standards

Academic Journals strongly supports the Open Access initiative. Abstracts and full texts of all articles published by Academic Journals are freely accessible to everyone immediately after publication.

Crossref is an association of scholarly publishers that developed Digital Object Identification (DOI) system for the unique identification published materials. Academic Journals is a member of Crossref and uses the DOI system. All articles published by Academic Journals are issued DOI.

Similarity Check powered by iThenticate is an initiative started by CrossRef to help its members actively engage in efforts to prevent scholarly and professional plagiarism. Academic Journals is a member of Similarity Check.

CrossRef Cited-by Linking (formerly Forward Linking) is a service that allows you to discover how your publications are being cited and to incorporate that information into your online publication platform. Academic Journals is a member of CrossRef Cited-by.

Academic Journals is a member of the International Digital Publishing Forum (IDPF). The IDPF is the global trade and standards organization dedicated to the development and promotion of electronic publishing and content consumption.

Contact

Editorial Office: ajest@academicjournals.org

Help Desk: helpdesk@academicjournals.org

Website: http://www.academicjournals.org/journal/AJEST

Submit manuscript online http://ms.academicjournals.org

Academic Journals
73023 Victoria Island, Lagos, Nigeria
ICEA Building, 17th Floor,
Kenyatta Avenue, Nairobi, Kenya.

Table of Content

Vol. 15(11), pp. 505-518, November 2021
DOI: 10.5897/AJEST2021.3073
Article Number: CB1206268190
ISSN: 1996-0786

http://www.academicjournals.org/AJEST

ACADEMIC JOURNALS
expand your knowledge

African Journal of Environmental Science and Technology

Full Length Research Paper

Spatio-temporal dynamics of land use on the expansion of coffee agroforestry systems in Cameroon's production basins

Marcien Kuete Fogang[1*], Marie Louise Avana Tientcheu[1], Christopher Tankou[2] and Eunice Ndo[3]

[1]Department of Forestry, Faculty of Agronomy and Agricultural Sciences, University of Dschang, Cameroon.
[2]Department of Crop Science, Faculty of Agronomy and Agricultural Sciences, University of Dschang, Cameroon.
[3]Institute of Agricultural Research for Development (IRAD), Cameroon.

Received 12 October, 2021; Accepted 12 November, 2021

Diachronic analysis of satellite images was used to assess the spatiotemporal dynamics of land use and land cover change in the coffee production basins of Cameroon, located in the forest agro-ecological zones (Moungo and Haut-Nyong) and the highland humid savannah (Noun). A survey of farmers was carried out to identify land use and changes in the area of coffee agroforests over time. While the period 1980 to 2001 was marked by an increase in the area of the forest/agroforest land-use unit, the period 2001 to 2019 shows significant regressions ranging from 14 to 22% of the total area of each basin. Significant changes in the land use units have repercussions on the areas dedicated to coffee growing, which have decreased significantly; today, the largest areas under cultivation are in Haut-Nyong (1.51±1.27 ha), the medium areas in Moungo (1.14±1.13 ha) and the smallest in Noun (0.67±0.72 ha). Coffee abandonment coupled with anthropogenic factors such as agriculture and housing expansion are mainly responsible for the degradation of coffee agroforests, with notable repercussions on land cover changes. The cocoa-coffee revival encouraged by sectoral Ministries in recent years seems to have encouraged cocoa production, since in agro-ecological regions; the increase in forest/agroforest area is mainly attributable to *Theobroma cacao* and *Elaies guineensis*.

Key words: Spatio-temporal dynamics, land use/land cover, agroforestry system, coffee agroforest, coffee area, agro-ecological zone.

INTRODUCTION

Land use change through deforestation and/or forest cover degradation due to unsustainable agricultural practices emits significant amounts of carbon into the atmosphere (Cortez and Stephen, 2009; Mangion, 2010). According to the Global Environment Facility (FEM, 2012), the activities of land use and forestry sector contribute 31% to global greenhouse gas (GHG) emissions that is, 14% in agriculture and 17% of

*Corresponding author. E-mail: marcien.kuete@yahoo.fr.

deforestation and land degradation due to unsustainable practices, which have profound impacts on maintaining ecosystem services. Research on land use and land cover change is important at a basic level to explore the dynamics and drivers of change (socio-economic or biophysical) associated with it in order to support conservation planning and policy development (Ellis et al., 2010); the processes and drivers associated with these changes being complex and resulting from the interaction of the human-environment system which is influenced by socio-economic, environmental and political-institutional aspects that can be considered as drivers (Rindfuss et al., 2004; Overmars and Verburg 2005, 2006).

The monitoring of land use and land cover changes in the Congo Basin is necessary in view of the significant decrease in forest area recorded during this century (Karsenty, 2004; Tchatchou et al., 2015). In this regard, forests and agroforests constitute a major component for the maintenance of tree cover (Ellis et al., 2010). Indeed, agroforestry systems (AFS) are recognized as privileged places for biodiversity conservation and important carbon reservoirs (Zapfack et al., 2002). Recent studies show that the management of agroforests based on perennial crops constitutes a means of afforestation of savannah ecosystems, through the introduction and or preservation of trees for shade and the provision of many other services (Jagoret et al., 2014). In Central Africa, a significant part of agriculture is based on complex AFS, mainly based on cocoa and coffee trees, which contribute to the income and food of millions of rural families. These complex cocoa- and coffee-based AFS are considered intermediate land-use systems between natural forest extraction and modern plantations (Foresta and Michon, 1997; Correia et al., 2008). The conversion of agroforests to non-agroforestry systems can occur if the economic and institutional conditions are not favourable compared to the deforestation process and thus generate similar environmental impacts (Ellis et al., 2010).

Cameroon, the second largest country in the Congo Basin in terms of forest area (20 million ha of forest) and the fifth most biodiverse country in the continent (WRI, 2006), is made up of five agro-ecological zones, three of which form the south of the country and are the main coffee and cocoa production basins. These are the monomodal forest zone (coastal and mountainous zone with a humid equatorial climate), the bimodal forest zone and the high altitude humid savannah zone (Western Highlands) with an equatorial climate (MINEPIA, 2011). The forest agro-ecological zones are recognized as Robusta coffee growing areas while the highlands are the preferred area for Arabica coffee. According to Kamga (2002), the cultivation of Arabica coffee in the highlands of West Cameroon, introduced in 1924 by the colonial administration has experienced an unprecedented boom. Thanks to this crop, the Bamileke peasant was able to improve his social status. However, the economic crisis of the 1980s, coupled with the devaluation of the CFA franc, led to a gradual abandonment of coffee cultivation due to the cost of inputs and the lack of subsidies in favour of market gardening and food crops (Fongang, 2008; Kuete, 2008). These phenomena have significantly marked the history of coffee growing and, by extension, the agrarian landscapes of Cameroon's coffee-growing regions. Considering the construction of coffee landscapes in the 1960s, followed by their deconstruction in the 1980s with the advent of the crisis, one could envisage encouraging prospects for a spatial reconfiguration of coffee agroforests in the different production basins thanks to the cocoa-coffee revival encouraged in recent years by the sectoral ministries, organizations and institutions under their supervision. However, this revival does not take into account the evaluation of changes in land use and occupation. It is therefore important to examine the influence of these changes in coffee growing on the landscape dynamics of humid forest and savannah ecosystems, which are recognized as the main production basins in Cameroon.

Remote sensing data are frequently used for landscape studies (Morant, 1999; Djiongo et al., 2020). Remote sensing offers an important data source for studying the spatio-temporal dynamics of several environmental parameters; it is necessary for monitoring land use. The objective of the study is to characterize the changes in land use patterns in the main coffee production basins in Cameroon between 1980 and 2018, taking into account the following eco-zones i.e. the Noun Division (Foumbot, Nkouoptamo) for the high savannah agro-ecological zone where Arabica coffee is grown and the Divisions of Moungo (Melong, Baré-Bakem, Nkongsamba 2) and Haut-Nyong (Angossas, Mboma) for the forest agro-ecological zones with monomodal and bimodal rainfall regimes, respectively, which are the preferred zones for Robusta coffee.

MATERIALS AND METHODS

Study site

The main coffee production basins of Cameroon are located in the southern part of Cameroon, between 2°10' and 7°00' North latitude and between 8°30' and 16°10' East longitude, covering an area of 242620 km^2 (Figure 1). It corresponds essentially to the West and North-West regions for the agro-ecological zone of humid highland savannah (AEZ 3) characterized by a tropical mountainous climate of sub-equatorial type influenced by a rugged relief and with a long rainy season and a short dry season of 2 to 4 months (UNDP, 2013); the South-West and Littoral regions for the monomodal forest zone (AEZ 4) where a hot and humid oceanic equatorial type climate prevails with two seasons; the Central, Eastern and Southern regions for the bimodal forest zone (AEZ 5), characterized by a sub-equatorial Congo-Guinean type climate with two dry seasons alternating with two rainy seasons. According to Letouzey (1985), the AEZ 3 is made up of a herbaceous stratum dominated by *Pennisetum purpereum* and *Imperata cylindrica* and the woody cover is highly disturbed by human activities. A mangrove flora composed of *Rhizophoras* and *Avicennia* in AEZ 4; AEZ 5 is composed on the one hand by the dense evergreen forest of low

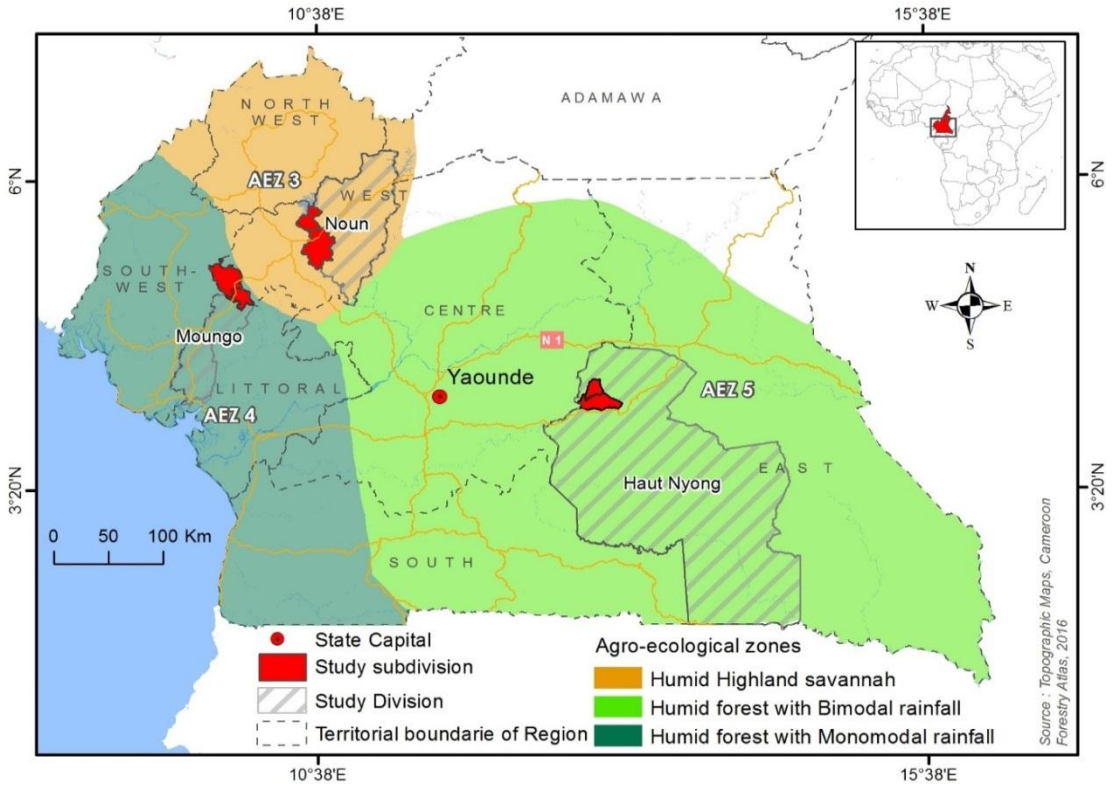

Figure 1. Location of study sites. **Source:** Topographic maps of Cameroon; Forestry Atlas, 2016.

and medium altitude and Atlantic of medium altitude and on the other hand, by the dense semi-deciduous forest of medium altitude. The Subdivisions of Foumbot and Kouoptamo are the study localities for AEZ 3; the Subdivisions of Melong, Baré-Bakem and Nkongsamba 2 are the study localities for EAZ 4; the Subdivisions of Angossas and Mboma are the study localities for EAZ 5.

Data collection and analysis

Remote sensing and field data

The remote sensing data consists of Landsat MSS, Landsat 7 ETM+ and Landsat 8 OLI_TIRS satellite images for the years 1980, 2001 and 2019, respectively. These images contain location information provided by National Aeronautics and Space Administration (NASA) and United State Geological Survey (USGS). The images have the advantage of being orthorectified, so they can be easily integrated into a geographic information system (GIS). These images have a resolution of 30 m for the multi-spectral bands and 15 m for the panchromatic band. They are provided in standard GeoTIFF format with a Universal Transverse Mercator (UTM) projection. The dry season images were used to discriminate between perennial crops and food crops and between rainy season crops. Landscape unit discrimination points were identified in the localities of the three production basins corresponding to four land use forms of interest in Noun and Moungo (forest/agroforest, clear forest, cropland, built-up areas/bare soil) and five in Haut-Nyong (valley vegetation, forest/agroforest, clear forest, cropland, built-up areas/bare soil).

DEM ASTER (Digital Elevation Model) images with a resolution of 30 m were first used to produce the Digital Terrain Model; coupled with field surveys, they were used to identify the altitudes at which coffee is grown in the production basins. A questionnaire was administered to 240 producers on the evolution of coffee-growing areas and the identification of land use types.

Data analysis

The first phases of the processing consisted of image pre-processing (atmospheric and radiometric corrections), combination of the different spectral bands and extraction of the study area from the image scenes for each of the three dates. The images used were all already geo-rectified according to the UTM WGS 84 projection system. Next, the normalized vegetation index (NDVI) analysis was used to highlight the vegetation surfaces. The NDVI varies from -1 to 1 with negative water values, bare and nearly bare soil values close to 0 and dense and green vegetation values close to 0.8 (Lambin and Ehrlich, 2007). It is the ratio of the Near Infrared (NIR) band minus the Red (R) band to the NIR + R band. The thresholding technique is then applied to extract information on AFS and forest formations. Finally, the composite bands were used to produce the best colour compositions to determine the spectral signatures of the objects for a supervised maximum likelihood classification of the land cover patterns. Four main classes of interest were identified: forest/agroforest, open forest, cropland and built-up/bare soil. The classification results were used to quantify land cover and highlight vegetation cover in 1980, 2001 and 2019. The pixel confusion matrix coupled with Global Positioning System (GPS) data from the field campaigns were used for final validation of the land cover maps. The image processing was carried out using ENVI 5.3 software. The processed images were then introduced into ArcGIS 10.3 software for the creation of maps and the calculation of areas.

The analysis of the dynamics was done by calculating the

average annual rate of spatial expansion (T) which measures the growth of macroeconomic aggregates between two given periods (Inoussa et al., 2011). Let S be the area, S1 and S2 corresponding to the areas of a land use class during the first and second periods.

$$T\ (\%) = \left[\frac{S2}{S1} - 1\right] * 100$$

- If S2 - S1 is positive, an increase in land cover unit is concluded;
- If S2 - S1 is negative, a regression of the land cover unit is concluded;
- If S2 - S1 is zero, a stability of the land use unit is concluded.

The development of the transition matrix, a method for describing in a condensed manner, in the form of a square matrix, the changes in state of the elements of a system during a given period (Schlaepfer, 2002). The transition matrix makes it possible to describe in a condensed manner, in the form of a square matrix, the changes in state of the elements of a system during a given period; it contains no information on the spatial distribution of the changes, nor on the processes and causes that led to the changes, but it does provide information on the proportion of assignment of a type "i" of land use to a state "j" that was achieved during the period in question (Bamba, 2010). The analysis of variance with SPSS 21 software has made it possible to compare the evolution of the averages of coffee areas in the production basins.

RESULTS

Land use in coffee growing areas

Status of land use in 1980, 2001 and 2019 in Noun

Figure 2 shows that land use differs from one date to another. In 1980, forest/agroforest occupied 18% of the total area, or 19596.5 ha. Crops occupied 13% (13988 ha) and clear forest 5.96%, that is, 6241.5 ha.

In 2001, the land use has clearly changed for some classes. The area occupied by forest/agroforest increased by 2% and reached 21% (21635.3 ha). Crops follow the same trend with a remarkable evolution of almost 10% of the occupied area between 1980 and 2001. The clear forest has considerably regressed compared to 1980; it does not reach 1% in 2001 and yet it occupied an area of over 5% in 1980. In 2019, built-up/bare soil still occupies a larger area than the other classes. Crops have followed a progressive curve and have evolved in terms of occupancy at the expense of other classes such as clear forest which holds the lowest percentage with 1.1%.

Status of land use in 1980, 2001 and 2019 in the Moungo

In Moungo, the changes and evolutions are as remarkable as in Noun (Figure 3). In 1980, forest/agroforest occupied a larger area than the other classes with 45.43% or 37907.1 ha of the total area.

The next largest area is cultivated with 33.95% (28332.8 ha), followed by built-up areas/bare soil and clear forest with 15.52 and 5.01% respectively. The real estate market with buildings had not yet expanded during this period. This is the reason why the area occupied by built-up/bare soil was not as important. The clear forest occupied only a small part of the total area. In 2001, both forest/agroforest and built/unbuilt land have changed compared to 1980. The area of forest/agroforest increased from 45.43% in 1980 to 55.05% (46677.4 ha) in 2001, that is, an increase of almost 10%, and the area of built-up area/bare soil increased from 15.52% in 1980 to 17.65% in 2001, that is, an increase of almost 1.5%. The clear forest and water have also experienced this evolution. Only crops have experienced a spectacular regression. They occupy 18.63%, which is minimal compared to the year 1980 when they occupied 33.95%. In 2019, crops have regained ground and occupy almost half of the total area with 45.16% (38346.8 ha). Among other things, they have nibbled away at the areas dedicated to forest/agroforest, which currently have only 22.31% (18,943.2 ha) of the area, whereas they occupied more than half of the total area in 2001. The clear forest has practically doubled its coverage rate with 16.44% (13960.3 ha) compared to 2001 when it was 8.57%.

Status of land use in 1980, 2001 and 2019 in Haut-Nyong

In Haut-Nyong (Angossas and Mboma), a new class is included in the analysis, namely valley vegetation (raffia swamp forest), which is a particularity of this zone (Figure 4). Globally, the class that has grown since 1980 to 2019 is the built-up/bare soil class with an evolution of more than 10% each time compared to the clear forest class which has suffered a degradation of its space going from 26.36% (16210.1 ha) of the occupied area in 1980 to 2.36% (1726.7 ha) in 2019. The other classes have undergone evolutions and changes over time; recording periods of oscillations that all have in common almost similar profiles in terms of evolution. In 2001, they reached their peak before falling in 2019.

Dynamics of land use patterns

From 1980-2001 to 2001-2019 in Noun

Between 1980 and 2001, forest/agroforest occupied more space with an increase in area of 2038.8 ha while clear forest lost over 90% of its area. The crop class gained the most in terms of area with a gain of over 11000 ha. The period 2001 to 2019 is characterized by gains in the clear forest and crop land use units and a decline in forest/agroforest and non-forest areas. Table 1 shows the differences in area gained or lost between the three dates (1980, 2001 and 2019).

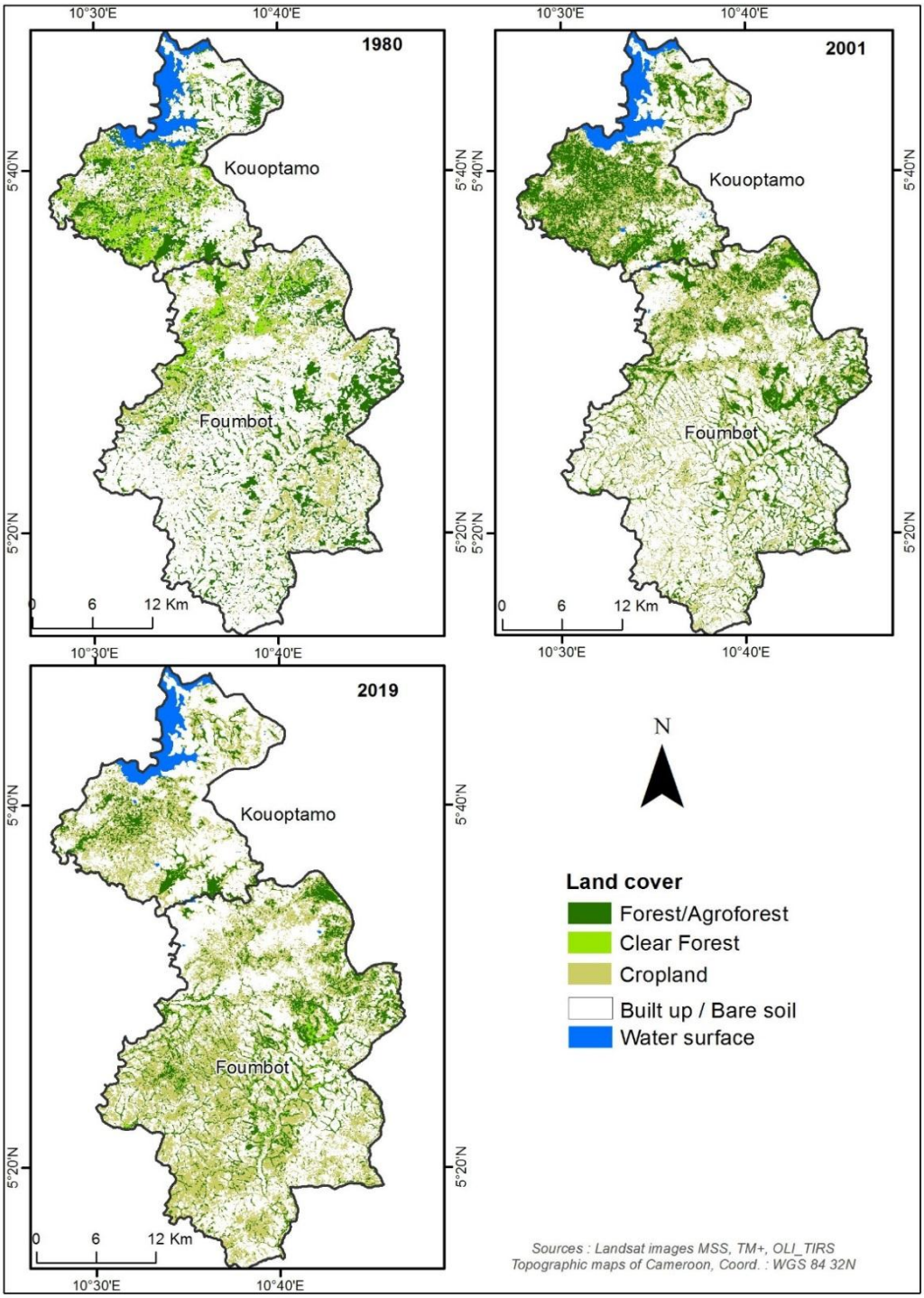

Figure 2. Land use/land cover classification in Noun Division (Foumbot and Nkouoptamo) in 1980, 2001 and 2019. Source: Landsat images MSS, TM+, and OLI-TIRS; Projection system: WGS 84 32N.

The transition matrix shows that between 1980 and 2001, 45.5% of the land in Noun underwent changes, including 42.30% of conversions, that is, 44281.6 ha, and 3.30%, that is, 3457 ha of modifications. The unchanged areas represent 54.40% of the total area of the study area, that is, 56943.2 ha. Table 4 highlights the changes that have affected forests at the expense of cultivated areas and built-up areas and bare soil. Between 2001 and 2019, 45.08% of the land in Noun underwent changes, 43.79% of which were conversions, that is, 45841.6 ha, and only 1.29%, that is, 1353.3 ha, were modifications. As for the areas without changes, they represent 54.92% of

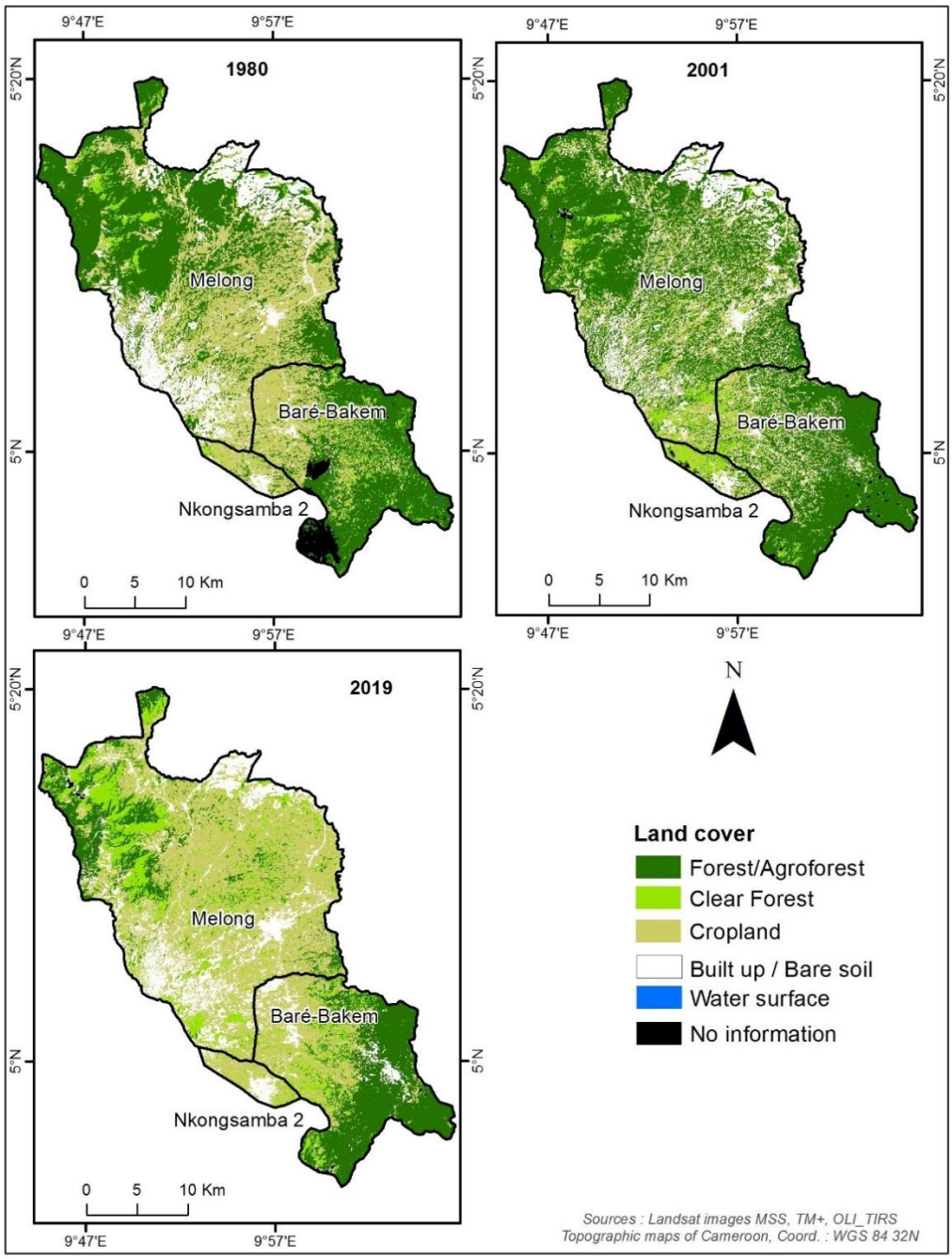

Figure 3. Land use/land cover classification in Moungo Division (Melong, Baré-Bakem and Nkongsamba 2) in 1980, 2001 and 2019. Sources: Landsat images MSS, TM+, and OLI-TIRS; Projection system: WGS 84 32N.

the total area of the study area, that is, 57487 ha (Table 5).

From 1980-2001 to 2001-2019 in the Moungo

Overall, the land use classes in this area have varied over time and no class has been able to maintain the extent of area that it has increased or decreased. Table 2 shows the differences in area (gained or lost) of the five land use classes between 1980 and 2019. Between 1980 and 2001, only crops experienced a decrease in terms of area and the other classes experienced remarkable increases. Forest/agroforest has the largest increase with 8770.2 ha; this class is strongly correlated with crops since an increase in area in one of these classes leads to

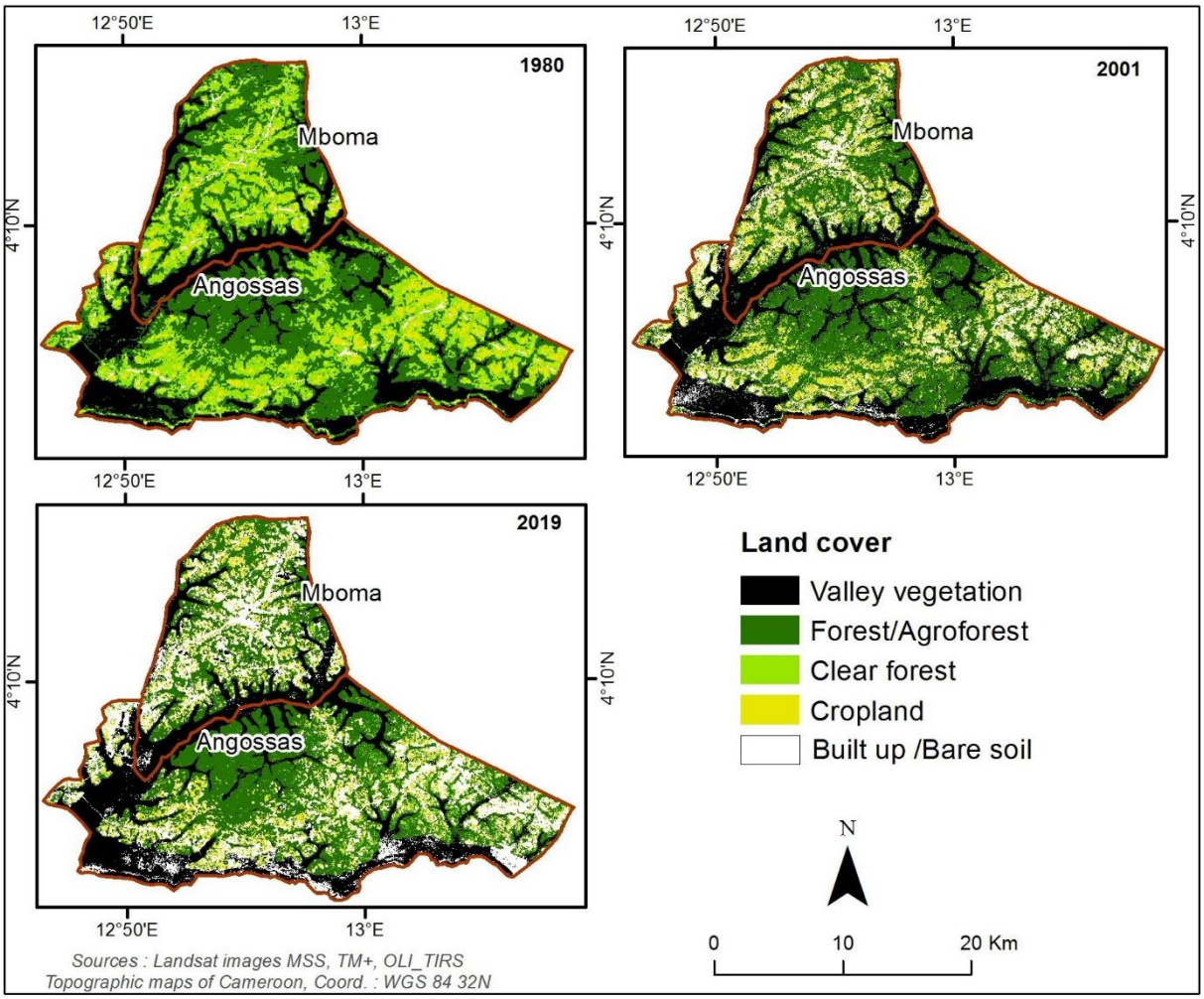

Figure 4. Land use/land cover classification in Haut-Nyong Division (Angossas and Mboma) in 1980, 2001 and 2019. Sources: Landsat images MSS, TM+, and OLI-TIRS; Projection system: WGS 84 32N.

Table 1. Areas of land use/land cover gained or lost (ha) between 1980 and 2019 in Noun.

Period	Areas in 1980	Areas in 2001	Areas in 2019	Area gained/lost between 1980 and 2001	Area gained/lost between 2001 and 2019
Land use patterns			**Areas (ha)**		
Forest/Agroforest	19596.6	21635.4	14164.4	2038.8	-7470.9
Clear Forest	6241.6	585.3	1242.1	-5656.2	656.7
Cropland	13988.9	25959.1	35291.5	11970.3	9332.4
Built up / Bare soil	61932.7	53423.4	51080.4	-8509.3	-2343.1
Water	2922.2	3078.5	2903.4	156.4	-175.1

a decrease in the other class and vice versa. The period 2001 to 2019 is marked by gains in the crop and clear forest land use units and a decrease in forest/agroforest. This confirms the interrelation between the forest/ agroforest class and crops.

Table 6 shows that between 1980 and 2001, 39.39% of the land in the Moungo underwent changes, of which 34.80% were conversions, that is, 28936.4 ha, and 4.59%, that is, 3813.6 ha, were modifications. The unchanged areas represent 60.61% of the total area of

Table 2. Areas of land use/land cover gained or lost (ha) between 1980 and 2019 in Moungo.

Period	Areas in 1980	Areas in 2001	Areas in 2019	Area gained/lost between 1980 and 2001	Area gained/lost between 2001 and 2019
Land use patterns			**Areas (ha)**		
Forest/Agroforest	37907.1	46677.4	18943.2	8770.2	-27734.2
Clear forest	4178.5	7263.8	13960.3	3085.2	6696.4
Cropland	28332.8	15792.6	38346.8	-12540.1	22554.2
Built up / Bare soil	12955.1	14969.8	13647.5	2014.6	-1322.2
Water	73.8	88.4	21.2	14.6	-67.2

Table 3. Areas of land use/land cover gained or lost (ha) between 1980 and 2019 in Haut-Nyong.

Period	Areas in 1980	Areas in 2001	Areas in 2019	Area gained/lost between 1980 and 2001	Area gained/lost between 2001 and 2019
Land use patterns			**Areas (ha)**		
Valley vegetation	14613.3	18080.1	14841.9	3466.8	-3238.2
Forest/Agroforest	24772.7	25944.7	23361.9	1172.1	-2582.9
Clear Forest	16210.1	1726.7	1436.4	-14483.4	-290.3
Cropland	4939.2	7998.4	6526.8	3059.2	-1471.7
Built up / Bare soil	956.2	7954.4	14746.3	6998.2	6791.8

Table 4. Dynamic characteristics of land use/land cover patterns from 1980 to 2001 in Noun.

2001/1980	Forest /Agro forest (ha)	Clear forest (ha)	Cropland (ha)	Built up/Bare soil (ha)	Water
Forest/Agroforest	9110.7	371.1	5439.2	4567.1	108.3
Clear forest	3085.9	26.8	2289.5	838.6	0.8
Cropland	2617.9	30.9	4268.5	7053.6	18.0
Built up/Bare soil	6754.3	156.5	13898.4	40854.6	268.9
Water	66.6	0	63.4	109.6	2682.6
	Modified areas in forest vegetation		Areas unchanged		

the study area, that is, 50390.7 ha. Between 2001 and 2019, 56.43% of the Moungo's land area underwent changes, of which 45.62% were conversions, that is, 38597.8 ha, and 10.81%, that is, 9141.1 ha of modifications. The unchanged areas represent 43.57% of the total area of the study area, that is, 36860.9 ha (Table 7).

From 1980-2001 to 2001-2019 in Haut-Nyong

Between 1980 and 2001, the first remark that stands out is that clear forest is the only class that has regressed and this area has reached 14483.4 ha. All other classes have gained in area. Between 2001 and 2019, valley vegetation is the class that lost the most area. Forest/agroforest is decreasing; in contrast to the period 1980 and 2001 when it had the largest area loss, it becomes the class with the least area loss during this period. Table 3 provides further clarification on land use in zone 5.

Table 8 shows that between 1980 and 2001, 48.64% of the land in Haut-Nyong underwent changes, of which 38.40% were conversions, that is, 23,614.3 ha, and 10.24%, that is, 6,298.6 ha, were modifications. As for the areas without changes, they represent 51.35% of the total area of the study area, that is, 31578.4 ha. Between 2001 and 2019, 46.02% of the land in Haut-Nyong underwent changes including 37.56% of conversions or 23178 ha and 8.46% or 5218 ha of modifications. As for the areas without changes, they represent 53.98% of the total area of the study area, that is, 33308 ha (Table 9).

Table 5. Dynamic characteristics of land use/land cover patterns from 2001 to 2019 in Noun.

2019/2001	Forest /Agro forest (ha)	Clear forest (ha)	Cropland (ha)	Built up/Bare soil (ha)	Water
Forest/Agroforest	8344.9	951.3	7800.5	4489.6	49.2
Clear forest	402.0	107.2	52.9	22.8	0.4
Cropland	3457.8	136.2	11156.7	11188.7	19.7
Built up/Bare soil	1949.2	47.1	16235.0	35118.1	74.1
Water	10.5	0.2	46.4	261.3	2760.1
	Modified areas in forest vegetation		Areas unchanged		

Table 6. Dynamic characteristics of land use/land cover patterns from 1980 to 2001 in the Moungo.

2001/1980	Forest /Agro forest (ha)	Clear forest (ha)	Cropland (ha)	Built up/Bare soil (ha)	Water
Forest/Agroforest	31790.6	1591.2	2252.5	2018.0	47.8
Clear forest	2222.4	1202.1	501.4	223.5	1.7
Cropland	9079.8	3658.2	10149.8	5388.2	7.3
Built up/Bare soil	2320.0	621.0	2742.8	7235.1	14.1
Water	43.7	0.8	1.2	14.4	13.1
	Modified areas in forest vegetation		Areas unchanged		

Table 7. Dynamic characteristics of land use/land cover patterns from 2001 to 2019 in the Moungo.

2019/2001	Forest /Agro forest (ha)	Clear forest (ha)	Cropland (ha)	Built up/Bare soil (ha)	Water
Forest/Agroforest	17557.0	8810.1	17423.9	2737.8	3.9
Clear forest	331.0	2278.9	3813.4	818.5	0.1
Cropland	414.9	1841.0	10267.7	3262.7	0.1
Built up/Bare soil	458.6	983.0	6768.9	6743.3	3.1
Water	20.5	5.1	10.4	31.9	14.0
	Modified areas in forest vegetation		Areas unchanged		

Table 8. Dynamic characteristics of land use/land cover patterns from 1980 to 2001 in Haut-Nyong.

2001/1980	Valley vegetation (ha)	Forest /Agro forest (ha)	Clear forest (ha)	Cropland (ha)	Built up /Bare soil (ha)
Valley vegetation	12418.8	1493.3	28.2	82.3	590.5
Forest/Agroforest	4805.3	15922.1	770.0	1790.5	1484.8
Clear forest	680.4	7208.3	773.7	4072.0	3475.7
Cropland	86.6	1112.1	137.4	1845.5	1757.6
Built up/Bare soil	27.0	118.5	11.6	180.8	618.3
	Modified areas in forest vegetation		Areas unchanged		

Influence of coffee growing on agrarian dynamics

In the Department of Noun, an Arabica coffee growing area (Foumbot and Kouoptamo Subdivisions), coffee growing is practiced between 800 and 1400 m altitude. The Kouoptamo area is higher in altitude and coffee is grown at an average altitude of 1200 m. In Moungo, the Robusta coffee production basin (Melong, Bare-Bakem

Table 9. Dynamic characteristics of land use/land cover patterns from 2001 to 2019 in Haut-Nyong.

2019/2001	Valley vegetation (ha)	Forest /Agro forest (ha)	Clear forest (ha)	Cropland (ha)	Builtup/Bare soil (ha)
Valley vegetation	12065.8	3156.9	152.1	368.5	2336.8
Forest/Agroforest	2061.1	15313.7	985.3	2632.6	4951.8
Clear forest	70.6	962.6	50.1	240.5	402.9
Cropland	157.0	2560.8	143.5	1882.1	3255.0
Built up /Bare soil	682.3	1594.2	110.8	1570.7	3996.3
	Modified areas in forest vegetation		Areas unchanged		

Table 10. Evolution of average coffee growing areas according to production zones.

Production basins	Locations	Average area at origin (ha)	Current average area (ha)
Noun	Foumbot, Nkouoptamo	1.25±1.02[a]	0.67±0.72[a]
Moungo	Melong, Baré-Bakem, Nkongsamba 2	1.59±1.07[b]	1.14±1.13[b]
Haut-Nyong	Angossas, Mboma	1.93±1.09[c]	1.51±1.27[c]

Means with identical letters in each column are equal to the significance level $\alpha = 0.05$, P = 95%.

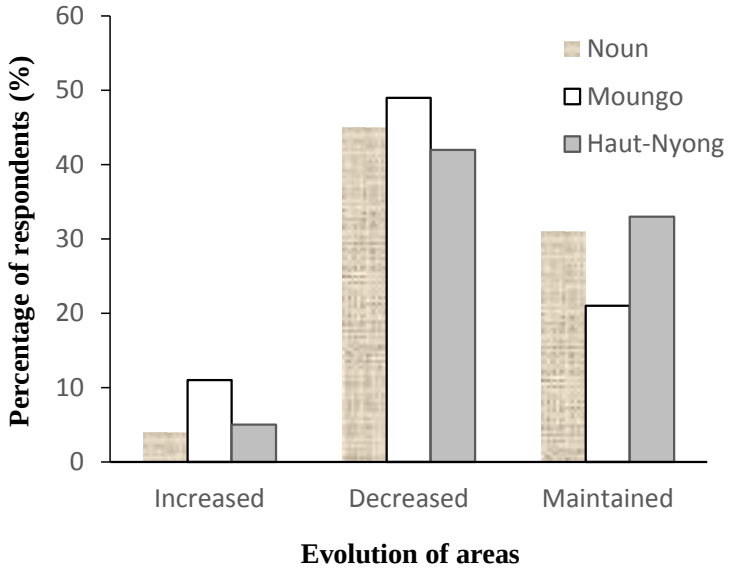

Figure 5. Producers' perception of the evolution of coffee areas over time according to production basins.

and Nkongsamba 2 Subdivisions), coffee is also grown at altitudes of up to 1,400 m. However, there are dissimilarities at the locality level, with the highest localities being in Melong and Nkongsamba 2. In Bare-Bakem, the altitude does not exceed 1000 m. In Haut-Nyong, another Robusta coffee production basin, the is altitude varies from 590 to 780 m (Mboma and Angossas Subdivisions) and coffee growing is practiced at all levels of altitude. The influence of coffee growing on the agrarian landscape of Cameroon's production basins significant and relates to the distribution of land per farmer according to the localities of each basin (Table 10 and Figure 5).

Table 10 shows that the largest areas under cultivation are in Haut-Nyong (1.51±1.27 ha), the medium areas in Moungo (1.14±1.13 ha) and the smallest in Noun (0.67±0.72 ha); however, Melong is the second largest area after Mboma. The smallest areas are found in Foumbot in Noun with 0.58±0.73 ha. For the first period (areas at origin), the analysis of variance shows that

there is a significant difference (0.010) between the area means between localities and area classes. The Newman-Keuls test for separation of means shows that the area means of Melong, Angossas and Mboma differ from those of the other four smaller localities. For the first period (areas at origin), the analysis of variance shows that there is a significant difference (0.010) between the area means between localities and area classes. The Newman-Keuls test for separation of means shows that the area means of Melong, Angossas and Mboma differ from those of the other four smaller localities.

For the second period (current areas), the analysis of variance shows that there is a significant difference (0.006) between the area means between localities and area classes. The test of separation of means shows that the area means of Melong and Mboma differ from those of the other five smaller localities. However, there is a significant difference between the area means of the different basins. However, Moungo is the basin that has experienced the most decreases and increases in area, with peaks of nearly 50 and 12% for decreased and increased areas respectively; the areas that have been maintained are found in Haut-Nyong (33%) and Noun (31%).

DISCUSSION

Land use/land cover dynamics

Studies on land cover change are essential for the development of effective natural resource management plans (Gilani et al., 2015). The diachronic analysis of the landscapes of the different coffee production basins developed from Landsat MSS, ETM + and OLI TIRS images, allowed a monitoring of landscape changes that occurred between 1980 and 2019. The knowledge of the terrain has made it possible to identify the constituent elements of the environment and to accurately characterize the occupation modes through thresholding methods and supervised classification. The use of remote sensing has already been used in the analysis of land cover dynamics by many authors (Tabopda, 2012; Ellis et al., 2010; Temgoua et al., 2018; Momo et al., 2018; Djiongo et al., 2020; Tsewoue et al., 2020), but this approach has the advantage of allowing for more accurate extraction of vegetation information. The confusion matrix reveals that the pixels of some land use units were confused with others; but the Kappa index obtained which varies between 0.90 and 0.98 for the images of each site confirms the statistical acceptability of these classifications.

The results of this study show after using the FAO soil classification system (2012) applied to our context, that coffee AFS are part of the forest/agroforest land use class. Since 1980, forest/agroforest compared to other land use classes has been the most important in Moungo in particular with 45% of the total area of the study area against 40% in Haut-Nyong and 18% in Noun. The 2001 period is marked by an increase in the area of this class in all production basins (55% in Moungo, 42% in Haut-Nyong and 21% in Noun). Between 2001 and 2019, there was a significant decline in the area of forest/agroforest, most notably in Moungo (22% in Moungo, 38% in Haut-Nyong and 14% in Noun). These decreases in area are in contrast to the continuous increases recorded in the crop and housing classes. In a similar study conducted on the eastern slope of the Bamboutos Mountains (Kuete, 2017; Fogaing, 2019), where population densities are higher, the period 2001-2017 is instead marked by a resurgence of forest/agroforest areas due to plantations of eucalyptus and other multipurpose woody species. These results on land use in Cameroon's coffee production basins, which show a continuous increase in cultivated areas, are similar to those obtained by Oszwald (2005); in fact, in a study conducted on agroforestry dynamics between 1980 and 2000, the author highlights deforestation in favour of cultivated areas, mainly for commercial purposes, through the establishment of coffee or cocoa plots; this period corresponds to a transition in Cameroon towards food and perennial crops (cocoa and oil palm).

The activity data that emerged show that overall, the period 2001-2019 is marked by greater changes (conversions and modifications) in land use units compared to the period 1980-2001. During the period 1980-2001, the greatest changes in land use units are recorded first in Haut-Nyong (48.6% of the total area of this study area) against 51.3% without changes; then in Noun with 42.3% of changes against 54.4% of unchanged areas; finally in Moungo with 39.9% of changes against 60.6% without changes On the other hand, during the period 2001-2019, Moungo recorded the greatest changes with 56.4% of the total area of this study area, followed by Haut-Nyong with 46% of changes; Noun was in last position with 45% of changes. These data differ from those obtained on the eastern slope of the Bamboutos Mountains (Kuete, 2017) where the most significant changes were observed during the period 1980-2001. These data differ significantly from those obtained by Sarr (2009) in a similar study in a drought affected ecoregion.

The identification of land use types from the forms of occupation showed that in addition to coffee AFS which are found in the forest class, sacred forests we also have raffia and bamboo in the valleys and other multipurpose woody trees; eucalyptus stands are found in Noun at all altitudinal gradients while coffee trees are found at medium and low altitudes as indicated by Mbarga et al. (2013) for the western highlands. In Noun (Foumbot and Kouoptamo Subdivisions), the study showed that coffee trees are found between 800 and 1400 m in Moungo and between 590 to 780 m in Haut-Nyong. Contrary to the eastern slopes of the Bamboutos Mountains, where

coffee is grown up to 1800 m in altitude and where all levels of altitude are exploited (potato and market garden crops at high altitude), the high altitudes of Noun and Moungo, which are mostly not exploited, are used for grazing. The non-forest areas (built-up areas/bare soil) are made up of built-up areas, rocky outcrops and bare soil. However, some of the bare soil was found to be cultivated areas due to the preparation of the soil for cultivation during the satellite imaging; this would refer to the larger agricultural areas than those assessed in this study.

Influence of coffee growing on the agrarian landscape of production basins

The introduction of coffee growing in Cameroon has had a significant impact on the agrarian landscape of the different production basins. In the years before the crisis, there was a rapid increase in the area under coffee, followed by a second period marked by a decline. There is a significant difference between the original and current areas under coffee. The average size of the original coffee-growing areas varied between 1.25±1.02 and 1.93±1.09 ha (with a peak of 2.02 ha in Haut-Nyong) depending on the production basin. Today, the largest areas under cultivation are in Haut-Nyong (1.51±1.27 ha), the medium areas in Moungo (1.14±1.13ha) and the smallest in Noun (0.67±0.72 ha); the localities of Haut-Nyong (Mboma and Angossas) and the locality of Melong have the largest average areas. These results show a certain evolution in the area under coffee; the work of Kaffo (2000) placed the average area in the village of Bafou (West Cameroon) at 1.8 ha. Taboula (2000) on the land and coffee crisis on the basaltic plateau of Bafou (West Cameroon) shows that the relief, certain paleoclimates limiting the available surfaces, rocky outcrops and mountainous slopes, and the inheritance system are the causes of these surfaces which he situates at an average of 700 m^2 on the piedmont and 2 ha on the mountain. However, it should be noted that the population growth is more important in this part of West Cameroon.

In general, this study shows a certain concordance with the periods that marked the history of coffee growing on the eastern slopes of the Bamboutos Mountains as studied by Kamga (2002) and Kuete (2008). The year 1980, the period of the coffee crisis, marks the peak of coffee cultivation. This is what justifies the dominance of the forest class in this period. Then, following the negative consequences of this crisis, including the fall in coffee prices, the abandonment of AFS is clearly felt in 2001 and 2019 with a dominance of bare soil and crops. This raises the question of the coffee revival encouraged for several years by the sectoral ministries, organizations and institutions under supervision, which seems to have remained embryonic. This reality is in line with the results of the work of Ellis et al. (2010) on the dynamics of land occupation and use in the marginal lowlands of the State of Veracruz in Mexico; these authors show that tree cover and coffee agroforests were largely conserved during the first decade after the coffee crisis, but losses recorded around 2010 mainly attributable to pasture and agriculture are leading the authorities to encourage the population to diversify, which alone may not stop deforestation.

Conclusion

The introduction of coffee growing in Cameroon by the colonialists in the 1920s saw a total adhesion of a good number of Cameroonian farmers in the 1990s following the liberalization of the sector. Despite the establishment of farmers' organizations that proliferated in West Cameroon following the disengagement of the state, or the installation of development agencies such as the Integrated Priority Action Zone of the East (ZAPI-East), Care Cameroon and Plan Cameroon, which gave a real impetus to development, the second crisis of the 1980s had a significant impact on the coffee economy and led farmers to adopt subsistence strategies. Multiscalar analysis of remote sensing images shows a significant change in the landscape. Land use in 1980 shows that forest/agroforest compared to other land use classes was the most important in Moungo, with 45% of the total area of the study zone, compared to 40% in Haut-Nyong and 18% in Noun.

The 2001 period is marked by an increase in the area of this class in all production basins (55% in Moungo, 42% in Haut-Nyong and 21% in Noun). Between 2001 and 2019, there was a significant decline in the area of forest/agroforest, most notably in Moungo (22% in Moungo, 38% in Haut-Nyong and 14% in Noun). These decreases in area are in contrast to the continuous increases recorded in the crop and housing classes. The identification of land use types based on tenure patterns showed that coffee AFS, forest, valley raffia and bamboo, and other multiple-use woody species are found in the forest/agroforest class; these coffee AFS are found at medium and low altitudes. In Noun (Foumbot and Kouoptamo Subdivisions), coffee trees are found between 800 and 1400 m, up to 1400 m in Moungo and between 590 and 780 m in Haut-Nyong. The high altitudes of Noun and Moungo are mostly undeveloped and used for grazing.

The non-forested areas (built-up areas/bare soil) are made up of built-up areas, rocky outcrops and bare soil. Coffee abandonment has had a significant impact on the development of coffee AFS. Following the negative consequences of this crisis in the 1980s, including the fall in coffee prices, the abandonment of the coffee AFS is clearly felt in 2001 and 2019 with a dominance of cultivated areas where many farmers prefer to devote

themselves to the cultivation of cocoa (mainly in Moungo and Haut-Nyong and a new introduction in Nkouoptamo in Noun), palm and banana.

CONFLICT OF INTERESTS

The authors have not declared any conflict of interests.

ACKNOWLEDGEMENT

The authors would like to thank the DP Agroforestry Cameroon for the financial support and technical means made available.

REFERENCES

Bamba I (2010). Anthropisation and spatio-temporal dynamics of forest landscapes in the Democratic Republic of Congo. Thesis presented in view of obtaining the degree of Doctor in Sciences; ULB; 205p.

Correia M, Diabaté M, Béavogui P, Guilavogui K, Lamanda N, De Foresta H (2008). Comparative analysis of structure and composition between coffee agroforest and natural forest in Guinea Forestière (Guinea, West Africa), 16p.

Cortez R, Stephen P (2009). Reducing Emissions from Deforestation and Forest Degradation (REDD) Introductory Course Participants' Reference Manual; World Wildlife Fund, 136p.

Djiongo JEB, Desrochers A, Avana MLT, Khasa D, Zapfack L, Fotsing E (2020). Analysis of Spatio-Temporal Dynamics of Land Use in the Bouba Ndjidda National Park and Its Adjacent Zone (North Cameroon). Open Journal of Forestry 10:39-57.

Ellis EA, Baerenklau KA, Marcos-Martínez R, Chávez E (2010). Land use/land cover change dynamics and drivers in a low-grade marginal coffee growing region of Veracruz, Mexico. Agroforestry Systems 80(1):61-84.

Fogaing JR (2019). Carbon assessment of agroforestry systems on the eastern slopes of the Bamboutos Mountains; PhD thesis, University of Dschang 245 p.

Fonds pour l'Environnement Mondial, FEM (2012). Les activités en matière d'Utilisation des Terres, de Changement d'Affectation des Terres et de Foresterie (UTCATF) 28 p.

Fongang FGH (2008). Les mutations du secteur agricole bamiléké (Cameroun) étudiées à travers ses acteurs : Une analyse à partir des localités de Fokoué et de Galim; Doctoral dissertation, AgroParis Tech 416 p.

Foresta HD, Michon G (1997). Agroforests: pre-domestication of forest trees orrue domestication of forest ecosystems? Netherlands Journal of Agricultural Sciences 45(4):451-462.

Gilani H, Shrestha HL, Murthy MSR, Phuntso P, Pradhan S, Bajracharya B, Shrestha B (2015). Decadal land cover change dynamics in Bhutan. Journal of Environmental Management 148:91-100.

Inoussa MM, Mahamane A, Mbow C, Saadou M, Yvonne B (2011). Spatiotemporal dynamics of open forests in the W National Park of Niger (West Africa). Science and Global Change/Drought 22(2):108-116.

Jagoret P, Kwesseu J, Messie CA, Michel I, Malézieux E (2014). Use values of woody species used in agroforestry: cocoa agroforests in central Cameroon. Bois et Forêts des Tropiques (321):45-54.

Kamga A (2002). Economic crisis, return of migrants, and evolution of the agrarian system on the eastern and southern slopes of the Bamboutos Mountains (West Cameroon). Doctoral dissertation, Toulouse 2.

Karsenty A (2004). Issues in recent forestry tax reforms in the Congo Basin. Bois et Forêts des Tropiques 281(281):51-60.

Kuete M (2008). Coffee, coffee farmers and politics in the highlands of West Cameroon. Les Cahiers d'Outre-Mer. Revue de géographie de Bordeaux 61(243):285-302.

Kuete FM (2017). Spatiotemporal dynamics of coffee agroforestry systems in the humid savannah ecosystems of Cameroon: the case of the eastern slope of the Bamboutos Mountains, highland zone of western Cameroon. Master's thesis; FASA-University of Dschang 60 p.

Lambin EF, Ehrlich D (2007). The surface temperature-vegetation index space for land cover and land-cover change analysis. International Journal of Remote Sensing 17(3):463-487.

Letouzey R (1985). Notice of the phytogeographic map of Cameroon at 1: 500 000 (1985): 2. M-SM: afro-montane region and submontane stage 27 p.

Mangion I (2010). Le futur mécanisme REDD face aux moteurs de la déforestation et de la dégradation des forêts au Brésil, en Indonésie et en RDC. Mémoire de Master en Sciences et Gestion de l'Environnement, Université Libre de Bruxelles/Institut de Gestion de l'Environnement et d'Aménagement du Territoire; 152p.

Mbarga MA, Akoa A, Abolo D, Mbang AA, Bedimo JM, Nomo LB, Akume ND (2013). Floristic structure and composition of Arabica coffee (Coffea arabica L.) agroforests in the western highlands of Cameroon. International Journal of Biological and Chemical Sciences 7(4):1474-1489.

Ministry of Livestock, Fisheries and Animal Industries, MINEPIA (2011). 18th Alive Executive Committee; Douala, Cameroon; 39p.

Momo SMC, Njouonkou AL, Temgoua LF, Zangmene DR, Wouokoue TJB, Ntoupka M (2018). Land-Use / Land-Cover Change and Anthropogenic Causes Around Koupa Matapit Forest Gallery, West-Cameroon. Journal of Geography and Geology 10(2):56-65.

Morant P (1999). Contribution of remote sensing to the analysis and mapping of the Armorican bocage landscape. Ingénieries-EAT (18), p-61.

Food and Agriculture Organization of the United Nations, FAO (2012). Global forest land use change 1990-2005; FAO-FORETS study; No. 169; 56p.

Overmars KP, Verburg PH (2005). Analysis of land use drivers at the watershed and household level: linking two paradigms at the Phillipine forest fringe. International Journal of Geographical Information Science 19:125-152

Overmars KP, Verburg PH (2006). Multilevel modeling of land use from field to village level in the Phillipines. Agricultural Systems 89:435-456

Oszwald J (2005). Dynamique des formations agroforestières en Côte d'Ivoire (depuis les années 1980 aux années 2000): suivi par télédétection et développement d'une approche cartographique; PhD dissertation, Lille 1; 304p.

Rindfuss RR, Walsh SJ, Turner BL, Fox J, Mishra V (2004). Developing a science of land change: challenges and methodological issues. Proceedings of the National Academy of Sciences of the United States of America 101(39):13976-13981

Sarr MA (2009). Cartographie des changements de l'occupation du sol entre 1990 et 2002 dans le Nord du Sénégal (Ferlo) à partir des images Landsat. Cybergeo : European Journal of Geography, Environnement, Nature, Paysage, article 472. [En ligne] URL : http://cybergeo.revues.org/22707.

Schlaepfer R (2002). Analyse de la dynamique du paysage. Fiche d'enseignement 4.2. Lausanne. Laboratoire de gestion des écosystèmes (GECOS), École polytechnique fédérale de Lausanne, Lausanne P11

Tabopda GW (2012). Characterisation and Monitoring of Deforestation in the Protected Areas of North Cameroon: Analysis Using Satellite Remote Sensing in the Kalfou Forest Reserve. In : Technologies and Innovations for Development. Springer, Paris pp. 249-264.

Taboula L (2000). « Crise foncière et crise caféière sur le plateau basaltique de Bafou », in GEODOC 2000, N°51, série Moca N°8, Université de Toulouse Le Mirail pp. 6-23

Tchatchou B, Sonwa DJ, Ifo S, Tiani AM (2015). Deforestation and forest degradation in the Congo Basin: current status, causes and outlook. Center for International Forestry Research DOI: 10.17528/cifor/005894

Temgoua LF, Momo SMC, Nguimdo VV, Tagne BC, Tanougong A (2018). Spatial and temporal dynamic of land-cover/land-use and

carbon stocks in Eastern Cameroon: a case study of the teaching and research forest of the University of Dschang. Forest Science and Technology 14(4):181-191.
Tsewoue MR, Tchamba M, Avana ML, Tanougong AD (2020). Spatio-temporal dynamics of land use in the Moungo, Littoral Region, Cameroon: influence on the expansion of banana-based agroforestry systems. International Journal of Biological and Chemical Sciences 14(2):486-500.
United Nations Development Programme, UNDP (2013). Support programme for the implementation of integrated and comprehensive approaches to climate change adaptation 28 p.
Zapfack L, Engwald S, Sonke B, Achoundong G, Madong BA (2002). The impact of land conversion on plant biodiversity in the forest zone of Cameroon. Biodiversity and Conservation 11(11):2047-2061.

Vol. 15(11), pp. 457-469, November 2021
DOI: 10.5897/AJEST2020.2935
Article Number: E00C4B568021
ISSN: 1996-0786

http://www.academicjournals.org/AJEST

African Journal of Environmental Science and Technology

Full Length Research Paper

Use of effective microorganisms to enhance cost-effective biogas purification at the household level

Selele Minza[1*], Mgana M. Shaaban[2] and Mbuligwe E. Stephen[2]

[1]Department of Environmental Science and Management, School of Environmental Science and Technology (SEST), Ardhi University, P. O. Box 35176, Dar es Salaam, Tanzania.
[2]Department of Environmental Engineering, School of Environmental Science and Technology (SEST), Ardhi University, Dar es Salaam, Tanzania.

Received 23 October, 2020; Accepted 15 September, 2021

This study investigated the use of effective microorganisms (EM) to enhance cost-effective biogas purification at household-level application. It involved experimental setups for biogas purification in two different runs: 4 L activated EM and 1 L dormant EM by bubbling biogas through EM purification units. Biogas composition was analyzed using an industry-standard biogas analyzer. The results indicated that EM has the potential for biogas purification through a biological process, to remove H_2S and CO_2 by involving photosynthetic bacteria (*Rhodopseudomonas palustris*) in the presence of light. The raw biogas average composition was 62.2% CH_4, 37.4% CO_2 and 1359.3 ppm H_2S. The 4L activated EM batch solution purified the raw biogas to 80.2% CH_4, 19.5% CO_2 and 786.1 ppm H_2S. The corresponding purification efficiencies are 60% for CO_2 and 49% for H_2S. Purified biogas could be used by the household to cook for 1.82 h (85%) while raw biogas could cover only 55%. The designed biogas purification system can cost only Tshs 91,010/= and purify about 15,000 L of biogas at EM cost of Tshs 9,100/month.

Key words: Biogas composition, photosynthetic bacteria, anaerobic digestion, biochemical processes, *Rhodopseudomonas palustris*, biological desulphurization.

INTRODUCTION

Biogas is among the fuels from biomass which has great importance and can effectively replace fossil fuels for obtaining electricity and heat, also in the field of transport (Zăbavă et al., 2019). In recent years, there has been an increasing desire for use of biogas because it is a renewable source of energy, which is less expensive, reduce environmental pollution, reducing problems of power energy, environmental vandalism, loss of resources, climate change and promote better public health (Ilyas, 2006). Many communities especially those who live in rural areas meet 90% of their energy needs with biomass, particularly by wood fuel and this dependency on fuelwood has led to a rapid deterioration of Tanzania's ecosystems (Felix and Gheewala, 2011). Biogas is produced biologically through the process of anaerobic digestion by which organic material is transformed into gaseous products, mainly methane and carbon dioxide, ammonia, hydrogen sulphide and water

*Corresponding author. Email: minza.selele@gmail.com.

vapour. Biogas contains methane (60%) and carbon dioxide (40%) as its principal constituents (Adnan et al., 2019). Other biogas constituents are in small amounts of other compounds like ammonia (NH_3), water vapour (H_2O), hydrogen sulphide (H_2S), methyl siloxanes, nitrogen (N_2), Oxygen (O_2), halogenated volatile organic compounds (VOCs), carbon monoxide (CO) and hydrocarbons (Awe et al., 2017; Mann et al., 2009). The composition and properties of biogas vary to some degree depending on feedstock types, digestion systems, temperature and retention time (De Hullu, 2008). Weiland (2010) reported that from the biogas, methane gas is of particular interest because it is a fuel that can be used for several applications while the main biogas impurities that may require removal in upgrading systems are CO_2, H_2S, NH_3, water and solid particles. These components are impurities that pose major impediments to the commercial use of biogas (Nallamothu et al., 2013). High CH_4 purity biogas has the same properties as natural gas, especially in terms of heating value; therefore, this clean biogas is qualified to be injected into a natural gas grid (Adnan et al., 2019). CO_2 has no energy yield through combustion and greatly reduces the energy yield per volume of biogas due to its high concentration. H_2S is toxic and highly corrosive, often damaging machinery/equipments used to transport and produce energy from biogas. It also forms a harmful pollutant, Sulphur dioxide, upon combustion (Kapdi et al., 2005). Removal of these impurities is necessary to make biogas an effective energy source.

A number of technologies are available for biogas upgrading. Carbon dioxide is mainly removed by water scrubbing, pressure swing adsorption (PSA) and polyethylene glycol scrubbing (Weiland, 2010; Mann et al., 2009). Several techniques available for the removal of hydrogen sulphide from biogas are out of reach for common end-users due to lack of knowledge, higher running costs, and insufficient operational skills (Kulkarni and Ghanegaonkar, 2019). Using water scrubbing systems, H_2S can be removed simultaneously with CO_2, whereas for PSA systems adsorption columns with activated carbon are usually employed for H_2S removal. These methods are expensive and often environmentally hazardous due to the nature of the chemicals used (Adnan et al., 2019). Problems associated with cost and sustainability prevents biogas from becoming a competitive alternative energy source. H_2S can be removed internally to the digestion process by biological desulphurization performed by microorganisms of the family Thiobacillus or by iron chloride dosing to the digester (Weiland, 2006). Phototrophic bacteria (*Chlorobium limicola*) can also be responsible for the oxidation of H_2S under anaerobic conditions in the presence of CO_2 and sunlight. Most thiobacteria are autotrophic, consuming CO_2 and generating chemical energy from the oxidation of reduced inorganic compounds such as H_2S (Zhao et al., 2010).

In Tanzania, the amount of biogas produced is used up without being purified and as a result, it fails to meet the energy demand of the people. This is due to the lack of affordable and reliable purification technology because most of the biogas purification technologies are very expensive and hazardous to the environment (Ng'wandu et al., 2009). These problems associated with cost and sustainability prevents biogas from becoming a competitive alternative energy source that is why it is not widely spread in Tanzania. Thus, there is underutilization of biogas.

Effective microorganism is a media solution composed of different types of microorganisms such as photosynthetic bacteria, lactic acid bacteria, yeast, actinomycetes and fermenting fungi (Olle and Williams, 2013). These microorganisms usually synchronize with other microbes in any natural environment. The types of bacteria which are responsible for biogas purification are the photosynthetic bacteria (*Rhodopseudomonas palustris)* which are capable of oxidizing H_2S by using carbon from CO_2 as a source of energy (Agriculture and Lokare, 2007). Although *R. palustris* is a purple non-Sulphur bacterium, it is flexible to switch among any of the four modes of metabolism that support life. It can grow with or without oxygen, and uses light, inorganic compounds, or organic compounds, for energy (Kernan et al., 2015). The amount of H_2S conversion to elemental Sulphur or sulphate depends on the amount of light the bacteria receive (Pokorna and Zabranska, 2015). EM has a history of being used for different applications, including wastewater treatment, agriculture, livestock, gardening and landscaping, composting, bioremediation, cleaning septic tanks, algal control and household uses (Zakaria et al., 2010). Mwegoha (2012), reported the highest methane composition of 69% was observed from the study conducted on anaerobic composting of pyrethrum waste with effective microorganisms at an optimal mixing ratio of the substrate to EM of 1:250 V/V at a dilution ratio of 1:4 m/m. According to the study conducted by Selele (2009), EM has been effective in the enhancement of biogas production and composition using food remains whereby the biogas production rate increase to about 32% as well as the percentage of methane in biogas composition increased to about 82%. However, the use of EM in the purification of biogas has not been investigated although EM contains photosynthetic bacteria (*R. palustris*) which are capable of oxidizing H_2S by using carbon from CO_2 as a source of energy to purify biogas. Therefore, this study aims at investigating the use of effective microorganisms to enhance cost effective biogas purification at household level.

MATERIALS AND METHODS

Experimental set up for purification of biogas

Biogas to be purified was produced from an existing 1 m^3 floating

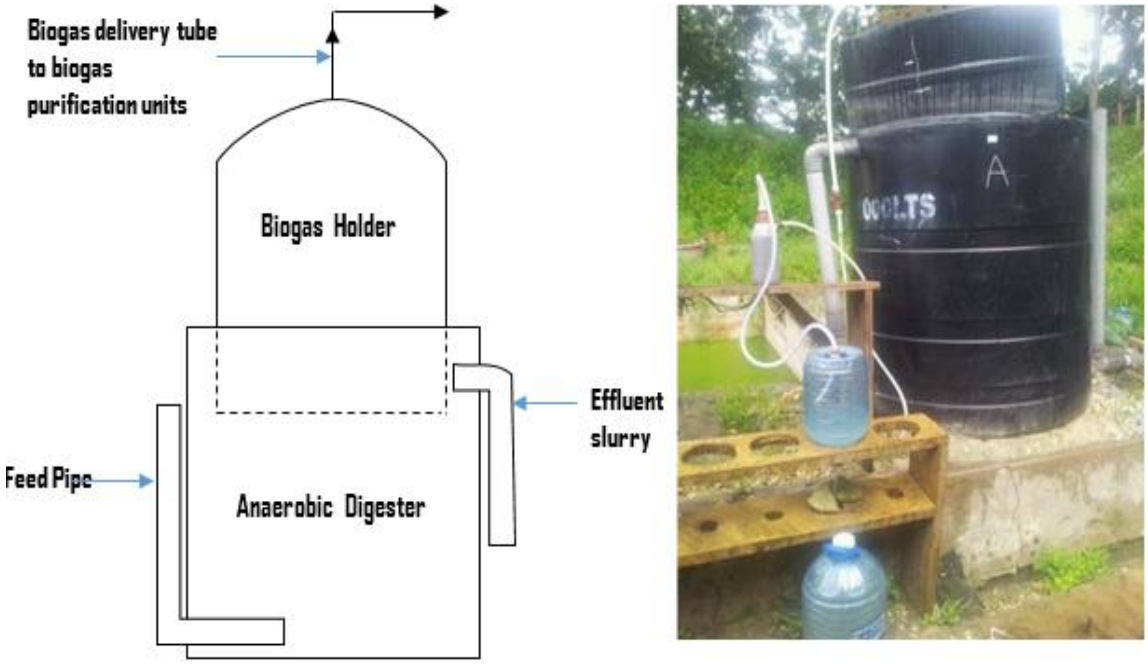

Figure 1. Experimental setup for biogas production and purification.

dome biogas plant (Figure 1) fed with kitchen waste from the Cafeteria at Ardhi University, Dar es Salaam, Tanzania. It involved the use of effective microorganisms (EM) as the media for biogas purification. Two different runs of biogas purification units (1 L dormant and 4 L effective microorganisms) were used. Biogas analysis was achieved by using a biogas analyser (GIR5500) manufactured by Hitech Instruments. EM used for this experiment was obtained from Ardhi University, Laboratory of Environmental Engineering, but initially, it was imported from EM Technology Limited (P. O. Box 1365-60100 Embu, and Nairobi, Kenya). The activation of EM solution was made by mixing 1 L of dormant EM, 1 L of molasses and diluted into 18 L de-chlorinated water at a ratio of 1:1:18 (v/v/v). The mixture had a pH of 4.09 and it was left to ferment for 7 days in a 20 L bucket at an ambient temperature between 28 and 31°C where at the end the pH dropped to 2.76.

Purification of biogas involved two units each containing EM solution as a media for purification. One of these batch units contained 1 L of dormant EM and the other one had 4 L of activated EM. The first unit used a 1 L batch of dormant EM because it contained a large number of microorganisms that react with both hydrogen sulphide and carbon dioxide but not with methane. In this case, 1.5-L container with dimensions 5 cm × 10 cm × 30 cm was used. The second unit was of a 4 L batch of activated EM in a 5-L container with dimensions 10 cm x 16.7 cm x 30 cm. During purification, biogas was tapped from the gasholder of a floating drum anaerobic digester to the purification units where it was allowed to bubble through EM batch solutions using a 0.635 cm diameter hose pipe in both units by monitoring the time taken by a specific amount of biogas to pass through the purification media

(

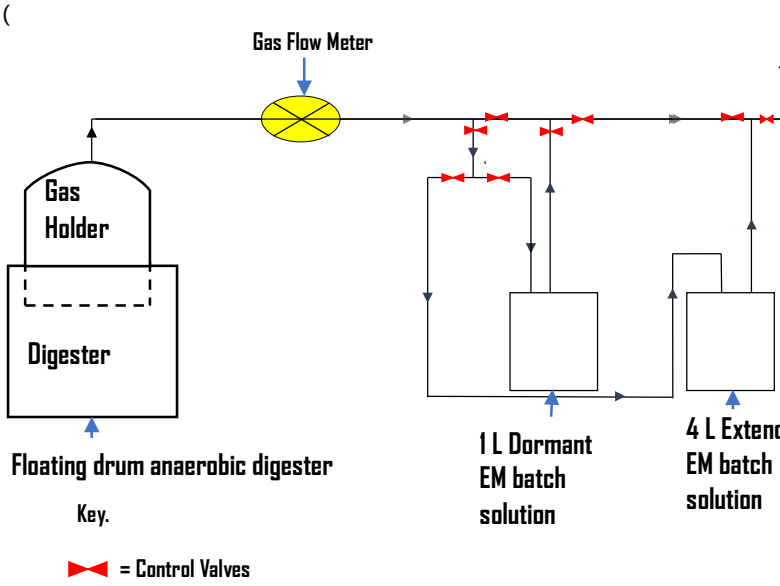

Figure).

During the purification of biogas, there was a variation in the time and the amount of biogas passed through because of the pressure difference from the biogas plant. The amount of pressure from the biogas plant was determined by the amount of biogas present and the mass of the loads added on top of the biogas holder. As the biogas passes to the gas analyzer, the moisture was trapped in the

moisture trap unit as shown in

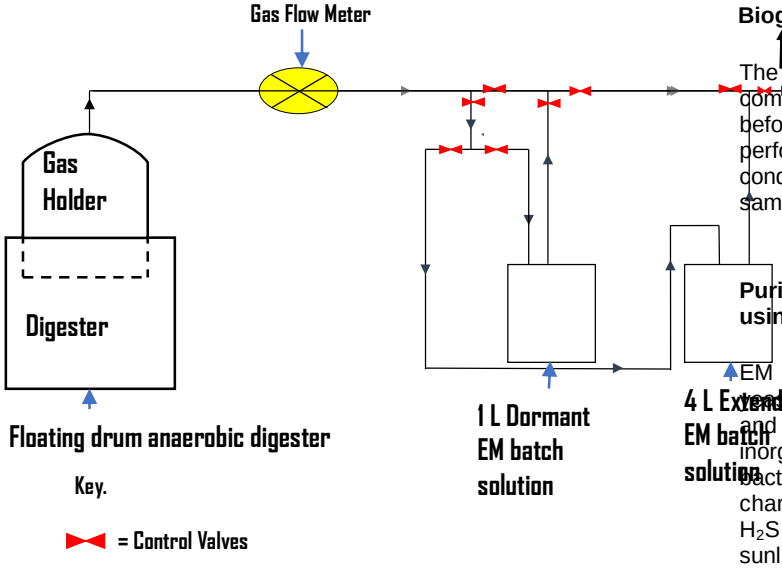

Figure . This experiment was conducted for 37 days until when the media was exhausted; that is, it lost the ability to purify the biogas. At this stage of media exhaustion, the concentration of gases in the composition of biogas in terms of percentage (CH_4 and CO_2) and ppm (H_2S) for the purified gas was almost the same as the raw gas, that is, 62.2% CH_4, 37.4% CO_2 and 1359.3 ppm H_2S.

Biogas composition analysis using Gas analyser GIR 5500

The GIR5500 (Gas analyser) was used to measure the percentage composition of biogas in terms of % CH_4, % CO_2 and H_2S ppm before and after purification as shown in Table . The analysis was performed by discrete sensors connected in series. Basic sample conditioning was supplied as standard along with a sampling pump, sample flow indication and a low sample flow alarm.

Purification mechanism for the removal of biogas impurities using EM

EM is made up of photosynthetic bacteria, lactic acid bacteria, yeast, actinomycetes and fermenting fungi which consume CO_2 and generates chemical energy from the oxidation of reduced inorganic compounds such as H_2S (Higa, 1998). Photosynthetic bacteria play the leading role in the activity of EM. The unique characteristic of the phototrophic bacteria is their ability to oxidize H_2S to elemental Sulphur under anaerobic conditions using sunlight and CO_2 as sources of energy (Equation 1). Hence, when biogas is passed through EM batch reactor, mainly CO_2 is consumed by phototrophic bacteria as a source of energy in the presence of sunlight to produce formaldehyde, water and Sulphur. Carbon dioxide is assimilated into cell material.

$$CO_2 + 2H_2S \xrightarrow{+Sunlight+EM+Photosynthetic\ bacteria} CH_2O + H_2O + 2S \quad (1)$$

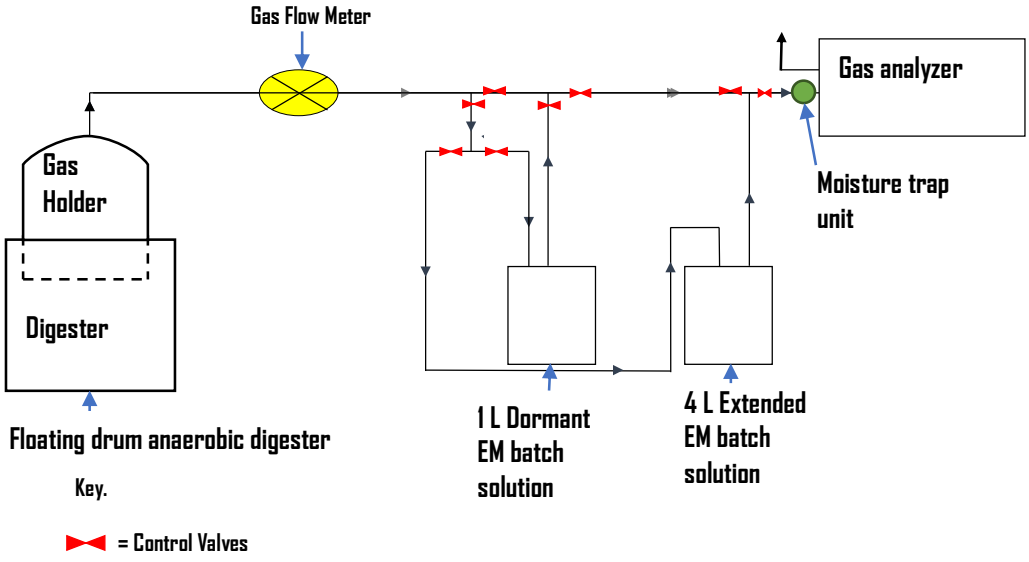

Figure 2. Schematic diagram of combined biogas purification units using both 1 L Dormant EM and 4 L Extended EM batch solutions.

Table 1. Gas analyzer specifications.

Gas sensor options	Range	Resolution
Methane	0 - 100%	0.1%
Carbon dioxide	0 - 100%	0.1%
Oxygen	0 - 25%	0.1%

Hydrogen Sulphide	0 - 5000 ppm	1 ppm

Lactic acid bacteria act on sugars and other carbohydrates produced by photosynthetic bacteria and yeast to produce lactic acids which result in the lowering pH below 2. Lowering pH might create an un-conducive environment for the photosynthetic bacteria. A study conducted by Sakurai (1997) reported that lactobacillus increased acidity of the media which was not conducive to photosynthetic bacteria and streptomyces during the co-existence of photosynthetic bacteria, streptomyces and lactic acid bacteria in solutions of effective microorganisms. However, the biochemical processes shown above (Equation 1) leads to the production of formaldehyde (CH_2O), batch EM solutions CO_2 and H_2S the purification process over time leads to the accumulation of formaldehyde which is toxic to photosynthetic bacteria. As the concentration of photosynthetic bacteria gets reduced over time due to the toxicity of formaldehyde, the removal rate of CO_2 and H_2S gets reduced with time.

Biogas utilization on cooking test

Both raw and purified biogases were utilized to test their efficiency in terms of cooking time. 100 L of biogas was burnt in a gas stove and the time taken to be utilized for cooking was monitored.

Data analysis

Data analysis was done using Microsoft Excel and the instant program. Statistical analysis was used to compare the performances of each biogas purification unit using different batch volumes of EM solution. The t-test was used to determine the differences in percentage removal of CO_2 from each of the biogas purification units.

RESULTS AND DISCUSSION

Biogas purification using 1 L Dormant EM and 4 L Activated EM batch media to remove CO_2

Performance of 1 L Dormant EM batch media in purifying biogas

Biogas purification using 1 L dormant EM batch media has shown that the percentage composition of CO_2 in the purified biogas kept on decreasing from 36.8 to 20.8%, whereas the percentage composition of CH_4 content kept on increasing from 62.9 to 79%. Removal of CO_2 and the percentage increase in the CH_4 content started from the beginning of the experiment from 36.8 to 20.8% for CO_2, and 62.9 to 79% for CH_4. As time went on, both respective percentages for removal of CO_2 and methane upgrade in the biogas kept on increasing. The reason for

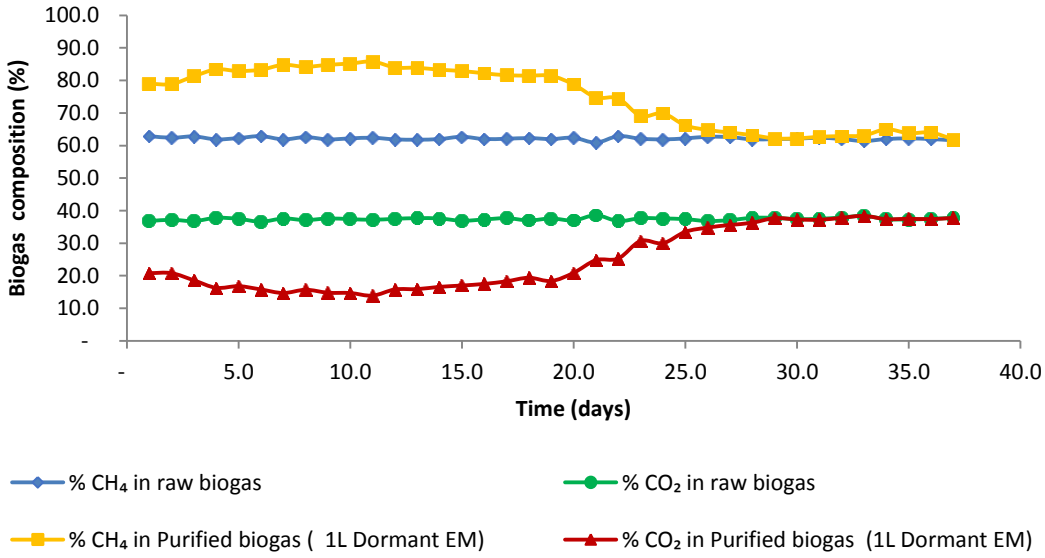

Figure 3. Daily gases in percentages composing biogas before and after purification using 1 L batch of dormant EM.

that might be due to the fact that from day 1 to day 3, the microorganisms were acclimatizing to the environmental conditions created by the introduction of biogas; however, as times went by, they got acclimatized and started acting on CO_2 as a source of energy resulting into more of them being reproduced. The percentage reduction of CO_2 in the purified biogas was a result of the mediation of the raw biogas by the photosynthetic bacteria (*R. palustris*) as shown in Equation 1. As reported by Hansen and Gemerden (1972), that *R. palustris* is capable of converting sulphide into sulphate without intermediate accumulation of elemental Sulphur. Therefore, during

purification of biogas using effective microorganisms, hydrogen sulphide may have been converted into elemental Sulphur or sulphate depending on the mode of metabolisms in which *Rps. palustris* is switched on.

The *R. palustris* bacteria in the purification media (that is, dormant and activated EM) were capable of oxidizing hydrogen sulphide present in the biogas to elemental Sulphur by using only light and CO_2 which is also present in the raw biogas for their growth. The process went on well until day 18 when there was a drop in the percentage increase of CH_4 although on day 19 there was a slight percentage increase in CH_4. Then from day 20 to day 26, there was a significant drop in percentage CO_2 removal whereby the concentration of CO_2 in purified gas was nearly equal to the concentration of CO_2 in raw biogas that ranged between 36.8 to 34.8%. Thereafter, there was no further removal of CO_2 as shown in Figure . This shows that at this point most of the phototrophic microorganisms might have been dead due to accumulation in the batch solution of formaldehyde over time that is toxic to photosynthetic bacteria. This could also be the main cause for the observations made on day 25 of the experimental run when the removal efficiency was almost zero. At this stage, the media was exhausted due to the absence of phototrophic bacteria to mediate the purification process. The overall average composition of biogas after purification was 74.8% CH_4 and 25.0% CO_2. By considering the time before exhaustion, the average biogas composition was 83.0% CH_4 and 16.7% CO_2 which was observed during the first 17 days before the media (EM) started to lose its efficiency in biogas purification (Figure).

Biogas purification process using 4 L activated EM

Biogas purification process using 4 L of activated EM showed that EM could remove CO_2 from the beginning of the experiment and it kept on increasing as time went by. This could be due to the reasons already mentioned above. The results have shown that percentage CO_2 composition in purified biogas was decreasing from 37.4% to an average percentage CO_2 by composition of 14.8% before exhaustion and 19.5% after exhaustion while percentage average methane composition was increasing from 62.9 to 85.6% before exhaustion and 80.2% after exhaustion before it began to lose its purification ability on day 27. From day 27, the removal of CO_2 started to decrease until it reached a point whereby the percentage CO_2 composition in raw biogas was equal to the percentage CO_2 content in purified biogas on day35 as shown in **Error! Reference source not found.**. At this stage, the media for

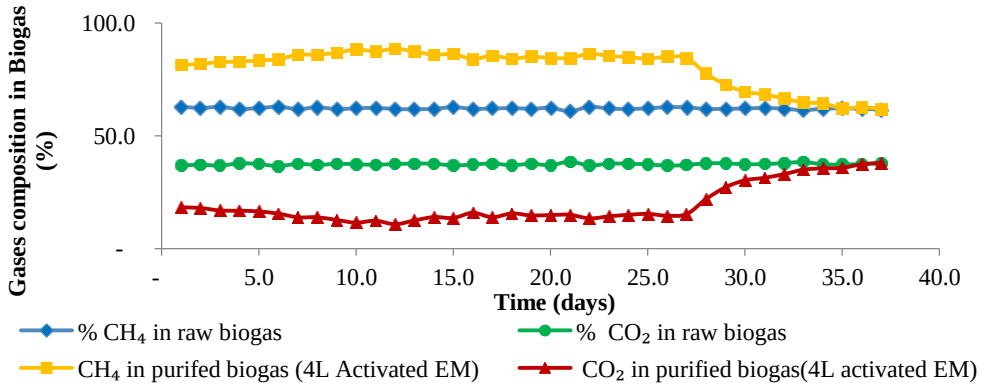

Figure 4. Daily gases in percentages composing biogas before and after purification.

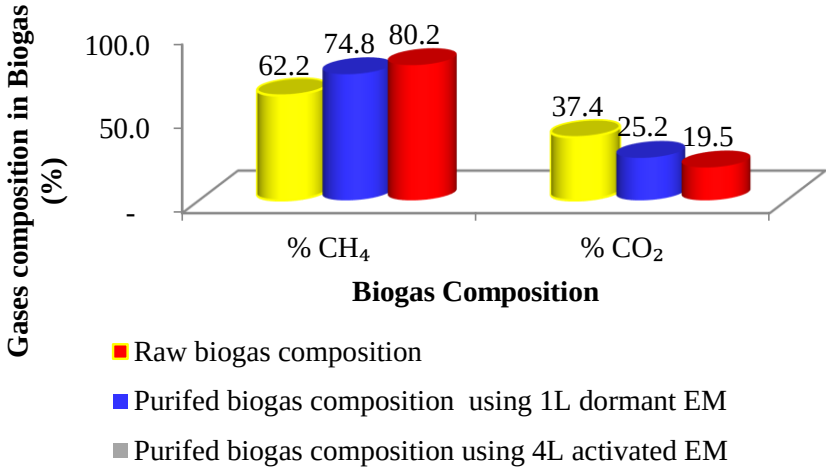

Figure 5. Overall average percentages of CH_4 and CO_2 gases composition in the biogas before and after purification.

purification (EM) had reached its exhaustion stage and the predominant reason for the exhaustion is due to the accumulation of formaldehyde over time in the batch solution that is toxic to photosynthetic bacteria over time.

Comparison of the biogas composition between the two purification units after purification

The results have shown that the overall average percentage CO_2 content in the purified biogas using 4 L activated EM is lower (about 19.8%) than that purified by using 1 L dormant EM (about 25.1%) (Figure), with the average removal efficiency of 47.9 and 34.2% in 4L activated EM and 1 L dormant EM respectively. The average percentage CH_4 content by the composition of purified biogas that went through the 4 L of activated EM was higher (about 80.3%) than the CH_4 gas content in the biogas purified using the 1 L dormant EM (74.8%) (Figure).

This might be due to the fact that the average time taken by the biogas to bubble through 4 L EM to the biogas analyser was longer (about 26.4 min) than that used by 1 L dormant EM (about 17.4 min) (**Error! Reference source not found.**).

The average amount of biogas passed through the biogas analyser for raw biogas was about 60 L/day at an average flow rate of 5.5 L/min, and 108 L/day at an average flow rate of 4.1 L/min in a 4L activated EM batch media and about 84 L/day with an average flow rate of 4.7 L/min in 1 L activated EM (

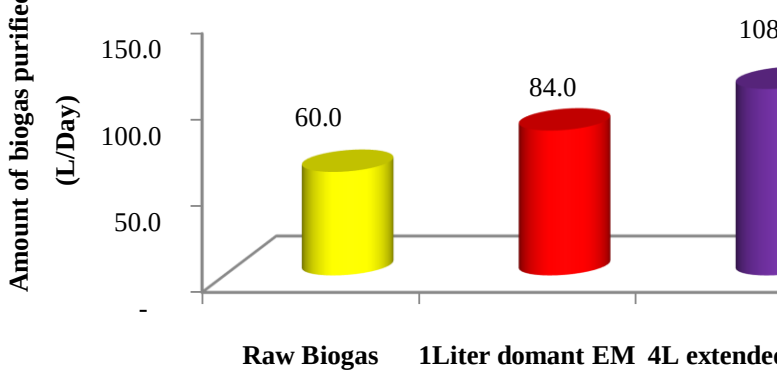

Figure). Therefore, a longer time provided more retention time for biogas to stay in the system, that is, biogas had more time to get in contact with the phototrophic microorganisms when the

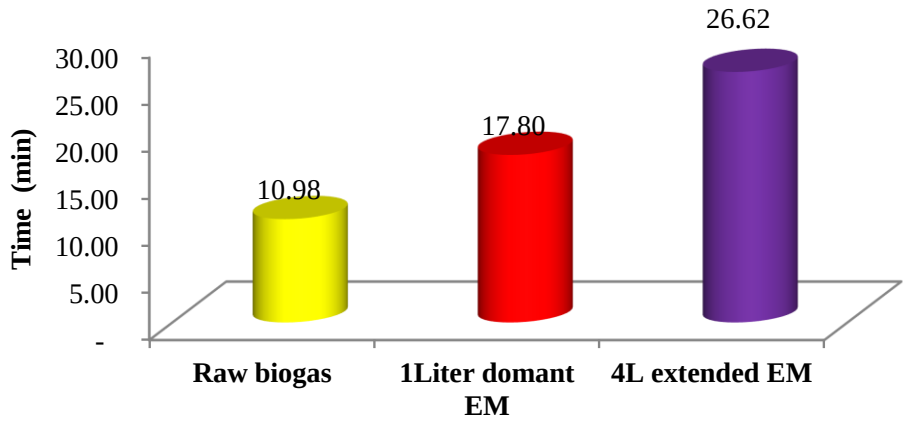

Figure 6. Average time is taken for biogas to bubble through EM.

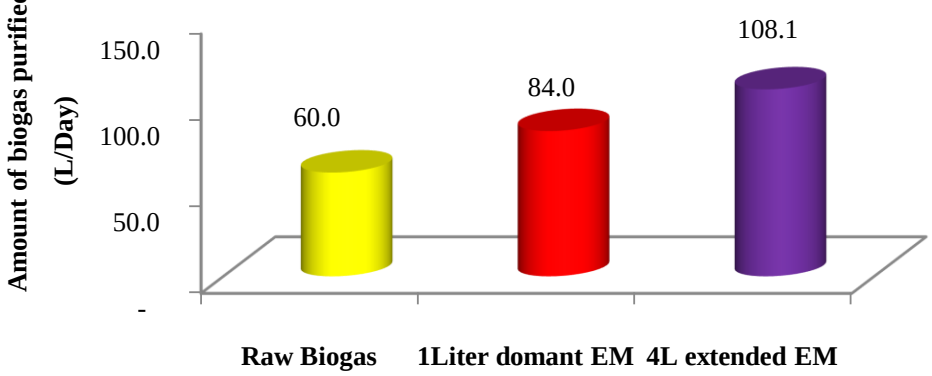

Figure 7. Average amount of biogas bubbled in a purification unit.

biogas was bubbling through the EM batch solution. The other reason could be that there were more phototrophic bacteria in the 4 L activated EM batch solution than in the 1 L dormant EM batch solution. The results from this paper have shown lower performance in terms of CO_2 removal as compared to the results reported by Ramaraj and Unpaprom (2016), that purification of biogas using microalgae resulted in purified biogas which contains about 96% CH_4 and 4% CO_2. The reason for this could be due to the use of different materials and methods.

Statistical analysis on the biogas purification performance from all units

The results have shown that the 4 L activated EM has shown high performance in biogas purification in terms of CO_2 removal efficiency as compared to 1 L dormant EM. A paired T-test statistical analysis shows the p-value between the two paired t-test was less than 0.0001 which is less than 0.05. Therefore, the difference between the two experimental runs was considered to be extremely significant.

Biogas purification processing batch media exhaustion rate

Determination of the purification processing batch media exhaustion rate is a function of the volume of biogas purified and the volume of the purification media through which the gas was passed. Therefore, the more the biogas was passed through the purification media the more the purification efficiencies got lowered

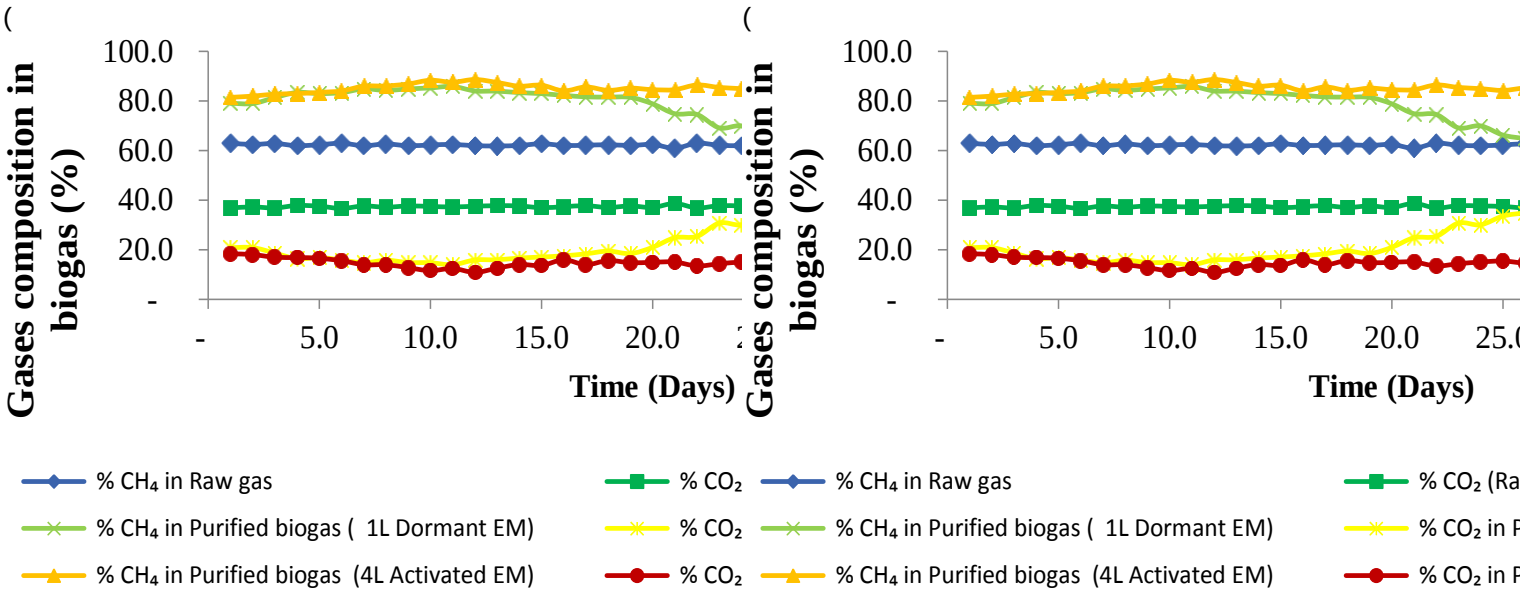

Figure). During the experimental run for a while, the biogas purification efficiency was observed to increase over time but later on, after some day's efficiency declined. By comparing the two purification processing batch media

Figure), the purification efficiency of the 1 L dormant EM batch media started to drop after 17 days at the

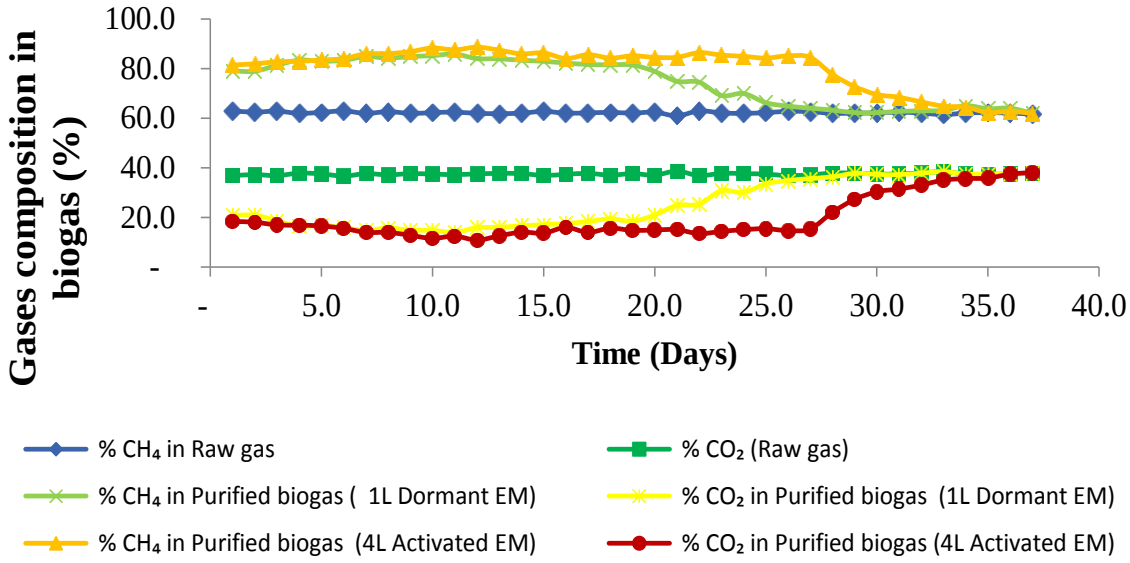

Figure 8. Biogas composing gases before and after purification.

average removal efficiency of 55.2% whereas the 4 L dormant EM batch media started to drop after 27 days at the removal efficiency of 59.95%. Although both purification batch media reached a point where their respective removal efficiencies started to drop, the results have shown that the 4 L activated EM batch media took a long time (about 27 days) to lose its ability to purify than the 1 L dormant EM batch media which took only 17 days. Considering the amount of biogas purified during those days, 1 L dormant EM batch media could purify

about 1409.5 L of biogas at a removal efficiency of 44.6% before exhaustion while the 4 L activated EM batch media could purify about 3002.5 L of biogas at a removal efficiency of 60% before exhaustion. Therefore, the longer the retention time the more the gas allowed to pass for purification.

Biogas purification using 1 L Dormant EM and 4 L Activated EM batch media for Hydrogen Sulphide Removal

The average concentration of hydrogen sulphide in raw biogas was 1353 ppm. During purification, the concentration of hydrogen sulphide in purified biogas was lowered to 539 ppm when purified in a purification unit of 1 L dormant EM batch solution and 313 ppm in 4 L activated EM batch solution at the beginning of the experiment. The results have revealed that the removal of H_2S in the purification units kept on decreasing gradually from day 1 to day 23 (1 L Dormant EM) and from day 1 to day 31 (4 L Activated EM); as a result, the daily concentration of hydrogen sulphide in purified biogas kept on increasing gradually before it was equal to the concentration of raw biogas (

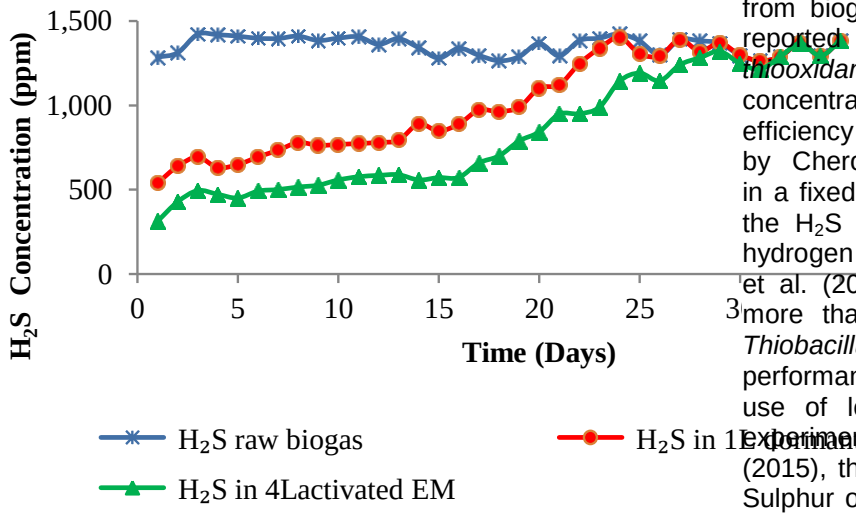

Figure).

Results have shown that more hydrogen sulphide was removed in the 4 L EM batch solution purification units with an average concentration of 786.1 ppm (

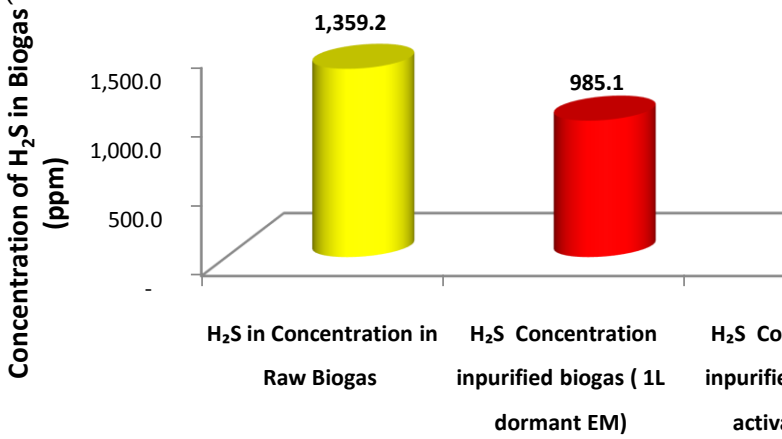

Figure) at an overall removal efficiency of 43.0% after exhaustion but the removal efficiency before exhaustion was 59.7%. In the purification unit of 1 L dormant EM batch solution, the average concentration of hydrogen sulphide was about 985.1 ppm at an overall removal efficiency of only 28.8% after exhaustion but the removal efficiency before exhaustion was 42.4%. The results from this study revealed that the removal efficiency of H_2S from biogas is low (59.7%) as compared to the study reported by Zhao et al. *(*2010), that *Acidithiobacillus thiooxidans*AZ11 are capable of reducing H_2S concentrations of 2200 ppm at a very high removal efficiency ranging from 94 to 99.9%. It was also reported by Cherosky (2012) that *Thiobacillus* bacteria operated in a fixed-film reactor were capable of removing 74% of the H_2S in biogas containing as high as 24000 ppm hydrogen sulphide concentration. At the same time, Choo et al. (2013) observed high H_2S removal efficiency of more than 98% in biogas purification using isolated *Thiobacillus thioparus* from swine wastewater. The lower performance observed in this study was attributed to the use of low light intensity (sunlight only) during the experiment as it was stated by Pokorna and Zabranska (2015), that the amount of H_2S conversion to elemental Sulphur or sulphate depends on the amount of light the bacteria receive. Hence, sufficient light is necessary for optimal performance. When only sunlight was used, the sulphide removal rate was four times less than when the light bulb was used (Zhao et al.,

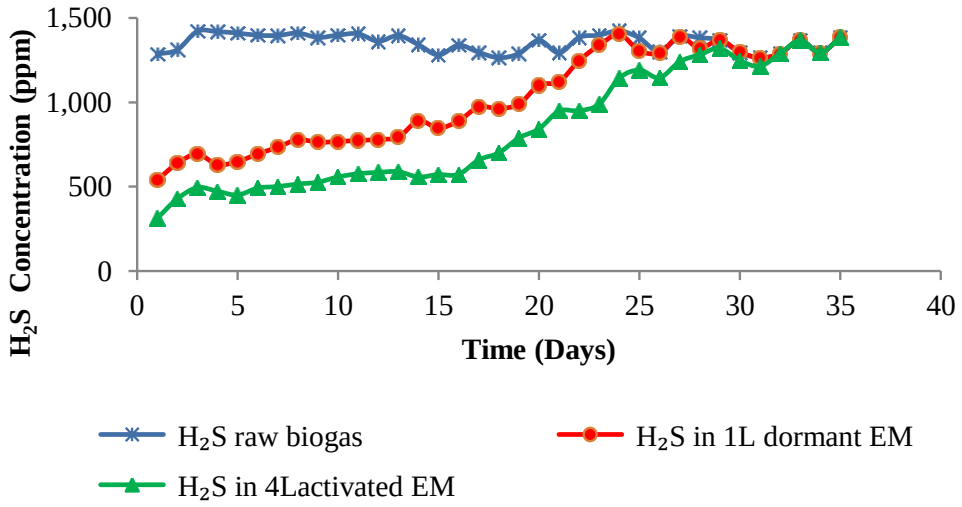

Figure 9. H_2S composition in the biogas before and after purification.

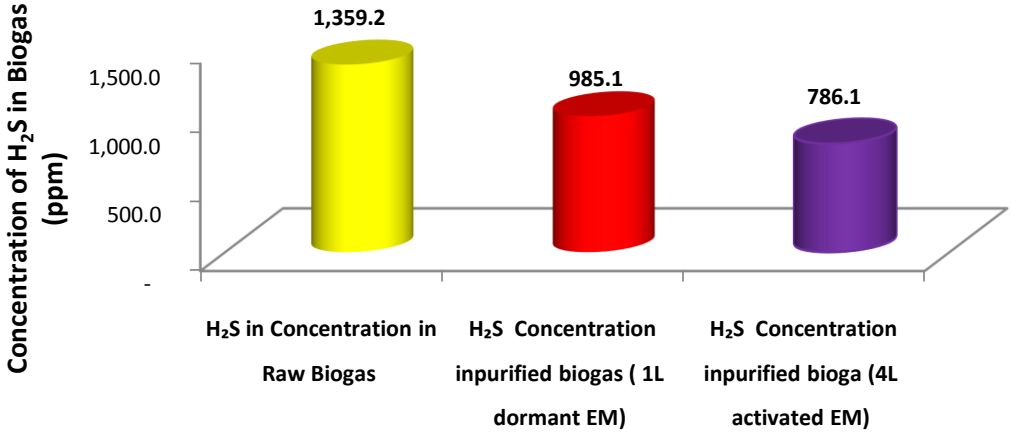

Figure 10. Average H_2S composition in the biogas before and after purification.

2010).

(

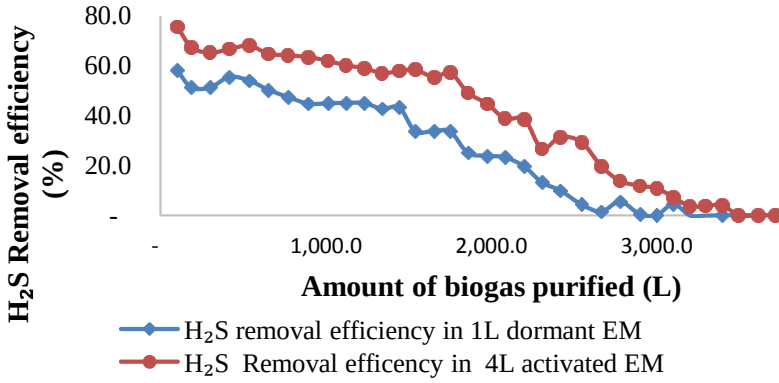

Figure). Thus, 4 L activated EM has shown high removal efficiency of H_2S than the 1 L dormant EM for the same amount of biogas purified. However, in all the cases discussed below, the removal efficiency of biogas

Relationship between the amounts of biogas purified using EM and the extent of biogas purification achieved

The amount and nature of EM as a purification media is the one that determines the rate of removal of H_2S present in the same amount of biogas being purified. For example, during the experimental run, it was observed that 1000 L of biogas was purified using a 4 L activated EM at an average H_2S removal efficiency of 61.9% whereas a 1 L dormant EM could purify the same amount of biogas but at an average H_2S removal efficiency of 45%. Therefore, the overall biogas-H_2S removal efficiency using the 4 L activated EM was about 49% while that of 1 L dormant EM was only about 35%

contents namely CO_2 and H_2S are governed by Equation 1. The biochemical processes shown above (Equation 1) leads to the production of formaldehyde (CH_2O). The CO_2 and H_2S removal rates are declining when using EM batch media since the accumulation of formaldehyde over time is toxic to photosynthetic bacteria over time.

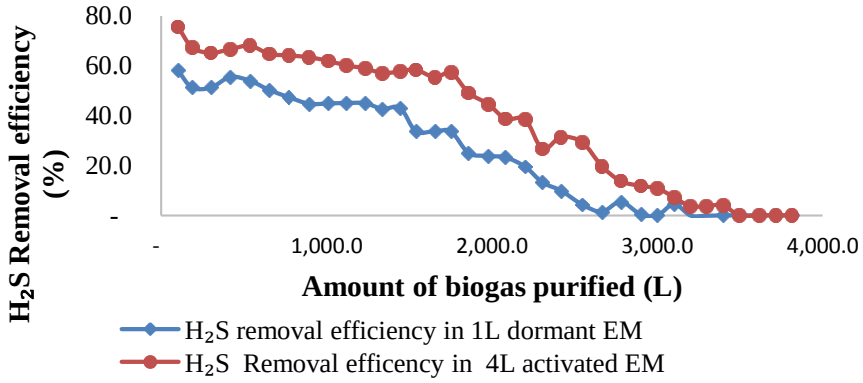

Figure 11. H_2S removal efficiencies with the amount of biogas purified.

purification using a 4 L activated EM batch media could remove about 60% of CO_2 content at a cumulative biogas amount of about 3000 L whereas the corresponding H_2S removal efficiency by the same 4 L activated EM batch media was less than 10% (

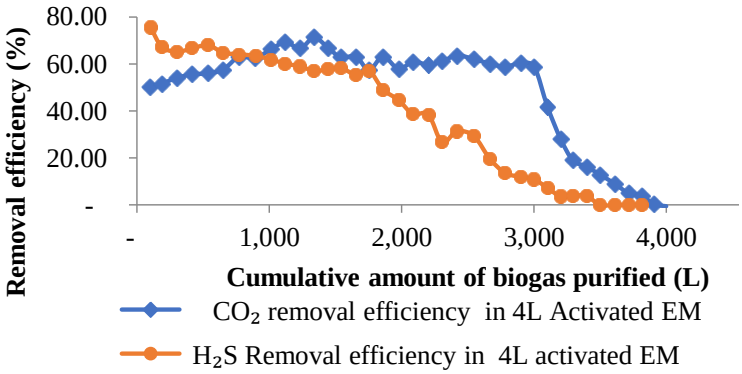

Figure). These results show that activated EM has a high affinity for CO_2 removal compared to H_2S. This observation is attributed to the presence of a lot of photosynthetic bacteria that are capable of reducing CO_2 to cell material with concomitant stoichiometric oxidation of reduced Sulphur compounds under anaerobic conditions in the presence of light as shown by Equation 1. Figure 12 emphasizes the fact that CO_2 and H_2S removal rates are in declining rate when using EM batch media since the accumulation of formaldehyde over time is toxic to photosynthetic bacteria.

Comparison of CO_2 and H_2S removal with respect to the amount of biogas purified

During the experimental run, it was observed that biogas

The experimental run also observed that 1 L dormant EM batch media could remove both CO_2 and hydrogen sulphide, but this could be achieved when the cumulative amount of biogas was low.

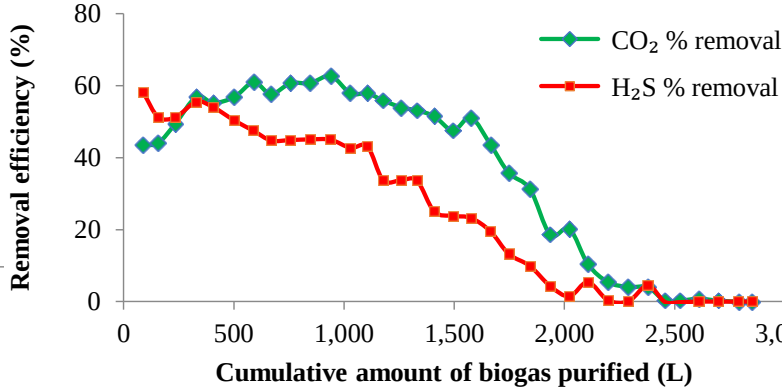

Figure show that 1 L dormant EM batch media could remove neither CO_2 nor Hydrogen Sulphide at a cumulative biogas amount of 3000 L. This suggests that 1 L dormant EM batch media was suitable for purification of biogas not more than 2031 L at a removal efficiency of 51.1%. The reason for this observation is that CO_2 and H_2S removal rates are declining rate when using EM batch media since the accumulation of formaldehyde over time is toxic to photosynthetic bacteria over time. However, comparing the 4 L activated EM batch media and the 1 L dormant EM batch media, the former has a higher removal capacity for both CO_2 and H_2S for the same cumulative amount of biogas purified.

Comparison of biogas utilization for cooking between raw and purified biogas

The amount of biogas produced from the biogas plants was burned using a biogas stove. The time required toburn 100 L of biogas was determined by testing both purified and raw biogas. Purified biogas recorded an average burning time of about 34.5 min for 100 L of biogas. This might be due to a high composition of methane of about 80.2% compared to raw biogas which took an average of 21.2 min to burn the same volume of biogas. A burning test was conducted to see how much cooking can be done by the purified gas. From this study, the average biogas production was 337.1 L/day. Based on the study conducted by Voegeli et al. (2009), it was reported that Tanzania average cooking time was estimated to be 2.15 h/day. Therefore, purified biogas could take about 1.82 h which is about 85% of the daily cooking hours, while raw biogas could take about 1.191 h equivalent to 55.4% of the total daily cooking hours.

Design of the household biogas purification unit using effective microorganisms

Results of this research have shown that 4 L activated EM can purify about 3000 L of biogas at an average CO_2 removal efficiency of 60.8%. Also, considering the amount of biogas to be generated from 2 kg of kitchen waste at a household level was 337.1 L/day, the design of the household biogas purification unit is demonstrated by assuming that all the amount of biogas generated must be purified and utilized.

Production of activated EM

Activated EM can be generated from the extension of 1 L dormant EM to produce 20 L of activated EM.

Number of 4 L activated purification units
=20 L of activated EM / 4 L activated EM
= 20/4

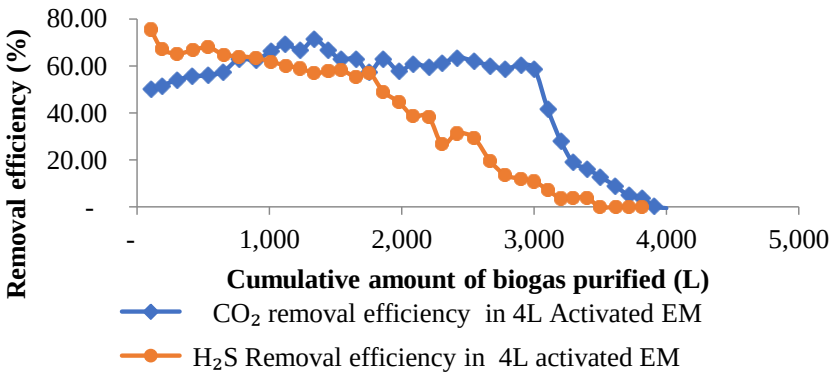

Figure 12. CO_2 and H_2S removal with respect to the cumulative amount of biogas purified using a 4 L Activated EM batch media.

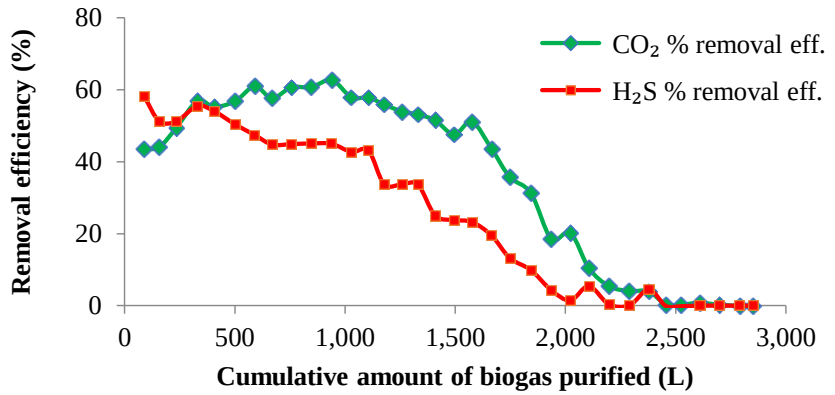

Figure 13. CO_2 and H_2S removal with respect to the amount of biogas purified in 1 L dormant EM batch media.

= 5 units

Amount of biogas to be purified by 20 L of activated EM

4 L of activated EM could purify 3000 L, taken as a design criterion.

Since 20 L of activated EM can produce 5 units of purification (Each unit is of 4 L),

= Amount of biogas purified in a 4 L × number of purification units

= 3000 × 5

= 15,000 L of biogas.

Number of days that 20 L of activated EM can be used at the household level

= Total amount of biogas to be treated/Average daily production of biogas

= 15,000/337.1

= 44.5 days

Cost associated with purchasing EM to be applied in the purification system

Cost of activated EM

1 L of Dormant EM	= 12,000 Tshs
1 L of morasses	= 1,500 Tshs
Total	= 13,500 Tshs

Monthly cost for EM

=Total EM cost × 30 days of a month/Number of days activated EM could be used

= 13500 × 30/44.5

= 9,101.1 Tshs

Therefore, the monthly cost of using EM purified biogas is about Tshs 9101.1.

Cost estimation of the biogas purification unit

The total initial cost of the purification units was estimated to be Tshs. 96,500. This cost covers the initial cost for purchasing dormant EM and Molasses which is about Tshs 13,500 and the cost for fabricating a purification unit which is about Tshs. 83,000.

Conclusion

It can therefore be concluded that both dormant and activated EM can be used for biogas purification to remove both CO_2 and H_2S at low cost for the household application. The purification process takes place through a biochemical reaction involving photosynthetic bacteria (*R. palustris*) in the presence of light, with a high affinity for CO removal compared to H_2S. This process results in the formation of formaldehyde (CH_2O) as one of the products, the accumulation of which lowers the purification efficiencies due to its toxicity to photosynthetic bacteria. The 4 L activated EM batch solution showed high removal efficiency of about 60 and 48% for CO_2 and H_2S respectively. Purified biogas with 80.3% methane content could take about 85% of the daily cooking hours, while raw biogas with a methane content of 62.2% could take only 55.4% of the total daily cooking hours. Therefore, the use of EM for biogas purification can be achieved at a low cost as a biogas purification unit using EM at the household level. The installation cost at the household level is about Tshs 83,000 and a monthly EM cost of about Tshs 9,101.1. With this biogas purification system application, the biogas user is enabled to use biogas with fewer impurities (CO_2 and H_2S) and high calorific value.

CONFLICT OF INTERESTS

The authors have not declared any conflict of interests.

ACKNOWLEDGEMENT

The authors appreciate the Tanzanian Ministry of Higher Education, Science and Technology through the World Bank Project for the financial support for development of this research.

REFERENCES

Adnan AI, Ong MY, Show PL, Nomanbhay S, Chew KW (2019). Technologies for biogas upgrading to biomethane. A review, Bioengineering 6(4):1-23.

Agriculture N, Lokare C (2007) Effective Microorganisms : Myth or reality ?' 14(2):315-319.

Awe OW, Zhao Y, Nzihou A, Minh DP, Lyczko N (2017). A Review of Biogas Utilisation, Purification and Upgrading Technologies', Waste and Biomass Valorization. Springer Netherlands 8(2):267-283.

Cherosky P (2012). Anaerobic Digestion of Yard Waste and Biogas Purification by Removal of Hydrogen Sulfide.Doctoral dissertation, The Ohio State University.

Choo HS, Lau LC, Mohamed AR, Lee KT (2013). Hydrogen Sulfide Adsorption by Alkaline Impregnated Coconut Shell Activated Carbon

8(6):741-753.
De Hullu J, Maassen J, van Meel P, Shazad S, Vaessen J (2008). Biogas upgrading, comparing different techniques. Eindhoven, Netherlands.
Felix M. Gheewala SH (2011). A review of biomass energy dependency in Tanzania. Energy Procedia 9(2):338-343.
Hansen TV, Gemerden H (1972). Sulfide Utilization by Purple Nonsulfur Bacteria'. Archiv für Mikrobiologie 86(1):49-56.
Ilyas SZ (2006). A case study to bottle the biogas in cylinders as a source of power for rural industries development in Pakistan. World Applied Sciences Journal 1(2):127-130.
Kapdi SS, Vijay VK, Rajesh SK, Prasad R (2005). Biogas scrubbing, compression and storage: perspective and prospectus in the Indian context. Renewable energy 30(8):195-202.
Kernan C, Chow PP, Christianson RJ, Huang J (2015). Experimental and computational investigation of biofilm formation by *Rhodopseudomonas palustris* growth under two metabolic modes. PloS one 10(6):e0129354.
Kulkarni MB, Ghanegaonkar PM (2019). Hydrogen sulfide removal from biogas using chemical absorption technique in packed column reactors. Global Journal of Environmental Science and Management 5(2):155-66.
Mann G, Schlegel M, Schumann R, Sakalauskas A (2009). Biogas-conditioning with microalgae. Agronomy Research 7(1):33-38.
Mwegoha W (2012). Anaerobic composting of pyrethrum waste with and without effective microorganisms. African Journal of Environmental Science and Technology 6(8):293-299.
Nallamothu RB, Abyot T, Rao BVA (2013). Biogas purification, compression and bottling. Global Journal of Engineering Design and Technology 2(6):34-38.
Olle M, Williams IH (2003). Effective microorganisms and their influence on vegetable production–a review. The Journal of Horticultural Science and Biotechnology 88(4):380-386.
Pokorna D, Zabranska J (2015). Sulfur-oxidizing bacteria in environmental technology. Biotechnology Advances 33(6):1246-59.
Ramaraj R, Unpaprom Y (2016). Effect of temperature on the performance of biogas production from Duckweed. Chemistry Research Journal 1(1):58-66.
Sakurai M (1997). Co-existence of photosynthetic bacterias streptomyces and lactic acid bacteria in solutions of effective microorganisms. International Conference on Kyusei Nature Farming 5:379-385.
Selele M (2009). Enhancement of the Biogas Plant Performance by Addition of Effective Microorganisms. M.Sc. Dissertation. Environmental Technology and Management. Ardhi University.
Voegeli Y, Lohri C, Kassenga G, Baier U, Zurbrügg C (2009). Technical and biological performance of the Arti compact biogas plant for kitchen waste-case study from Tanzania. In12th International Waste Management and Landfill Symposium, S. Margherita di Pula, Cagliari, Italy pp. 5-9.
Weiland P (2006). Biomass digestion in agriculture: a successful pathway for the energy production and waste treatment in Germany. Engineering in life sciences 6(3):302-309.
Weiland P (2010). Biogas production: current state and perspectives. Applied microbiology and biotechnology 85(4):849-60.
Zăbavă BŞ, Voicu G, Ungureanu N, Dincă M, Paraschiv G, Munteanu M, Ferdes M (2019). Methods of Biogas Purification–A Review. Acta Technica Corviniensis-Bulletin of Engineering 12(1):65-68.

Zakaria Z, Gairola S, Shariff NM (2010). Effective microorganisms (EM) technology for water quality restoration and potential for sustainable water resources and management.
Zhao Q, Leonhardt E, MacConnell C, Frear C, Chen S (2010). Purification technologies for biogas generated by anaerobic digestion. Compressed Biomethane, CSANR, Ed, 24.

Vol. 15(11), pp. 470-492, November 2021
DOI: 10.5897/AJEST2021.3042
Article Number: E27A0EC68105
ISSN: 1996-0786

http://www.academicjournals.org/AJEST

ACADEMIC JOURNALS
expand your knowledge

African Journal of Environmental Science and Technology

Full Length Research Paper

Analysis of the deposit conditions of sedimentary series of fluvio-lacustrine and aeolian origin in the Djourab desert, in Northern Chad

MOUSSA Abderamane[1*], MAHAMAT NOUR Abdallah[1], ABDERAMANE Hamit[1], MACKAYE H. Taisso[1], LIKIUS Andossa[1], SCHUSTER Mathieu[2], DURINGER Philippe[2], GHIENNE Jean-François[2] and VIGNAUD Patrick[3]

[1]Laboratory of Hydro-Geosciences and Reservoirs, Department of Geology and Paleontology, University of N'Djamena, N'Djamena, Chad.
[2]Institut de Physique du Globe de Strasbourg, Université de Strasbourg, EOST, 1 rue Blessig, 67084 Strasbourg Cedex, France.
[3]Laboratoire Paléontologie Evolution Paléoécosystèmes Paléoprimatologie, Université de Poitiers, Poitiers, France.

Received 6 July, 2021; Accepted 20 October, 2021

The detailed sedimentary study of the deposit sequences of the ancient hominid sector (SahelanthropustchadensisalisToumaï) of Toros-Menalla, presented here addresses new aspects of the sedimentary geology of the Chad Basin through an original field study of Moi-sediments: Pliocene of the northern basin of CHAD. This is an original contribution that sheds light on new knowledge of sedimentary series of fluvio-lacustrine and aeolian origin in the Djourab desert which are essential for understanding the paleoenvironments and paleoclimates of Chad, the Sahara and Africa. Aged from the Terminal Miocene to the present day, these deposits which constitute the last stages of the filling of this basin are exclusively of the continental type and concern in the broad sense the following four major sedimentary systems: Fluvial, deltaic, lacustrine and aeolian. From a lithological point of view, these sedimentary series are very heterogeneous and include sandstones, sands, clays and diatomites.

Key words: Sedimentary deposit, Djourab, Toros-Menalla, Chad, fluvio-lacustrine, Aeolian.

INTRODUCTION

In Africa and more particularly in the Chad Basin, the dynamics of paleoenvironments during the Mio-Pliocene played a crucial role in the history of the emergence and evolution of ancient hominids (Novello et al., 2015, 2017; Barboni et al., 2019; Bobe et al., 2020). Despite the importance of the Neogene and Quaternary continental sedimentary series present at the scale of the Chad basin, they are still poorly known and very little studied, in particular due to the absence of a robust chronological framework and especially their particular conditions: outcrops (Duval et al., 2021). The interpretation of the facies of these sedimentary series has so far not been the

*Corresponding author. E-mail: mnourabdallah@gmail.com.

subject of specific studies, in particular because of poor outcrop conditions and the difficulty of correlating outcrops between them both in age and facies (Minisini et al., 2018).

A first contribution to the knowledge of the Cenozoic continental sedimentary formations of the Chad basin was made in the 1970s (Servant-Vildary, 1973) and was particularly interested in the paleoclimatic message of these series. Another more recent study (Schuster, 2002, Moussa et al., 2016) is more focused on the one hand on the paleoenvironments of the mio-pliocene series with ancient vertebrates and hominids of the Djourab erg and on the other hand on the major lacustrine episode of the Holocene embodied by Lake Mega-Chad (Bristow et al., 2018; Yu et al., 2020). But a real stratigraphic study and a sedimentological analysis of these sedimentary series are missing.

The objective of this work is to attempt to reconstruct the deposition environments of the Chad basin during the last 7 million years and to make the link between the arenitic facies of the edges of the lake and the clay facies in the center of the Chadian basin and to propose a typical stratigraphic sequence in this area.

Particular attention will be paid to the sedimentary environments of the hominid sites in the northern part of the basin. This part of the current desert Chadian basin has been systematically excavated since 1994 by the Franco-Tchadien Paleontological Mission (MPFT). Currently more than 400 fossiliferous sites have emerged, the oldest of which have yielded the oldest hominid known to date (Toumaï: Sahelanthropus tchadensis) (Brunet et al., 2002; Alemseged et al., 2020). The fossiliferous sites are dated jointly by biochronology (faunistic associations) and by radiometric dating (Be10) (Brunet et al., 1995, 1996, 1997; Vignaud et al., 2002; Lebatard et al., 2008; Branco Pavanotto et al., 2020) vary between 3.5 and 7.32 million years (Ma). All the fossil sites in northern Chad form a strip of outcrop, oriented east-west, covering an area of approximately 2,500km^2. It constitutes a key zone which has played a role of oscillating buffer according to hydroclimatic fluctuations (Armitage et al., 2015; Bristow and Armitage 2016; Sewell, 2019).

The facies described range from lake to wind, passing through deltaic or peri-lacustrine margino-littoral facies.

This study is an original contribution to the knowledge of sedimentary series in the Chad basin. It brings new data for the understanding of paleoenvironments and paleoclimates of Chad, the Sahara and Africa from the late Miocene to the present.

METHODOLOGY

Study site

In northern Chad in the eastern part of the Djourab desert, the Toros-Menalla (TM) fossiliferous sector is the most important of those discovered by the MPFT. More than 300 sites have been prospected and analyzed. They are in an area between 16° 09 ' and 16° 17'N and 17° 28' and 18° 07 'E (Figure 1). The sites extend over approximately 200 km from east to west and 30 km from north to south. The fossiliferous sites and deposits of the Djourab desert (1) are defined as non “empty” outcrops (having yielded at least one fossil) separated from each other by sand dunes (Mackaye, 2001). The five fossil-bearing sectors of Djourab are: the Toros-Menalla (TM) sector, the Kossom-Bougoudi sector (KB), the Kollé sector (KL), the sector of Koro-Toro (KT) and finally the fossiliferous sector of the cliff of Angamma (ANG) (Mackaye, 2001). The outcrops are in large, flattened areas that denote the Miocene series. They are generally flat or very slightly wavy; the most important rarely exceed a few meters. The TM outcrops are located to the south of the lowest part of the Chadian basin called "Low Country" and whose altitude oscillates around 160 m. This depression in the northern Chadian basin is directly opposite a very active wind ravine in the Erdis basin, wedged between the Tibesti and Ennedi mountains. Locally, deflation can reach 2 to 3 cm per year. The TM zone is close to the Bodélé depression, well known to be the most important zone of wind power exploitation of Saharan sands and which leads to the denudation of the summit part of the Miocene (Warren et al., 2005). In the middle of this gigantic sea of sands and aeolian dunes, the outcrops of TM appear in the form of erosion windows. The deposits and facies of fossil outcrops have been described by Schuster (2002) and Moussa et al. (2016) who described the recurrence of an elemental desert-lake model as mainly sandy-detrital, sandy-clayey, and more rarely clayey or diatomite series. In the specific TM sector, the bottom of the trenches is made up of a sandy series characterized by large, inclined litters 10 m wide or more. It is interpreted as a major wind episode (Schuster, 2002; Schuster et al., 2006, 2009; Novello et al., 2015, 2017).

Cuts and outcrops

Several fossiliferous sites of Toros-Menalla (TM) including TM 266 have been the subject of precise cross-section surveys (Figure 2). The sections (or stratigraphic logs) have been correlated with each other over about 30 km showing the good lateral continuity of the large deposits on the scale of the meter. They also show rapid lateral variations at the scale of decimetric sequences as is usually the case in continental systems. The outcrops studied and the sections surveyed are in an area of 250 km² limited around the fossiliferous site of TM 266.

The approach adopted here is simple since it relies almost essentially on field observations and the interpretation of the large morpho-sedimentary structures characteristic of deposit environments described for the first time by Servant-Vildary (1973), Vignaud et al. (2002), Schuster (2002), Schuster et al. (2003) and Moussa et al. (2016); Bristow et al. (2018). The absence or even the weak vegetation cover and the good preservation of morpho-sedimentary structures prove to be an asset for the observations (Bianchini et al., 2019). A lot of terrain images were used to interpret the different facies. The sections were drawn on a computer using software such as Adobe Illustrator and Photoshop. Photo-interpretation of facies was of great use in this study.

On the ground, the outcrops of a few meters or the escarpments as in the quarries are rare and the ground is too flat, we have to carry out very difficult cuts on the witness ridges or to dig trenches to make the observations of the various deposits (Bianchini et al., 2019; Branco Pavanotto et al., 2020). The area of the Toros-Menella (TM) sites is close to the Bodélé depression (120 m), well known to be the most important wind farm in the Saharan sands and which leads to the denudation of the top part of the Miocene

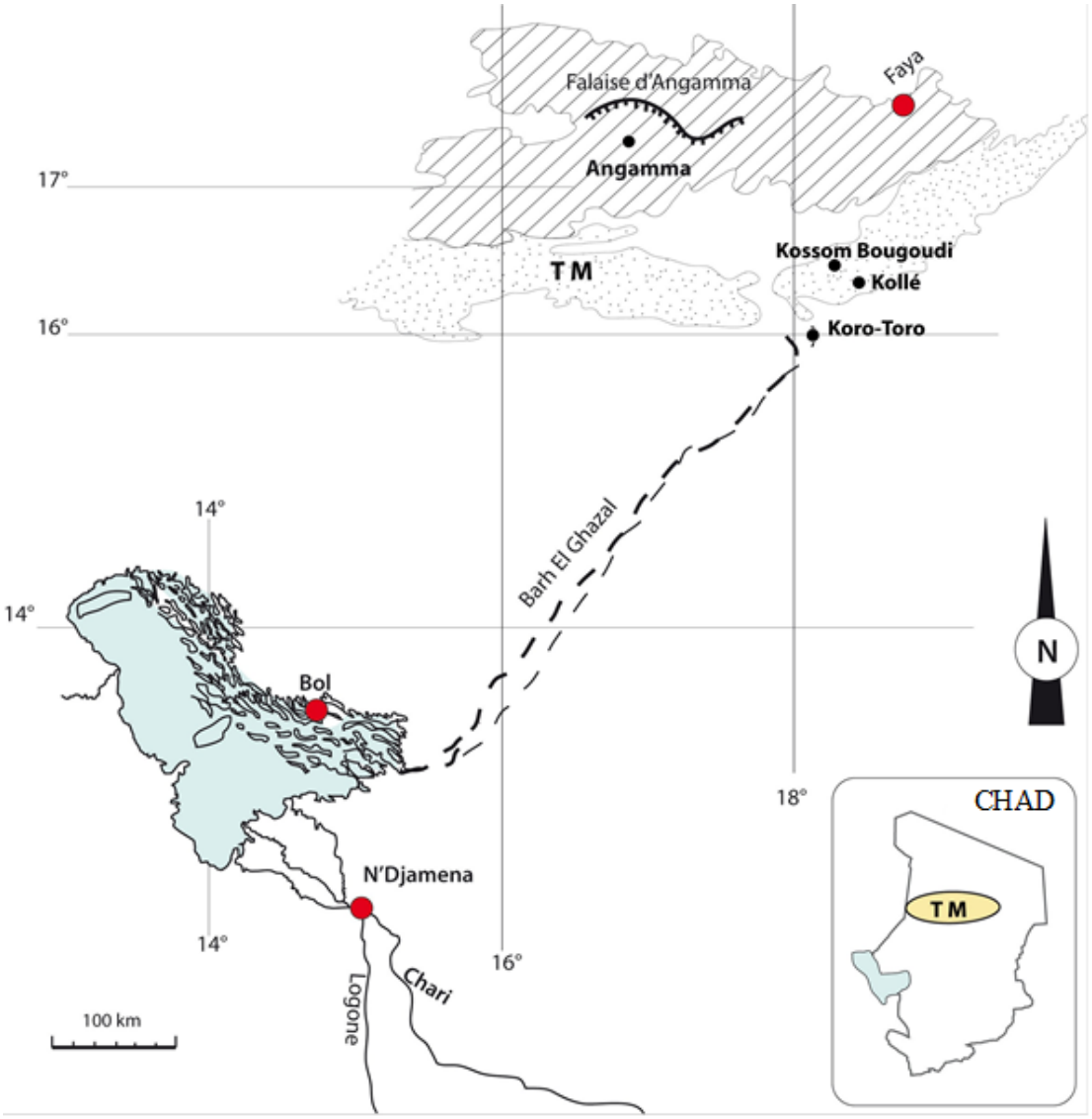

Figure 1. Schematic map of the location of the Djourab fossil sites prospected and discovered by the MPFT (Franco-Chadian Paleoanthropological Mission) since 1994. The Toros-Menalla (TM) sector alone contains more than 300 fossil sites, including the TM 266 fossil site. which delivered the remains of Toumaï (Sahelanthropustchadensis) in 2002 and a large fauna of vertebrates

(Warren et al., 2005; Bristow et al., 2018).

RESULTS AND DISCUSSION

Main lithological units

Three main lithological units follow one another from thebase to the top of the sections (Vignaud et al., 2002; Moussa et al., 2016): (1) clear sands with large bundles of oblique bedding at the base (Basal aeolian unit), (2) sandy sandstones and weakly indurated clayey sandstones in the middle part (Anthracotheriid unit), and (3) green clays and diatomites in the upper part (Lacustrine unit). The typical profile (Figure 3) is a synthetic profile reconstructed using several sections taken at different locations in the TM 266 sector.

Light sands with large oblique bedding beams

The basal part of the profile (at least 2 m thick) is composed of light fine-grained to very fine sand, rarely cemented except in the highest parts. The quartz grainsare well sorted, rounded and dull. This unit is

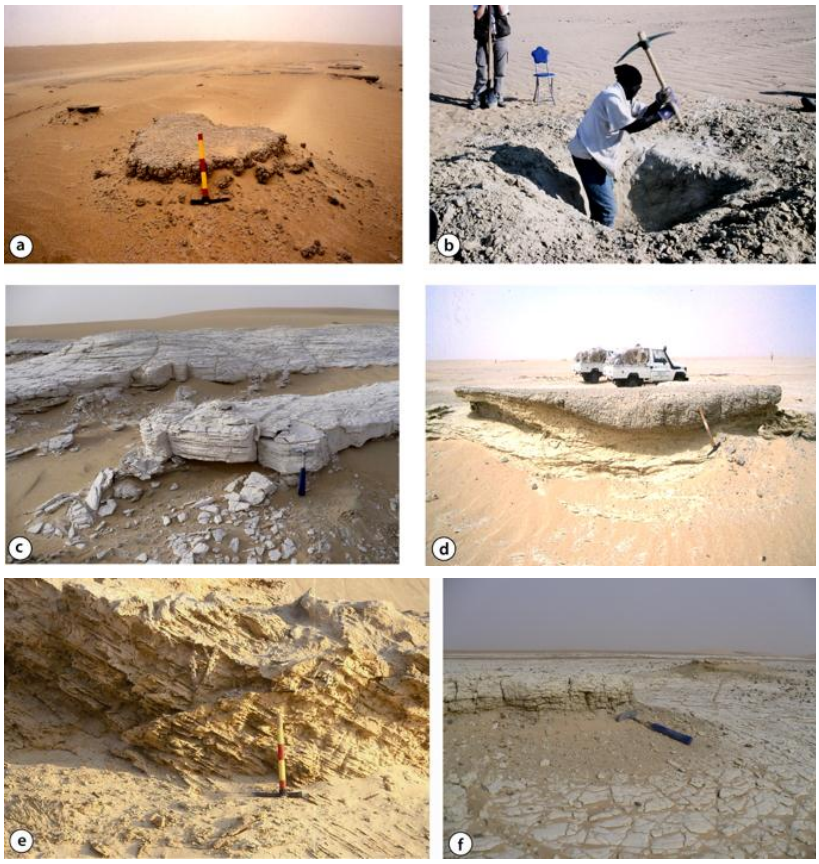

Figure 2. General view of the outcrops of the fossiliferous sites of Toros-Ménalla (TM). Fossil sites appear between dunes, in eroding interdune spaces (deflation). The cuts are metric in size and part of the outcrops buried under the sand were excavated at the base. (a) and (d) Clay outcrops; (c) and (f) diatomites; (b) extension of a cut by digging a well. (e) Oblique bedding of aeolian sands located at the base of the fossiliferous series.

characterized by the presence of large bundles of oblique bedding (Figure 3). The roots only appear in the upper part of the profiles. This unit constitutes an excellent lithostratigraphic landmark because it is the only one presenting such beams of oblique bedding and the only truly sandy one. Also, there are never any fossils in this level.

Fossiliferous clay sandstone

The middle part of the cut (Figure 3) is formed by the fossiliferous sandstone and sandstone-clay unit. This sandstone unit that delivered the remains of the hominids (Sahelanthropustchadensis) as well as the entire vertebrate fauna is officially named Anthracotheriid unit (Vignaud et al., 2002; Novello et al., 2015). It is formed by weakly to strongly indurated clayey sandstones. Unlike the basal part of the section, this facies appears more clearly cemented, in part thanks to the clay matrix and sometimes diatomaceous. Quartz grains are generally well graded, but their maturity is quite variable. This sand-clay unit is often characterized by small oblique bedding, visible only from place to place due to the high density of roots which have partially or totally erased the original structures. Root ducts are ubiquitous in this unit as are termite nests. They usually occupy horizons about 20 cm thick which alternate with facies without roots or with much attenuated root density. Unlike the lower sandy unit, current ripples and oscillation ripples are sometimes observed in this sand-clay unit, especially towards the top of the profile, and on clay or diatomaceous levels.

Diatomites/clays

The upper part of the typical TM 266 profile (Figure 3) is made of diatomaceous earth or clay, sometimes both. This lake unit marks the end of arenitic facies (Schuster et al., 2005; Yu et al., 2020). Its thickness is often reduced to a few decimeters at most in the TM 266 zone.

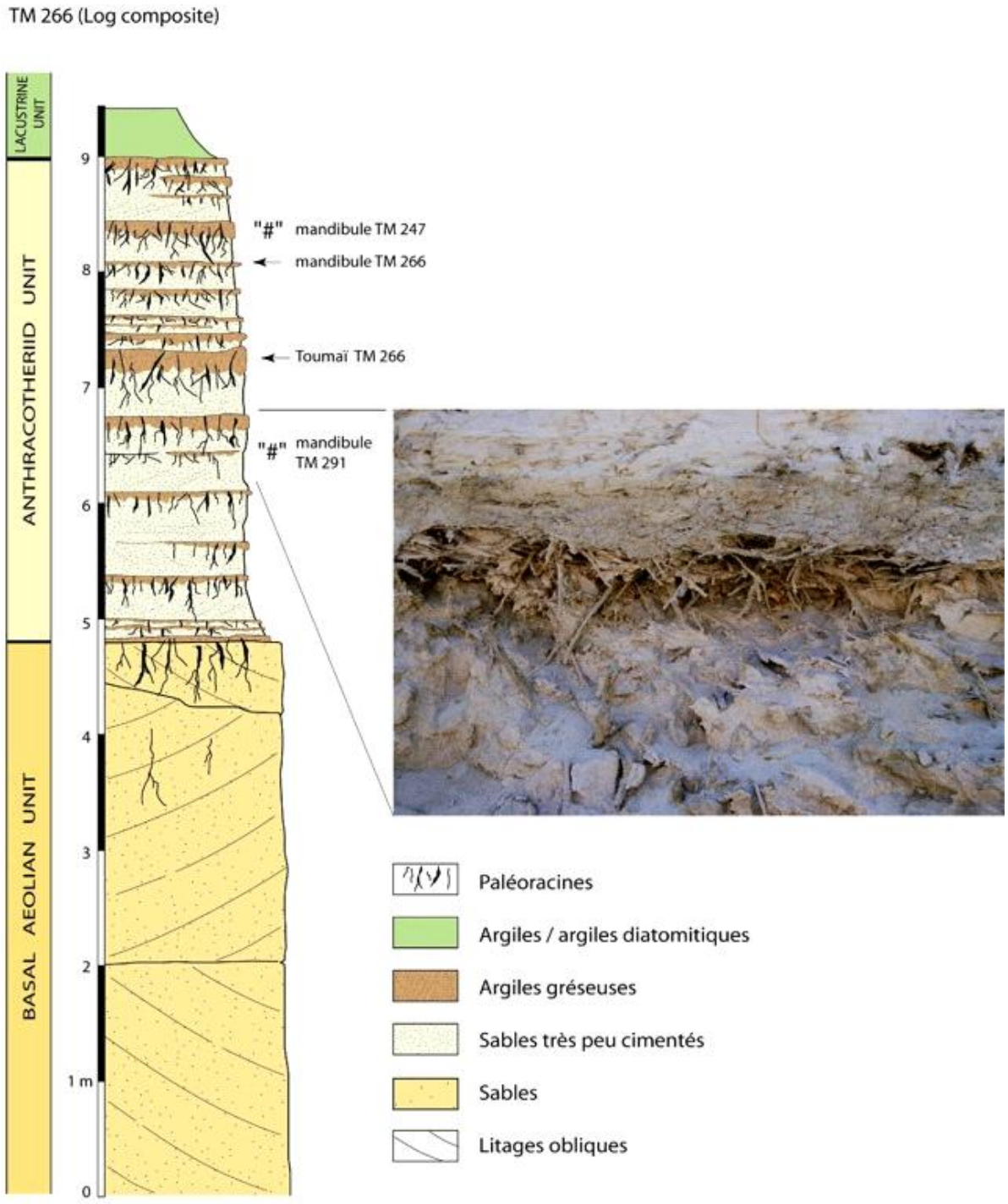

Figure 3. Synthetic reference section of Toros-Ménalla TM 266 (16° 15'N, 17° 29'E) illustrating the 3 major lithological units of the TM zone with, (1) the sandy unit with large oblique bedages at the base, (2) the sandy-clayey facies with roots which alternate with sandy facies without structure in the middle part and (3) the argilo-diatomite facies at the top. All the fossils, in particular the remains of Hominids discovered on this site come from the middle part of the section (Anthracotheriid unit).

This lacustrine facies reaches its maximum thickness in the most western sectors of the TM outcrop band, in particular TM 254 (Figure 4) which is characterized by an entirely diatomaceous lacustrine phase (Figure 4). This

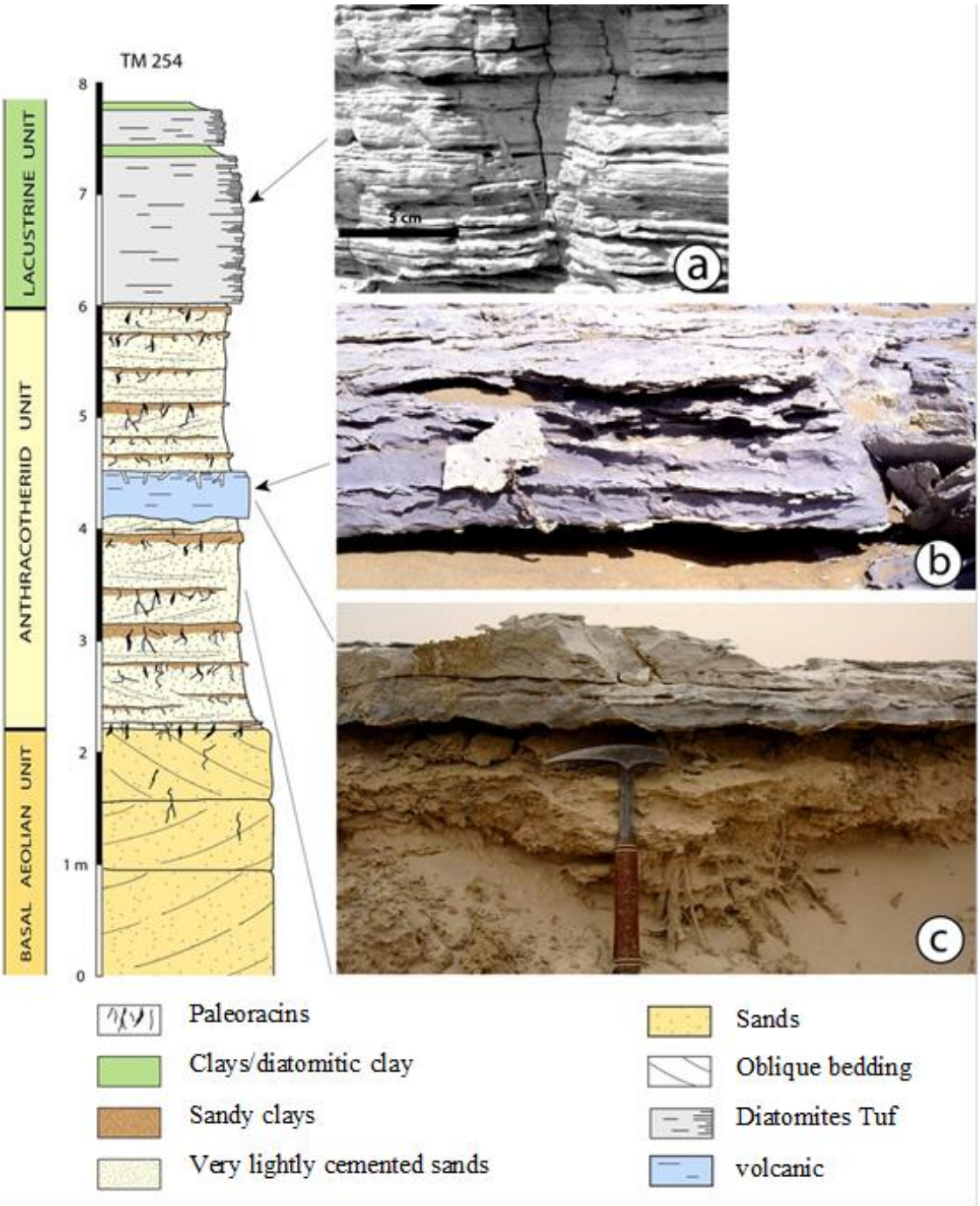

Figure 4. Lithostratigraphic profile of the TM 254 site (16 ° 17'N, 17 ° 20'E) showing the exceptional development of the entirely diatomite lacustrine facies at the top of the section (a) and the presence of a level of volcanic ash in the middle of profile (b). This ash level could only be observed on the TM 254 site and over a distance not exceeding 1.5 km. (c) Shows a detail of the lower part of the ashy level, covering a paleosol with numerous remains of fossil roots in place.

unit is set up in faciological discordance on the fossiliferous sandstone-clay series or very often interstratified in the form of shreds in the fossiliferous series (Brunet et al., 2002; Barboni et al., 2019). These clay-diatomaceous deposits generally contain only aquatic vertebrates (fish) while sandstones deliver almost

only terrestrial vertebrates. Diatomites are pure white and more gray or greenish in color if mixed with silts or clays. Finely bedded diatomites are typically lacustrine deposits. The transition from diatomaceous earth to clay is gradual and takes place over just a few centimeters (5 to 10 cm). The clay is olive-green, compact, homogeneous, and weakly bedded. Locally, it can be silty, especially at the base, in contact with the underlying sandstones (Schneider and Wolf, 1992).

Deposit facies

Four main types of facies are described in the order of their vertical succession from the base to the top of the sections: (1) sandy facies with oblique megalitages, (2) rooted facies, (3) sandstone facies with small bedding obliques, and (4) clay, diatomite and/or clay-diatomite facies.

Facies sandy steels with oblique megalitages

This sandy facies forms the basis of the detrital series of the Terminal Miocene which yielded the remains of Toumaï (Sahelanthropustchadiens) (Brunet et al., 2002; Bristow and Armitage 2016). This facies is made up of very fine sands, of a light color (white to light yellow) and not micaceous. The sand is generally well sorted without any clay matrix. The quartz grains have reached maturity (spherical, rounded, blunt and dull). Cementation is non-existent. There are no fossils in these facies, except in the top part where there are locally a few root ducts and a few rare sandstone balls with a flat base interpreted as mushroom millstones of mushroom termites (Duringer et al., 2006, 2007). The detailed study of oblique bedding (Figure 5) shows an alternation of avalanche laminae (flow) made up of thick laminae of coarser sand and settling laminae (fall) made up of thin laminae of fine sand. These two types of laminae are described to be characteristic of eolian forests (Hunter, 1977; Maithel et al., 2021).

The root ducts which cross obliquely the bundles of oblique bedding appear only at the top of the profile. They are preserved in the form of solid or hollow tubes 5 to 50 cm in length, sometimes interrupted by oblique bedding. On large outcrops, the thickness of the oblique bedding bundles decreases upward. The total thickness of the sandy series is not known but probably exceeds 10 cm. The upper part of this sandy facies is systematically truncated by an erosion surface on which are deposited generally coarser sandy facies. Sometimes when the surfaces of the drills are preserved, wind ripples appear oriented perpendicular to the axis of progradation of the drills. These figures are exceedingly rare in the Aeolian fossil facies. At the fossiliferous sites of TM, the oblique megalitages at the top of the unit are truncated by erosion, showing convex oblique surfaces whose orientation indicates the direction of the paleovents at the time of their formation (Figures 6 and 8).

These sandy facies composed of fine to very fine sands, not at all cemented (all more recent sandy facies are) is mainly made up of many well-sorted, well-rounded, and non-micaceous quartz grains. For many authors, these are criteria that suggest a wind origin (Hunter, 1977, 1985; Swezey, 1998; Maithel et al., 2021). However, the most important criterion is the presence of an alternation of avalanche lamina (flow) and settling lamina (fall) of different particle size, in the oblique bedding (Figure 6). The presence of wind ripples perpendicular to the direction of progradation of the large oblique bedding on the ground confirms the development of aeolianpaleodunes (Figures 7 to 10). The drawing on the ground of the oblique megalitages of pluri-decametric and even hectometric scale also confirms the aeolian origin of this deposit. In addition, the total absence of any criterion typical of watercourses such as the presence of pebbles, soft pebbles, bedding of current ripples or waves, confirms the wind interpretation. This interpretation agrees with the first observations made by Schuster et al. (2006) and Moussa et al. (2016) which make it the oldest record of dunes in the region with an age reaching over 7 million years. These fossil dunes are therefore the oldest evidence of desert conditions in the Sahara (Schuster et al., 2006). Paleovent direction measurements (Vignaud et al., 2002; Schuster et al., 2006) on the oblique beds of the paleodunes indicate a direction of the winds generally oriented towards the South-West, that is, in the same direction as the current dunes of Djourab. The perfect superposition of the directions of the current prevailing winds (harmattan) and the wind of the Miocene is an interesting data for paleoclimatic reconstructions. The presence of a few root ducts (plants) and a few rare sandstone balls in the upper part of this facies testifies to the end of the desert period in favor of a more humid Sahelian-type climate. This essentially Aeolian sandy facies result mainly from an arid desert phase which ended a little before 7 Ma. The perfect superposition of the directions of the current prevailing winds (harmattan) and the winds of the Miocene is an interesting data for paleoclimatic reconstructions.

Root facies

The root facies is undoubtedly the most characteristic of the entire TM zone. It is the “flagship” facies of the Antrhacotheriid area. It is the one who delivered most of the vertebrate fossils, including Toumaï (Brunet et al., 2002; Bobe et al., 2020). This facies is characterized by an alternation of sandy levels and sandy-clay levels with roots and fossil termite nests of decimetric to pluri-decimetric scale (Figure 11). The sands between the

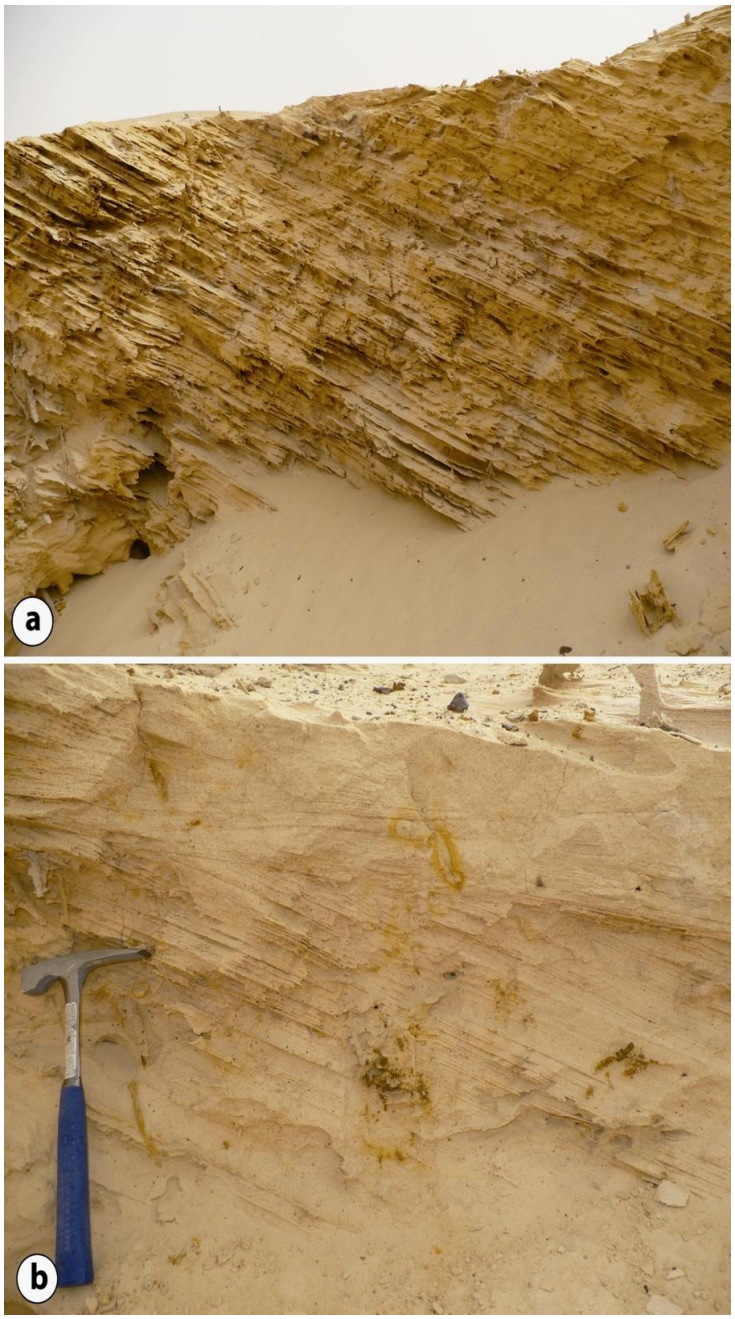

Figure 5. Aeolian deposits at the Miocene Terminal (Toros-Menalla). (a) Large oblique bedding planes of decametric size. The upper part of the profile is truncated by erosion. (b) Superposition of two oblique bedding beams separated by a reactivation surface under which there are some traces of oxidized roots. The alternation of fine laminae of fine sand and thick laminae of coarse sand is characteristic of dune forests. Source: Hunter (1977).

rooted passes are often like the aeolian sands described earlier but in the absence of obvious sedimentary structures their interpretation remains uncertain if not that they seem genetically linked to the rooted horizons (Schuster et al., 2005). The transition between the two is also always diffuse and gradual, at least for the vertical passage “sand-paleosols” (Lemoalle et al., 2012). The bio-turbated part with roots is loosely cemented clay

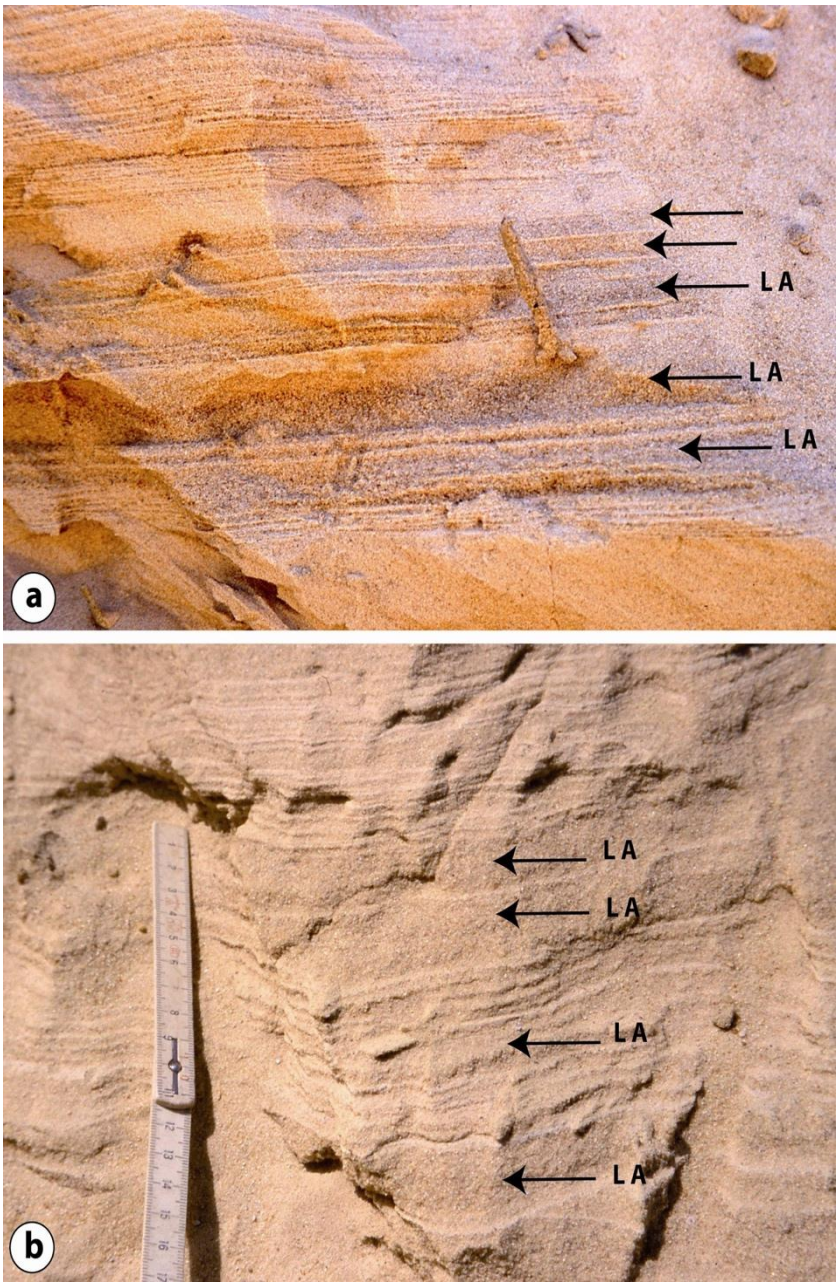

Figure 6. Typical aeolian deposits (a and b) showing the detail of the lamina types: the thick laminae indicated by the black arrows are made up of coarser sands than the fine settling laminae.

sandstone often greenish in color. This color is accentuated with the increase in the proportion of clay. This rooted facies is formed by a confused network of branched and bifurcated root conduits. The shape and size of the root ducts are very variable, but they are mostly circular in section and their diameter decreases from top to bottom of the profiles. The root ducts being slightly more cemented than the surrounding area, they appear in relief (Servant-Vildary, 1973). Some examples taken from the different TM sites show the passage between the rooted paleosol facies to the clay lacustrine facies (Figure 11). This passage is often clearly visible and underlined by an erosion surface (Figures 11 and 13). From a sequential point of view, the downward passage from greenish clayey sands with roots to light sands is always clear even if the very gradual decrease

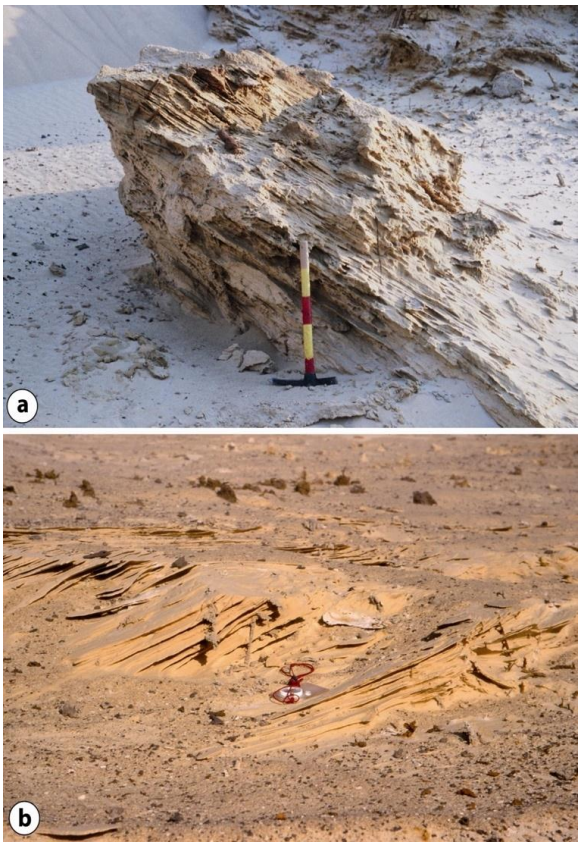

Figure 7. The palaeodunes of the Miocene Terminal de Toros –Ménalla. (a) Flat oblique bedding with a steep slope (greater than 30 degrees) (b) Image showing the damping of the oblique bedding at the foot of the dune with the installation of some roots.

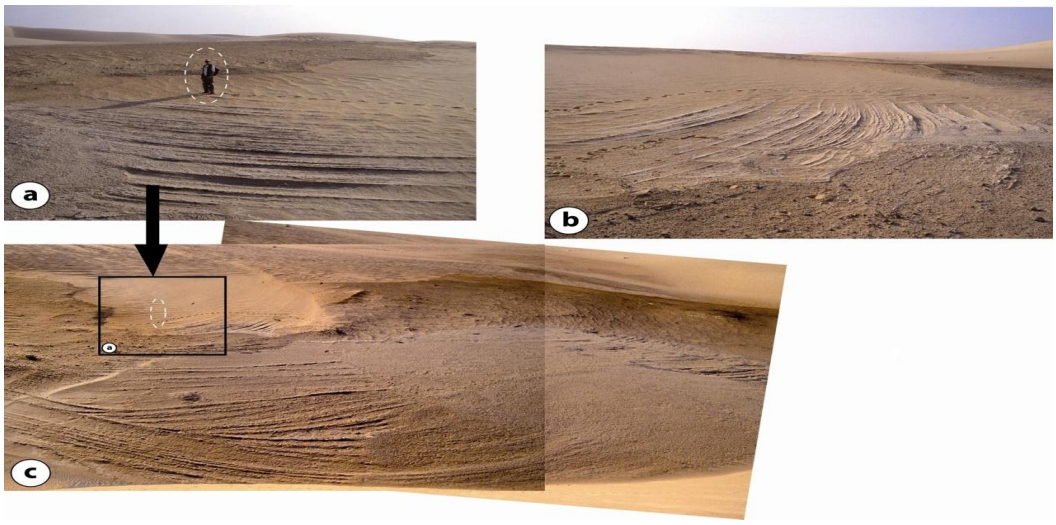

Figure 8. Aeolian facies of the Miocene Terminal outcropping at the surface in the Toros-Menalla sector. (a) Exceptional outcrop showing the bedding in giant troughs drawn on the ground and brought to light by erosion. Such structures suppose large dunes exceeding well over ten meters. Note the footprint and the character which gives the giant scale of the megalitages structures.

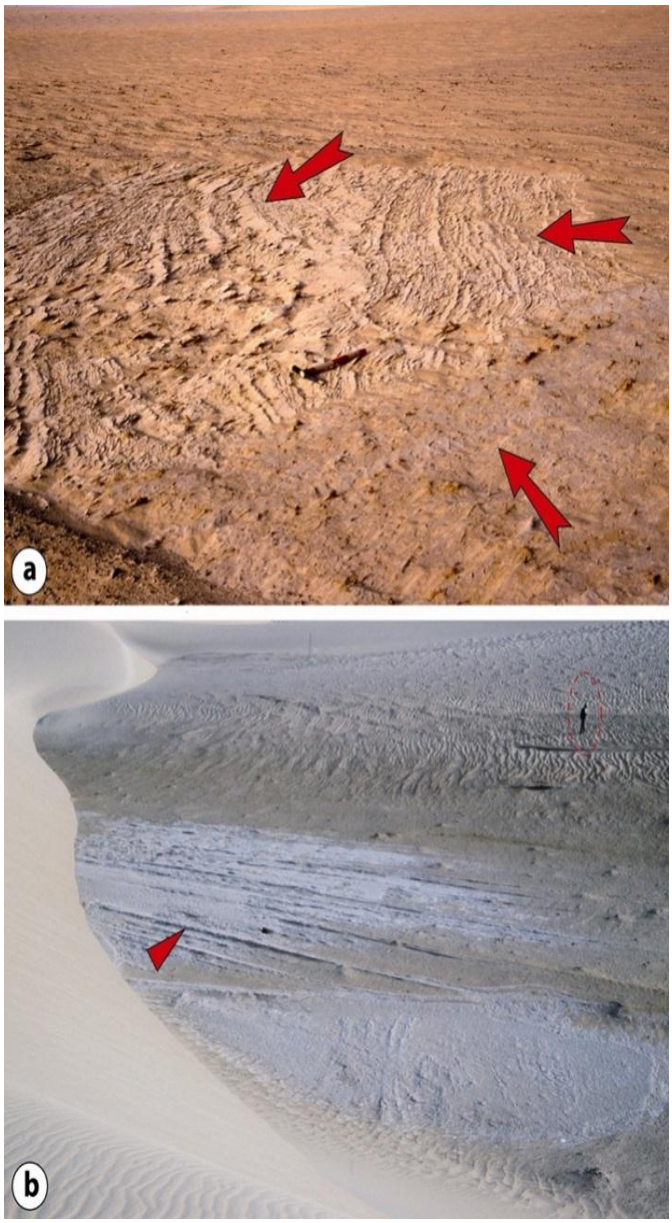

Figure 9. Traces of fossil dunes outcropping on the surface in the fossiliferous sector of TM. The red arrows indicate the direction of movement of the dunes. Photo (b) shows that the direction of migration of paleodunes goes in the direction of migration of current dunes (half-arrow in red) (person for scale). Generally speaking, the orientation of the Miocene paleodunes is comparable to that of the current dunes of Djourab.

in the root network downwards sometimes gives the illusion of a continuous passage. Partly at the top, the passage from the horizon with roots to the overlying white sands can be erosive or very gradual.

These rooted facies are the basic elementary motif which repeats itself vertically almost endlessly. It reflects the development and installation of a paleosol with roots on sands which could be wind turbines at least in part. Figure 11 is undoubtedly one of the most demonstrative examples. Dense, confused, and branched structures correspond well to root ducts and cannot be confused with burrows/galleries and/or other biological or sedimentary structures. Indeed, numerous indices/ recognition criteria make it possible to distinguish them

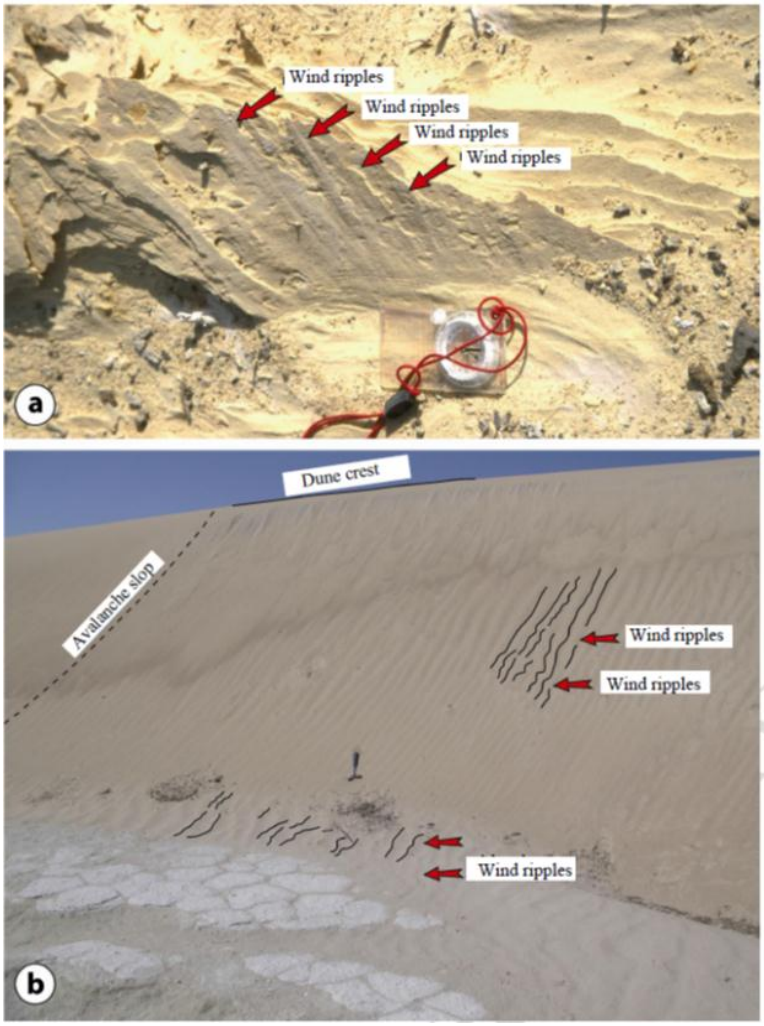

Figure 10. (a) Presence of wind ripples perpendicular to the progradation axis of Miocene paleodunes compared to identical structures on current dunes (b).

Figure 11. This image illustrates the reality of the revegetation of the aeolian sands on the sites of the Miocene Terminal of Toros-Menalla. The alternation of paleosol facies with Aeolian facies is also well marked. The upper limit of the paleosol is underlined by a red dotted line. The arrows show the density of the roots passing through the Aeolian facies.

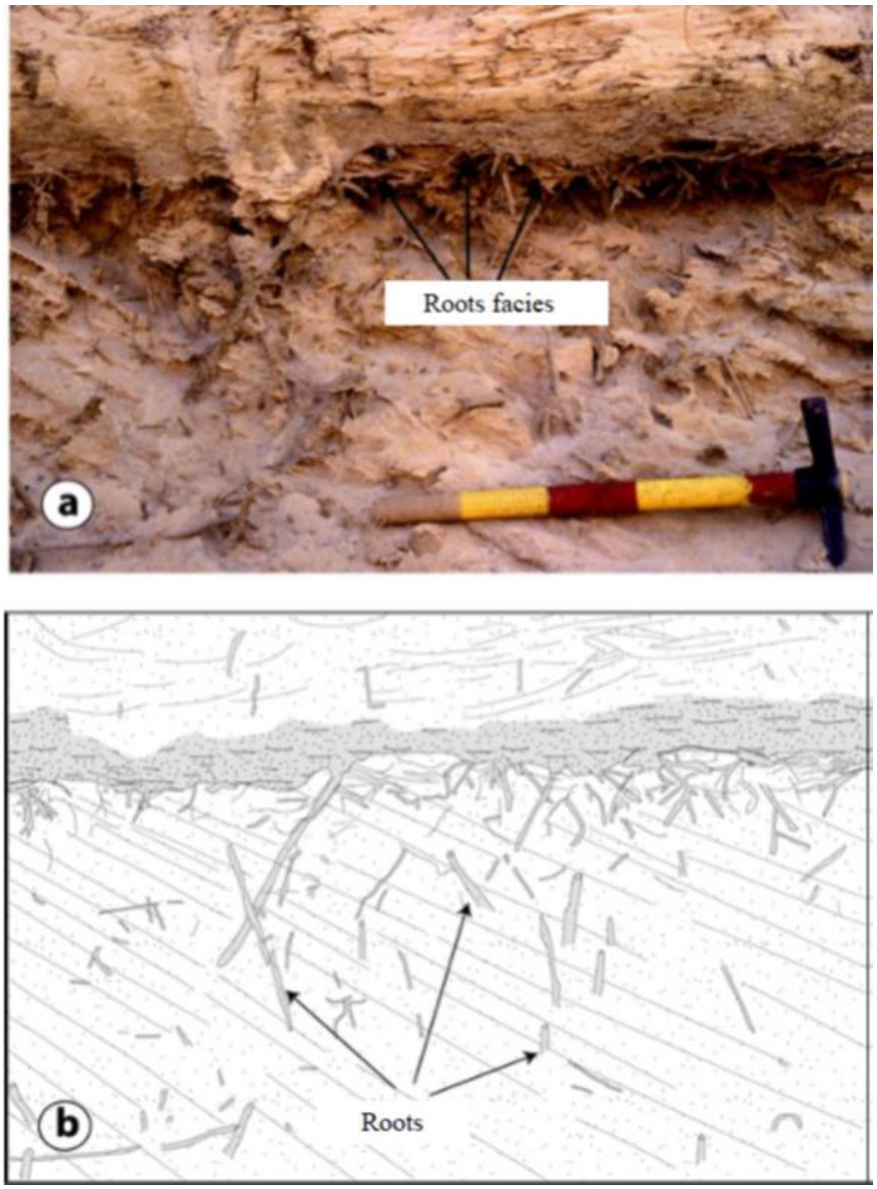

Figure 12. Example of passage from aeolian sandy facies to clayey sand facies with roots formed during the revegetation of aeolian dunes during a wetter phase. Note the gradual overpass between paleosols and clear sands that mark the gradual return to a more arid environment after the wet phase.

from other structures. The ramifications and irregularities of shapes and diameters are very good criteria for recognizing root ducts (Plaziat, 1971). Figures 12 and 13 show the state of conservation of the exceptional ramifications of some of these root ducts.

These root facies are therefore interpreted as the revegetation of aeolian sands during wet phases which alternate with drier, Sahelian or totally desert phases.

The rhythmicity of the alternations is difficult to estimate because there is no significant difference in the age of the faunas collected from the base to the top of the Anthracotheriid Formation. In comparison with the climatic variations of the African Holocene, these cycles have at least 5,000 to 10,000 years, which would give, as first approximation, a range of 100,000 to 200,000 years at least for the whole unit to Anthracotheriid.

Sandstone facies with small oblique bedages

This sandstone facies are especially well developed in the upper part of the Anthracotheridae unit and

Figure 13. (a) and (b) Sandy-clayey facies with paleosols of the Terminal Miocene (Toros-Ménalla). This rooted facies (paleosols) is characterized by very dense root canal networks and termite nests indicated by the red arrows. The roots have penetrated the Aeolian sandy facies at the base of the paleosol.

particularly in contact with the major lacustrine series with which it is unmistakably linked (Figures 14 and 15). It is formed by a moderately to strongly cemented sandstone. The cementation is of clay and clay-diatomite origin (Schuster et al., 2005). The quartz grains, well sorted, are generally larger in size than in all the other facies (Ghienne et al., 2002; Moussa et al., 2016). These facies, unlike the sandy facies with oblique megalitages, is characterized by the development of small oblique bedding bundles of centimeter to pluricentimetric size. It is also characterized by the presence of current ripples, oscillation ripples and sometimes clay drapes (Figure 14). Oscillation megarids have been observed at certain sites, demonstrating the importance of lake or perilacustrine dynamics (Lemoalle et al., 2012; Maley and Maley 1981; Armitage et al., 2015). The abundance of clays in these facies is very variable, of the roots, and some levels are completely devoid of it. The base of this facies is still very clearly erosive on the underlying facies (Minisini et al., 2018).

The appearance in these facies of current ripples and oscillation ripples, as well as clay drapes on the ripples, testifies for the first time with certainty of the immersion of the surface under a sheet of free water in motion (Olivry et al., 1996). Generally, placed at the top of the sequence of root paleosol facies, this facies undoubtedly marks the development of extensive flood zones.

It is typical transitional facies of the edge of a lake in which ripples and roots coexist for a certain time before giving way to the body of water (Lemoalle et al., 2012). Sometimes the sequences show a gradual passage between aeolian dunes, vegetated or not, and the lake, passing through phases with ripples and clay drapes (Pias, 1970). Such transgressive sequences are known in the Bol sector on the northern outskirts of present-day Lake Chad where the dunes are vegetated when the

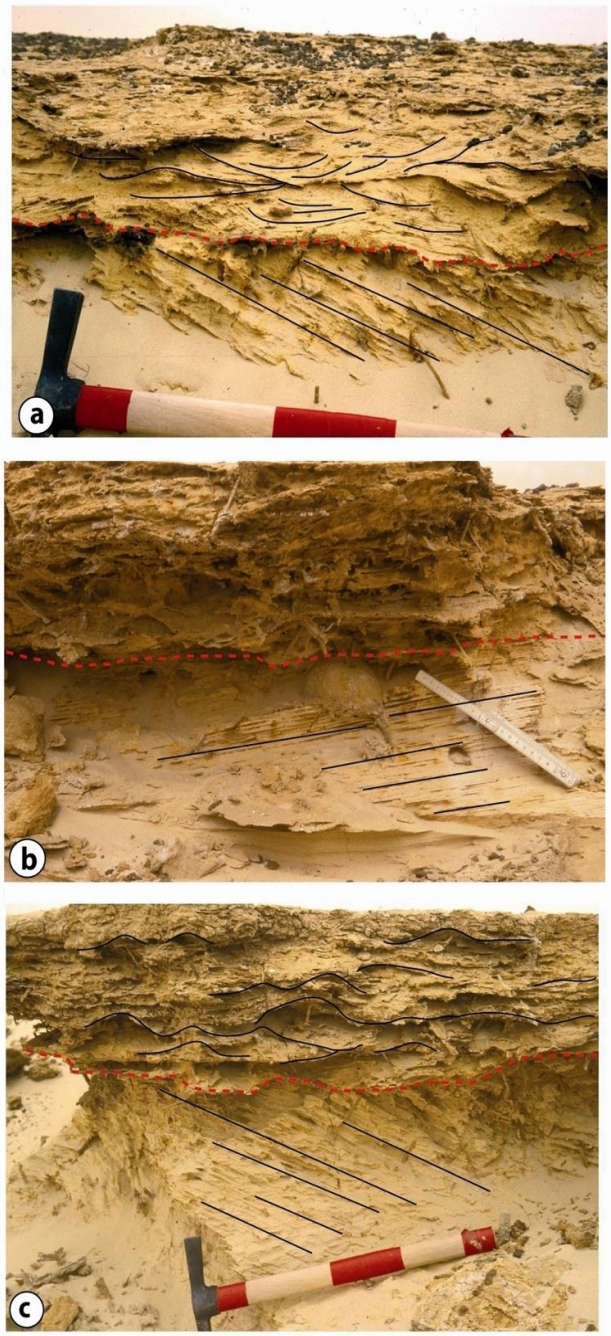

Figure 14. Sandstone perilacustrinefacies with small oblique bedding (a, b, and c) covering Aeolian facies. The majority of terrestrial vertebrate fossils come from this facies. (a) This image highlights large oblique bedages of aeolian nature in the lower part. The upper part is characterized by very small bundles of oblique bedding formed by current ripples. This very dynamic facies does not show any roots. (b) and (c) The Aeolian facies of the base of the photos (large oblique bedages) is covered by a “flaser” type facies showing the alternation of small beams of oblique bedding of current ripples and sea ripples. oscillation separated by clay layers. This facies shows an alternation of period of agitation (sand and sandstone) and periods of calm during which the clays are deposited.

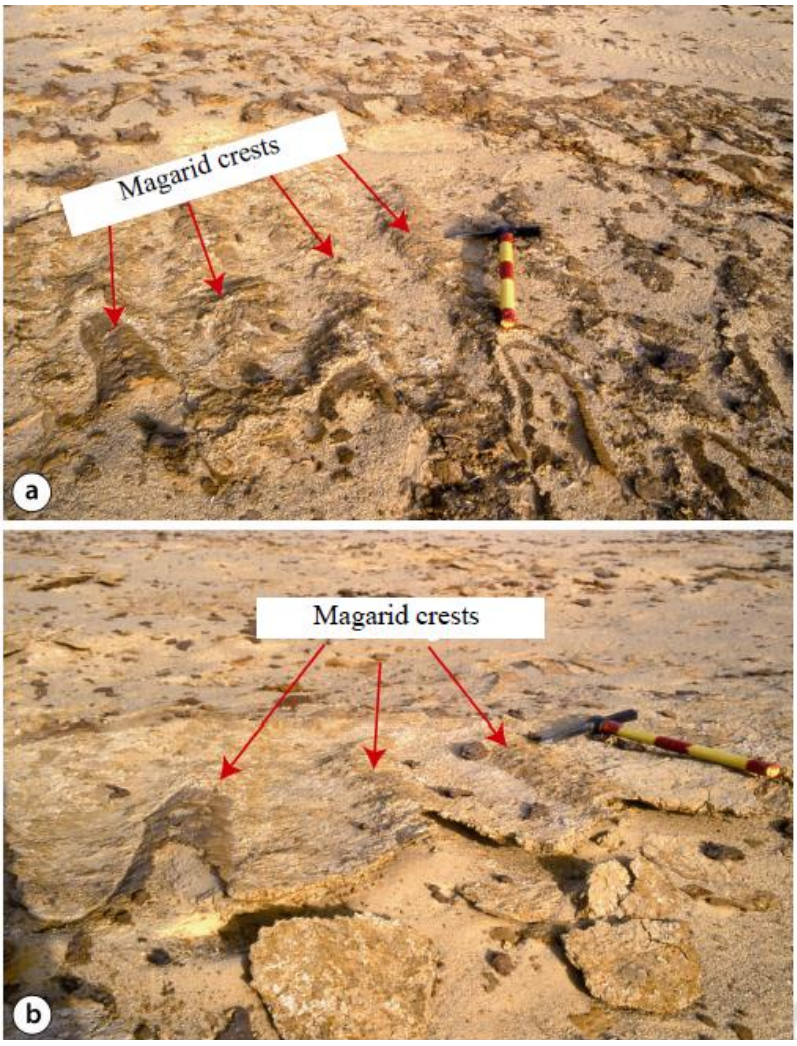

Figure 15. Sandstone facies with small oblique bedding (peri-lacustrine). Sandstone surface showing oscillating megarid ridges (a) (hammer for ladder). Such megarides also present in marine environments, characterize very high energy environments. This type of wrinkle only develops in very coarse sands, or in fine gravel.

water level rises before being totally submerged (Leblanc et al., 2006; Moussa et al., 2016).

These facies are riddled with roots and bioturbations. It highlights the gradual installation of an undoubtedly perennial water body. The red dotted line indicates the limit between the two facies (Aeolian at the base and peri-lacustrine at the top).

This peri-lacustrine facies is the transition facies marking the flooding and progressive submersion of this sector during a phase of lacustrine transgression.

Facies clayey, diatomite and clay-diatomite steels

Lacustrine sediments are characterized by two types of facies (Figures 16 and 17): clays and diatomites, and sometimes by a mixture of the two. This lacustrine facies almost always rests on an erosion surface (Figure 18). The clay or diatomaceous facies marks the end of the deposition sequence. It rests directly on the root facies (paleosols) or on the sandstone facies with small oblique bedages (peri-lacustrine) or, in certain sections, directly on the Aeolian formations of the base.

Clay facies

This lacustrine facies is formed of a more or less homogeneous green clay on the fossiliferous sites of TM (Figure 16a) never very thick with a few rare exceptions.

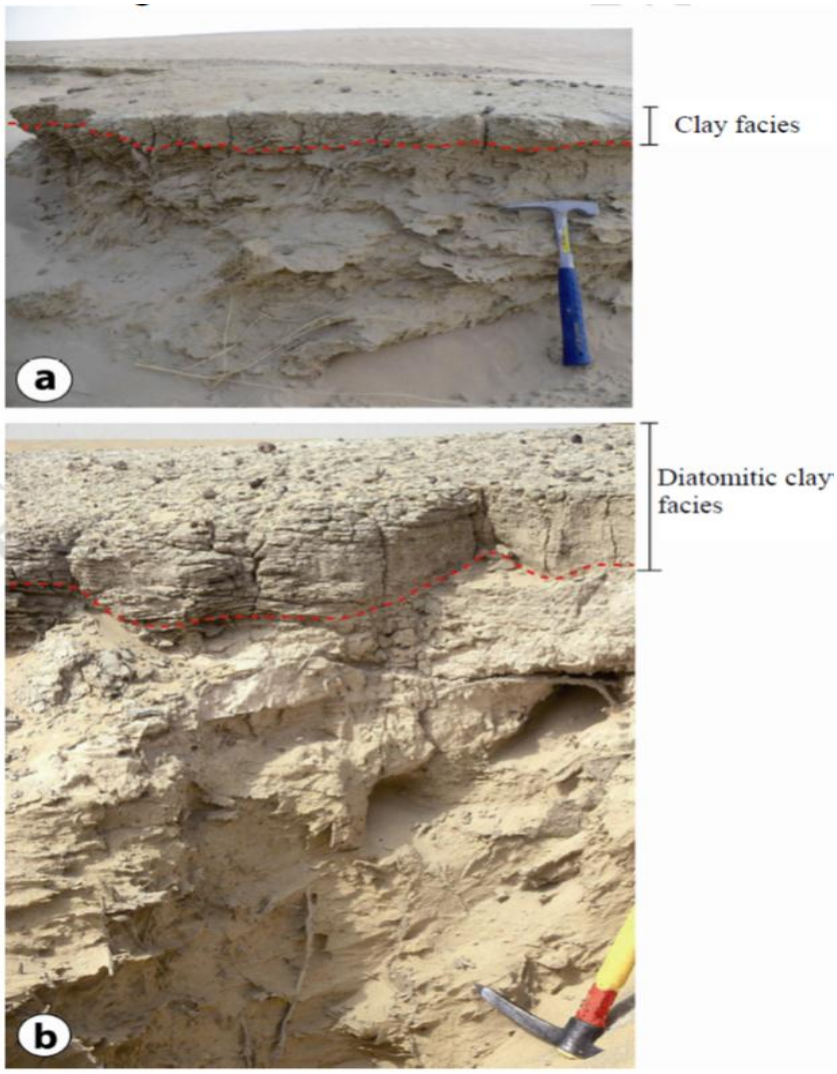

Figure 16. Clayey and clay-diatomite lacustrine facies deposited in discordance on the sandy roots facies. (a) The diffuse contact undoubtedly testifies to a very gradual establishment. (b) Example showing a clearer erosion surface.

It often occurs as discontinuous lenses within sandstones and clayey sandstones. The diatomite/clay passage is not always clear and the transition is generally made by a mixture of the two facies. Diatomaceous earth becomes greener and greener when mixed with clay (Figure 17b). Very few sedimentary figures can be observed within these facies.

Diatomite facies

Diatomites appear as white spots that run the length of outcrops at the Toros-Menalla sites, especially on TM 254 where they form prominent outcrops, sometimes even small ledges in the landscape. The lacustrine diatomite facies is composed of pure white diatomites, or sometimes mixed with clays or/and silts which give them a gray tint (Figure 17). Diatomite is a rock very low density formed entirely or almost entirely of frustules of diatoms (unicellular algae with siliceous tests). Diatomites are often compact or finely bedded. Their thickness varies greatly depending on the outcrops, reaching up to a few centimeters. The lower contact with the underlying facies is still very clear. Diatomites are not very rich in vertebrate fossils, often limited to the remains of fish, turtles and crocodiles.

Even if diatoms abound in the marine environment, the development of substantial deposits is the exclusive fact of lake environments.

The diatomite facies and the clayey facies mark the

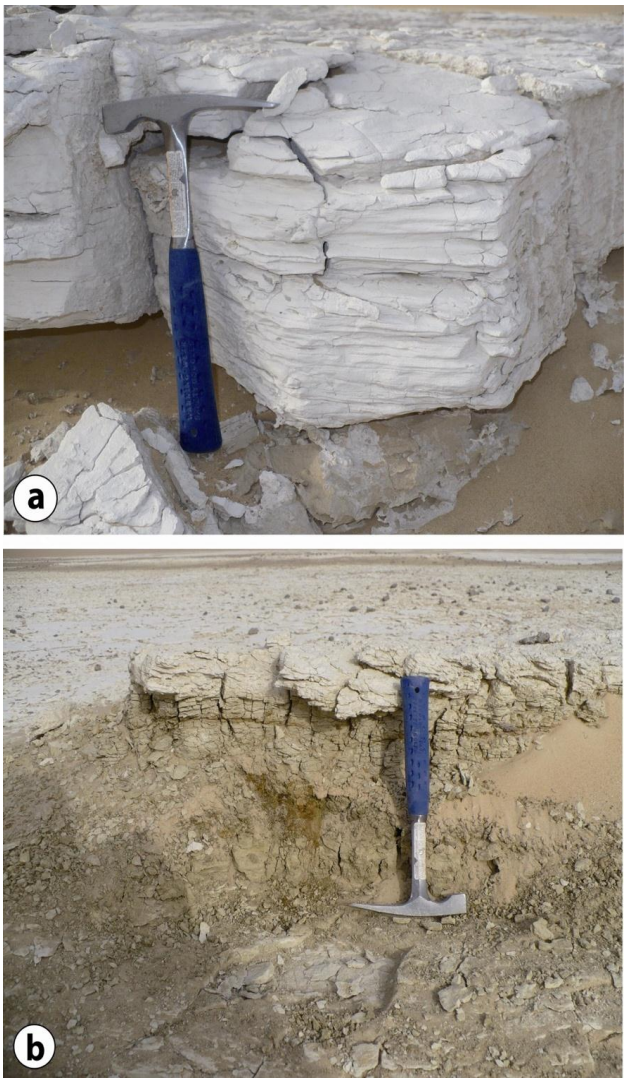

Figure 17. Diatomite lacustrine facies of TM fossil sites. (a) Pure, compact and weakly bedded white diatomites. (b) Mixture of diatomite and clays above the sandy-clay facies. The passage between clay and diatomite seems to be continuous and gradual.

installation of a perennial lacustrine environment during the Terminal Miocene on the fossiliferous sites of Toros-Ménalla. These clayey and diatomite facies correspond to transgressive lacustrine deposits (wet phases) which progress on the Aeolian facies (arid phases), the sandy-clay facies with paleosols and/or on the peri-lacustrine facies (Figure 18). These clayey and diatomite lacustrine facies can be compared with lake phases of the Mega-Chad type (Ghienne et al., 2002; Schuster, 2002; Schuster et al., 2003, 2005, 2009; Bouchette et al., 2010). Similar studies have shown relatively comparable sedimentary successions in the Mio-Pliocene age deposits of Chad (Duringer et al., 2000; Schuster, 2002; Bianchini et al., 2019). On some sections studied near Koro-Toro, Servant (1973) describes the installation of a transgressive lacustrine phase on aeolian deposits. The sedimentological characteristics of the lacustrine facies (clayey and diatomite) presented earlier allow us to precisely demonstrate the presence of a transgressive lacustrine phase in the fossiliferous sites of Toros- Menalla (TM).

Typica deposit sequences

The composite section of TM 266 (Figure 19) shows the gradual passage of aeolian sands, to Sahelian, peri-

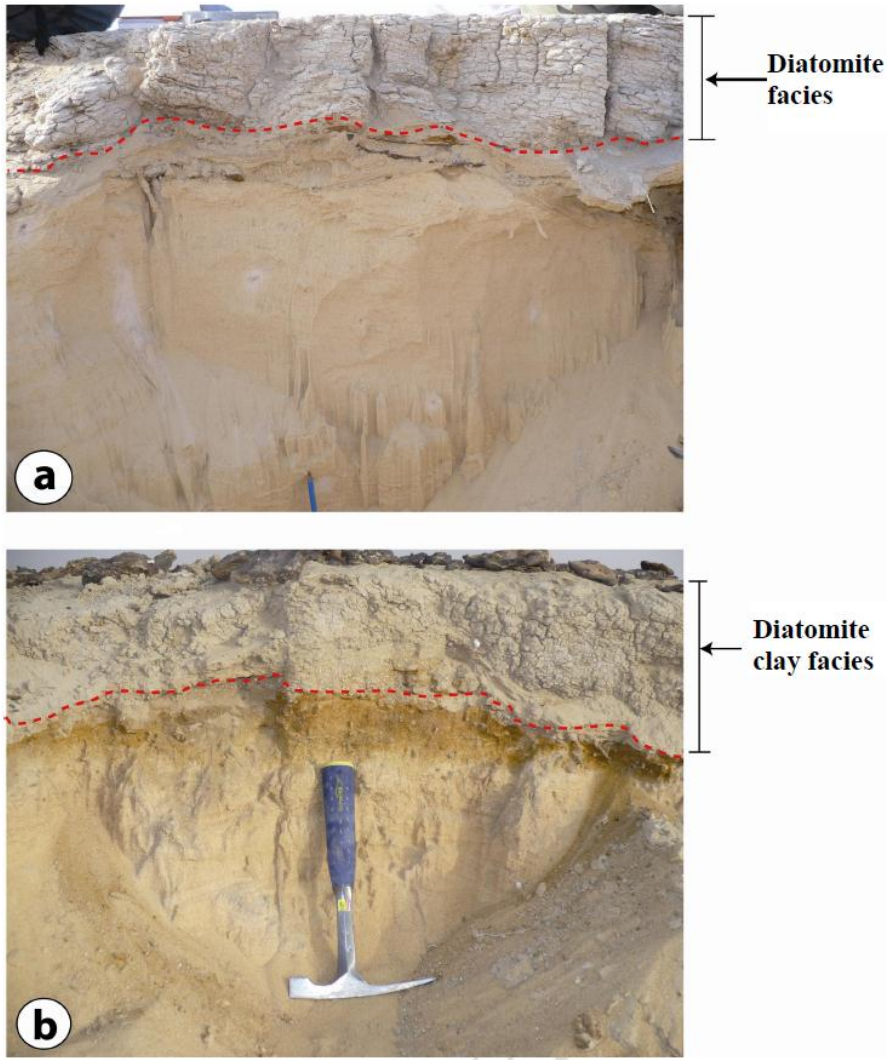

Figure 18. Example of clear erosive contact between diatomites and underlying sands. (a) and (b): Diatomites in discordant contact on sands of aeolian nature. The contact of photo (b) is marked by ferro-manganese oxidations.

lacustrine and then lacustrine sequences (Schuster et al., 2005). The ideal sequence drawn (Figures 19 and 20) traces the vertical evolution of the facies during this climatic drift (Lemoalle et al., 2012; Bristow et Armitage, 2016).

This standard sequence of the eolo-lacustrine series of the Terminal Miocene of the fossiliferous sites of Toros-Ménalla is characterized by the superposition of the four facies described previously with successively the Aeolian facies, the paleosol facies, the peri-lacustrine facies, and the lacustrine facies (Figure 19).

This "typical" sequence raised at the interface of two contrasting environments (desert at the base and lacustrine at the top) shows Aeolian facies covered by a paleosol (paleosol facies) with root ducts and bioconstructions of insects passing to sands: peri-lacustrine (peri-lacustrine facies) with small oblique beddings surmounted by diatomites or lacustrine clays (lacustrine facies) (Ghienne et al., 2002; Novello et al., 2017). Pattern variations within this “typical” sequence can be significant, such as being sometimes eroded, or even absent (Figure 20). Thus, clayey lacustrine facies can rest either directly on paleosols without an intermediate peri-lacustrine term, or directly on aeolian formations (Servant-Vildary, 1973). Fossil deposits are also often found with a transgressive base that allows a concentration of fossils (Brunet et al., 2002; Duval et al., 2021). The typical environments described in this sequence are therefore as follows:

(1) The basis of the sequence materializes a dry arid environment with the development of real dunes of large

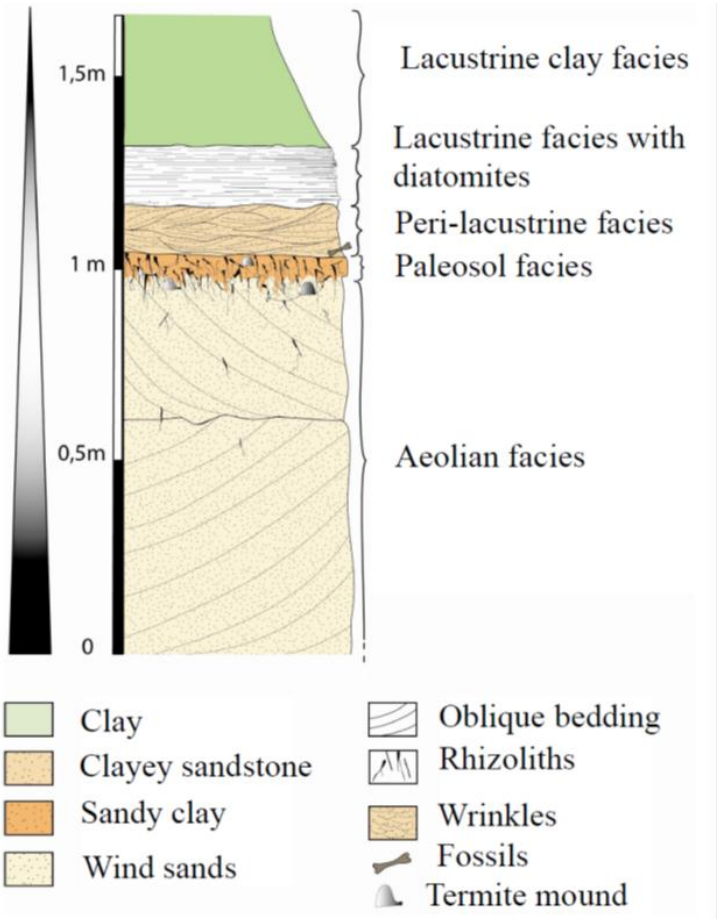

Figure 19. Type “dunes-lake” sequence from the Upper Miocene of Chad. This sequence traces the history of a major palaeoenvironmental variation of climatic origin marked by the installation of a lake which transgresses a desert. The first major changes begin with the marked development of revegetation on the dunes at the start of a wetter phase. The gradual installation of roots at the top of the dunes is the best example of this. The establishment of the wrinkles marks the development of a perilacustrine zone, which then appears submerged by the final transgression of the lake.

dimensions like those of ergs still exist today in the Djourab desert.

(2) The top of the sequence corresponds to a lake environment of the classic Mega Lake type.

(3) The middle part is literally a buffer zone between these two extreme environments. The transition to more humid climatic conditions will gradually vegetate the desert. During these "green phases", it allows the development of numerous paleosols. “Arid-humid” climatic fluctuations are at the origin of the alternation of sandy facies without structures (aeolian or Sahelian) with sandy-clay facies with paleosols.

(4) Near the lakes which are gradually spreading, peri-lacustrine facies is developing marked by the appearance of facies with current ripples and oscillation which gradually replaces the root facies of paleosols.

The first deposits correspond to a desert environment (Aeolian facies), gradually passing to lakeside deposits by a succession of paleosols (paleosol facies) increasingly marked by the increasing proximity of the lake (peri-lacustrine facies) and this sequence ends with the transgression of a perennial lake (lacustrine facies with diatomites and clays).

Conclusion

Based on the interpretation of the facies, the sedimentological study of the fossil Hominid sites of the late Miocene reveals four successive environments: the

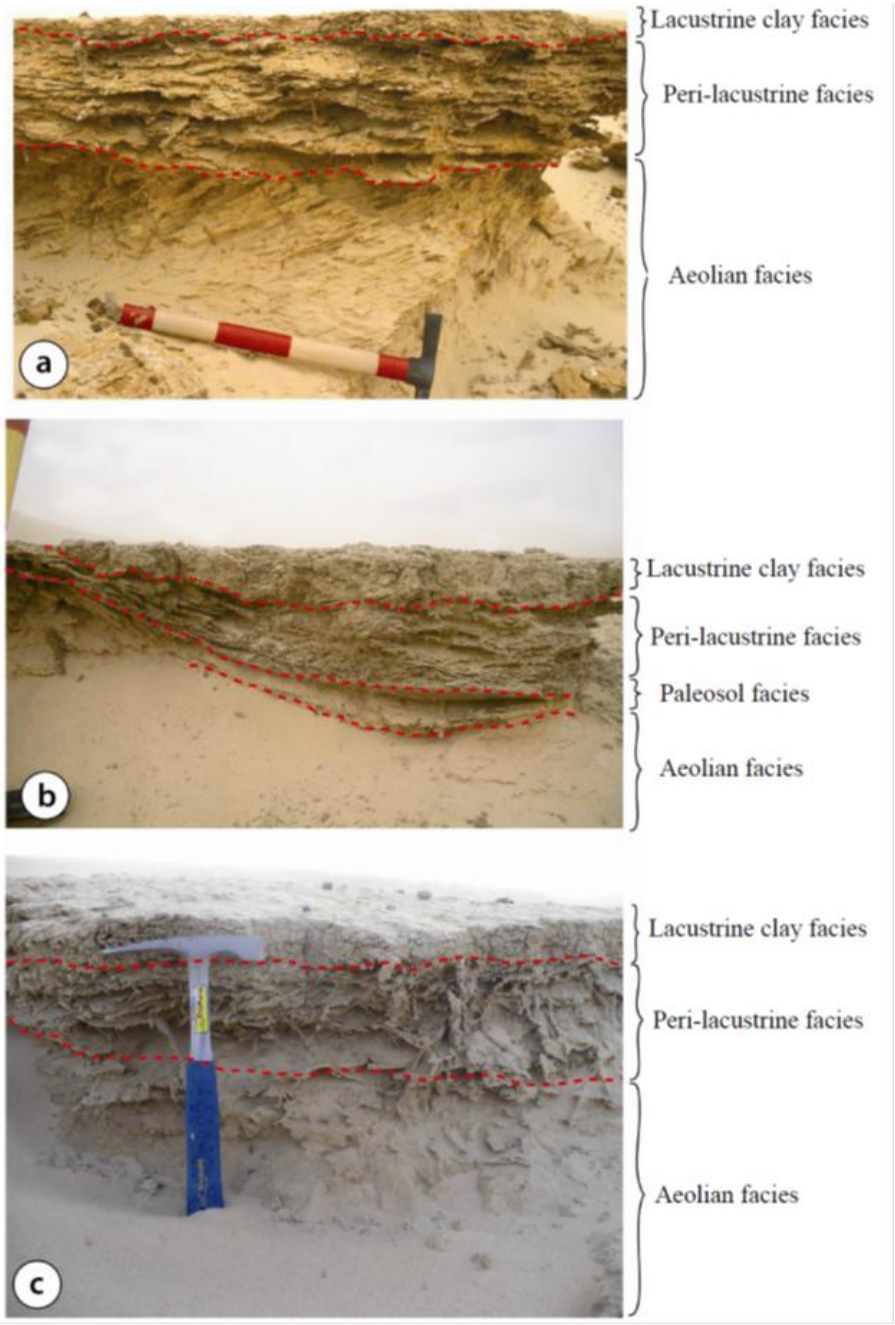

Figure 20. The three photos (a, b and c) show the vertical variations of the facies in the Upper Miocene fossil sites of Chad. Image (b) shows the superposition of the four facies with a paleosol sequence intermediate between the Aeolian and peri-lacustrine facies.

first deposits correspond to (1) an aeolian desert environment (aeolian facies), gradually passing to lakeside deposits by a succession (2) of paleosols (root facies or paleosols) increasingly marked by the increasing proximity (3) of the lake (peri-lacustrine facies). The sequence ends with the transgression (4) of a perennial lake (lacustrine facies with diatomites and clays). The fossiliferous facies (Anthracotheriid layers) set up between the two major Aeolian phases (at the base) and lacustrine (at the top), show an alternation of Sahelian phases episodically vegetated during wetter phases. The "dune-soils" sequence constitutes the recurring elementary motif of the deposit. From place to place, the insertion of clays or lacustrine diatomites

manifests a transgressive pulsation with the installation of peri-lacustrine environments favoring the development of a more aquatic fauna. The installation of fauna clearly characterizes these “greener” phases.

By examining all the fossiliferous sites between 3 and 7 million years ago, we see that this northern part of the basin has almost always been a buffer zone oscillating according to climatic fluctuations between the lake, the edge of the lake, the Sahelian zone, and total desert. In this eolo-lacustrine transition zone, where the ancient hominids evolve, the lacustrine episodes are only temporary phases corresponding to the transgressions of the perennial central lake whose pulsations follow the climatic rhythm of the wet and dry phases. The Bol archipelago, located northeast of present-day Lake Chad, symbolizes an excellent model of this type of environment, where the lake and the desert merge.

CONFLICT OF INTERESTS

The authors have not declared any conflict of interests.

REFERENCES

Alemseged Z, Wynn JG, Geraads D, Reed D, Barr WA, Bobe R, McPherron SP (2020). Fossils from Mille-Logya, Afar, Ethiopia, elucidate the link between Pliocene environmental changes and Homo origins. Nature communications 11(1):1-12.

Armitage SJ, Bristow CS, Drake NA (2015). West African monsoon dynamics inferred from abrupt fluctuations of Lake Mega-Chad. Proceedings of the National Academy of Sciences 112(28):8543-8548.

Barboni D, Ashley GM, Bourel B, Arraiz H, Mazur JC (2019). Springs, palm groves, and the record of early hominins in Africa. Review of Palaeobotany and Palynology 266:23-41.

Bianchini S, Solari L, Del Soldato M, Raspini F, Montalti R, Ciampalini A, Casagli N (2019). Ground subsidence susceptibility (GSS) mapping in Grosseto Plain (Tuscany, Italy) based on satellite InSAR data using frequency ratio and fuzzy logic. Remote Sensing 11(17):2015.

Bobe R, Manthi FK, Ward CV, Plavcan JM, Carvalho S (2020). The ecology of Australopithecus anamensis in the early Pliocene of Kanapoi, Kenya. Journal of human evolution 140:102717.

Bouchette F, Schuster M, Ghienne JF, Denamiel C, Roquin C, Moussa A, Duringer PH (2010). Hydrodynamics in the Holocene Lake Mega-Chad. Quaternary Research 73:226-236.

Branco Pavanatto AE, Stock Da Rosa ÁA., Temp Müller R, Roberto Da Silva L, Ribeiro AM, Martinelli AG, Dias Da Silva S (2020). Bortolin site, a new fossiliferous locality in the Triassic (Ladinian/Carnian) of southern Brazil. Sociedade Brasileira de Paleontología.

Bristow CS, Armitage SJ (2016). Dune ages in the sand deserts of the southern Sahara and Sahel. Quaternary International 410:46-57.

Bristow CS, Holmes JA, Mattey D, Salzmann U, Sloane HJ (2018). A late Holocene palaeoenvironmental ‘snapshot’of the Angamma Delta, Lake Megachad at the end of the African Humid Period. Quaternary Science Reviews 202:182-196.

Brunet M, Beauvilain A, Coppens Y, Heintz E, Moutaye AHE, Pilbeam D (1995). The first australopithecine 2500 kilometres west of the Rift Valley (Chad). Nature 378:273-275.

Brunet M, Beauvilain A, Coppens Y, Heintz E, Moutaye AHE (1996). *Australopithecusbahrelghazali*, une nouvelle espèce d'Hominidé ancien de la région de Koro Toro (Tchad). Comptes rendus de l'Académie des sciences. Série 2. Sciences De La Terre Et Des Planètes 322(10):907-913.

Brunet M, Beauvilain A, Geraads D, Guy F, Kasser M, Mackaye HT, Mac Latchy LM, Mouchelin G, Sudre J, Vignaud P (1997). Tchad : un nouveau site à Hominidés pliocène. C. R. Acad. Sci. Paris 324:341-345.

Brunet M, Guy F, Pilbeam D, Mackaye HT, Likius A, Ahounta D, Beauvilain A, Blondel C, Bocherens H, Boisserie JB, De Bonis L, Coppens C, Dejax J, Denys Ch, Duringer PH, Eisenmann V, Fanone G, Fronty P, Geraads D, Lehmann TH, Lihoreau F, Louchart A, Mahamat A, Merceron G, Mouchelin G, Otero O, PelaezCampomanes P, Ponce De Leon M, Rage JC, Sapanet M, Schuster M, Sudre J, Tassy P, Valentin X, Vignaud P, Viriot L, Zazzo A, Zollikofer CH (2002). A new hominid from the Miocene of Chad, central Africa. Nature 418(6894):145-151.

Duringer P, Brunet M, Cambefort Y, Likius A, Mackaye HT, Schuster M, Vignaud P (2000). First discovery of fossil dung beetle brood balls and nests in the Chadian Pliocene Australopithecines levels. Lethaia 33(4):277-284.

Duringer P, Schuster M, Genise JF, Mackaye HT, Vignaud P, Brunet M (2007). New termite trace fossils: Galleries, nests and fungus combs from the chad basin of Africa (Upper Miocene - Lower Pliocene). Palaeogeography Palaeoclimatology Palaeoecology 251(3-4):323-353.

Duringer P, Schuster M, Genise JF, Likius A, Mackaye HT, Vignaud P, Brunet M (2006).The first fossil fungus gardens of Isoptera: oldest evidence of symbiotic termite fungiculture (Miocene, Chad basin). Naturwissenschaften 93(12):610-615.

Duval M, Sahnouni M, Parés JM, van der Made, Abdessadok S, Harichane Z, Cheheb RC (2021). The Plio-Pleistocene sequence of Oued Boucherit (Algeria): A unique chronologically-constrained archaeological and palaeontological record in North Africa. Quaternary Science Reviews 271:107116.

Ghienne JF, Schuster M, Bernard A, Duringer Ph, Brunet M (2002). The Holocene giant Lake Chad revealed by Digital Elevation Models. Quaternary International 87(1):81-85.

Hunter RE (1977). Basic types of stratification in small eolian dunes. Journal of Sedimentary Petrology 24(3):361-387.

Hunter RE (1985). Subaqueous sand-flow cross strata. Journal of Sedimentary Petrology 55(6):886-894.

Lebatard AE, Bourlès D, Duringer P, Jolivet M, Braucher R, Carcaillet J, Schuster M, Arnaud N, Monié P, Lihoreau F, Likius A, Mackaye HT, Vignaud P, Brunet M (2008). Cosmogenic nuclide dating of Australopithecus bahrelghazali and Sahelanthropustchadensis: Mio-Pliocene Hominids from Chad. Proceedings of the National Academy of Sciences 105(9):3226-3231.

Leblanc M, Favreau G, Maley J, Nazoumou Y, Leduc C, Stagnitti F, Oevelen PJ. van, Delclaux F, Lemoalle J (2006). Reconstruction of Megalake Chad using Shuttle Radar Topographic Mission data. Palaeogeogr. Palaeoclimatol. Palaeoecol 239(1-2):16-27.

Lemoalle J, Bader JC, Leblanc M, Sedick A (2012). Recent changes in Lake Chad: Observations, simulations and management options (1973–2011). Global and Planetary Change 80:247-254.

Mackaye HT (2001). Les proboscidiens du Miocène du Tchad : Biodiversité ; biochronologie ; paléoécologie ; et paléobiogéographie. Thèse de doctorat de l’Université de Poitiers (France) 209 p.

Maithel SA, Brand LR, Whitmore JH (2021) Characterization of hard-to-differentiate dune stratification types in the Permian Coconino Sandstone (Arizona, USA). Sedimentology 68(1):238-265.

Minisini D, Eldrett J, Bergman SC, Forkner R (2018). Chronostratigraphic framework and depositional environments in the organic-rich, mudstone-dominated Eagle Ford Group, Texas, USA. Sedimentology 65(5):1520-1557.

Moussa A, Novello A, Lebatard AE, Decarreau A, Fontaine C, Barboni D, Sylvestre F (2016). Lake Chad sedimentation and environments during the late Miocene and Pliocene: New evidence from mineralogy and chemistry of the Bol core sediments. Journal of African Earth Sciences 118:192-204.

Novello A, Barboni D, Sylvestre F, Lebatard AE, Pailles C, Bourles DL, Likius A (2017). Phytoliths indicate significant arboreal cover at Sahelanthropus type locality TM266 in northern Chad and a decrease in later sites. Journal of human evolution 106:66-83.

Novello A, Lebatard AE, Moussa A, Barboni D, Sylvestre F, Bourlès DL,

Paillès C (2015). Diatom, phytolith, and pollen records from a 10Be/9Be dated lacustrine succession in the Chad basin: insight on the Miocene–Pliocene paleoenvironmental changes in Central Africa. *Palaeogeography, Palaeoclimatology, Palaeoecology* 430:85-103.

Olivry JC, Chouret A, Vuillaume G, Lemoalle J, Bricquet JP (1996). Hydrologie du lac Tchad (Vol. 12). https://www.unitheque.com/Livre/orstom/Monographie_hydrologique/ Hydrologie_du _lac_Tchad-10440.html

Pias J (1970). La végétation du Tchad: ses rapports avec les sols, variations paléobotaniques au quaternaire; contribution à la connaissance du bassin tchadien, Vol. 6. IRD Editions. https://www.worldcat.org/title/vegetation-du-tchad-ses-rapports-avec-les-sols- variations-paleobotaniques-au-quaternaire/oclc/12583332

Plaziat JC (1971). Racines ou terriers ? Critères de distinction à partir de quelques exemples du Tertiaire continental et littoral du bassin de Paris et du midi de la France. Conséquences paléogéographiques. Bulletin de la Société Géologique de France 7:1-2.

Schneider JL, Wolf JP (1992). Carte géologique et hydrogéologique de 1/500 000 de la republique du Tchad, mémoire explicatif, 531. Paris: BRGM, P.531. https://www.worldcat.org/title/carte-geologique-et-cartes-hydrogeologiques-a-11- 500-000-de-la-republique-du-tchad-memoire-explicatif/oclc/26094222/

Schuster M (2002). Sédimentologie et paléoécologie des séries à vertébrés du paléolac Tchad depuis le Miocène supérieur. Thèse de doctorat de l'Université Louis Pasteur, Strasbourg I. 152 p.

Schuster M., Duringer Ph, Ghienne JF, Roquin C, Sepulchre P, Moussa A, Lebatard AE, Mackaye HT, Likius A, Vignaud P, Brunet M (2009). Chad Basin: paleoenvironments of the Sahara since the late Miocene. ComptesRendus Geosciences 341:612-620.

Schuster M, Duringer Ph, Ghienne JF, Vignaud P, Beauvilain A, Mackaye HT, Brunet M (2003). Coastal conglomerate around the Hadjer el Khamisinselbergs (western Chad, central Africa): new evidence for Lake Mega-Chad episodes. Earth Surface Processes and Landforms 28(10):1059-1069.

Schuster M, Duringer Ph, Ghienne JF, Vignaud P, Mackaye HT, Likius A, Brunet M (2006). The age of the Sahara Desert. Science 311:821.

Schuster M, Roquin C, Duringer Ph, Brunet M, Fontugne M, Mackaye HT, Vignaud P, Ghienne JF (2005). Highlighting Holocene Lake Mega-Chad paleoshorelines from space. Quaternary Science Reviews 24(16-17):1821-1827.

Servant-Vildary S (1973). Stratigraphie et néotectonique du Plio-Pléistocène ancien du Tchad d'après l'étude des Diatomites. C.R. Acad. Sc. Paris, t. 276 (9 mai 1973). Série D- 2633.

Sewell L (2019) Using a multiproxy analysis of springbok fossils to track 2 million years of vegetation changes experienced by hominins in southern Africa. (PhD Thesis). Bournemouth University.

Swezey C (1998). The identification of eolian sand and sandstones (L'identification des sables et gréséoliens. C.R. Acad. Sci. Paris, Sciences de la terre et des planètes / Earth and Planetary Sciences 327(8):513-518.

Vignaud P, Duringer P, Mackaye HT, Likius A, Blondel C, Boisserie JR, De Bonis L, Eisenmann V, Etienne ME, Geraads D, Guy F (2002). Geology and palaeontology of the Upper Miocene Toros-Menalla hominid locality, Chad. Nature 418(6894):152-155.

Warren A, Bristow C, Chappell A, Engelstaedter S, Mbainayel S, Todd M, Washington R (2005). The dustiest place and Earth. Nature 434:816-819.

Yu Y, Kalashnikova OV, Garay MJ, Lee H, Notaro M, Campbell JR, Marquis J (2020. Disproving the Bodélé depression as the primary source of dust fertilizing the Amazon Rainforest. Geophysical Research Letters 47(13):e2020GL088020.

Vol. 15(11), pp. 493-504, November 2021
DOI: 10.5897/AJEST2021.3031
Article Number: C74C85968183
ISSN: 1996-0786

http://www.academicjournals.org/AJEST

African Journal of Environmental Science and Technology

Full Length Research Paper

Improving future temperature projections with bias correction methods in Lake of Guiers/Senegal

Alioune Badara Sarr[1,2]

[1]Laboratoire d'Océanographie, des Sciences de l'Environnement et du Climat (LOSEC), UFR Sciences et Technologies, Université A. SECK de Ziguinchor, Sénégal.
[2]IRD-ESPACE-DEV, Maison de la Télédétection 500 rue Jean-François Breton, F-34093 Montpellier Cedex, France.

Received 3 June, 2021; Accepted 27 August, 2021

Climate models are generally used to evaluate the climate change impacts. However, they have important biases at the regional or local scales. This study evaluates the future temperature projections in Lake of Guiers/Senegal. For this, the daily maximum and minimum temperature from the ensemble mean of five (5) Coordinated Regional climate Downscaling Experiment (CORDEX) regional climate models (RCMs) under the greenhouse gas scenarios RCP4.5 and RCP8.5 and three (3) bias correction methods (Linear scaling, variance scaling and quantile mapping methods) were used. The performance of raw ensemble mean of the models was first evaluated against the WFDEI data. The results show that this latter exhibits some limitations to reproduce the minimum and the maximum temperature at the Lake scale. In order to make temperature data more accurate, the three bias correction methods were used. Results show that bias correction methods improve well the simulated minimum and maximum temperature. The future temperature projections show an increase of temperature which are faster in bias-corrected data. From the results it is indicated that it is necessary to implement appropriate adaptation measures to address these climate changes.

Key words: Climate change, regional climate models, coordinated regional climate downscaling experiment (CORDEX), bias correction methods, Lake of Guiers.

INTRODUCTION

Most of the studies conducted on the West African climate show an increase in temperatures in the Sahel region (IPCC, 2013; Ly et al., 2013; Giorgi et al., 2014). These temperature increases can impact the hydrological cycle and agriculture yields (Salack et al., 2011; Gelata and Gobosho, 2018; Sarr and Camara, 2018). They can also lead to problems in the supply of fresh water to populations through the evaporation phenomena, especially in Sahelian countries which are characterized by a short rainy season (3 to 4 months) and with variability in rainfall distribution (Tall et al., 2016; Luo et al., 2018). Therefore, climate change scenarios are needed in West Africa, particularly in Sahel to evaluate these impacts.

In West Africa climate changes have often been studied with global climate models (GCMs). However,

E-mail: aliounebadara.sarr@ird.fr. Tel: +33 752524563.

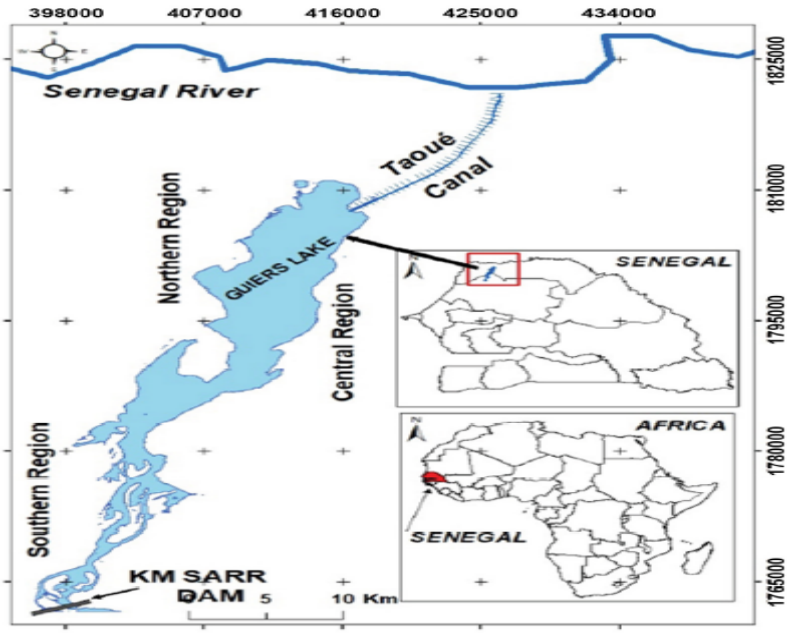

Figure 1. Study area.
Source: Diédhiou et al. (2019).

these models have large disparities in this region. In fact, GCMs have difficulty simulating certain surface heterogeneities because of their low spatial resolution (200 to 300 km). Thus, these GCMs are important only when it comes to representing global climate change. That is to say on a large scale. To address these issues, regional climate models (RCMs) are increasingly being used to dynamically disaggregate global climate models (Paeth et al., 2011). In this context, several experiments have been undertaken to produce coordinated experiments using several regional climate models (RCMs). This is the case of PRUDENCE (Baguis et al., 2010), ENSEMBLES-AMMA (Déqué et al., 2012). However, these coordinated experiments focused on limited areas. CORDEX is an international program implemented by several research centers which aim is to produce reliable climate change scenarios for impact studies. The ability of CORDEX RCMs to reproduce the present climate in West Africa has been assessed in numerous studies (Nikulin et al., 2012; Gbobaniyi et al., 2014; Klutse et al., 2015; Akinsanola and Ogunjobi, 2017). The climate change scenarios are obtained by forcing CORDEX RCMs by the Coupled Models Intercomparison Project phase 5 (CMIP5) GCMs from 1951 to 2100 (Giorgi et al., 2009). RCMs are the same basic physical principles as GCMs, but with higher horizontal resolution (~10-50 km). They are much more appropriate for impact studies because of their ability to represent the climate in complex areas such as West Africa. However, the simulated climate is not again in perfect agreement with observation. In fact, these RCMs also have limitations when it comes to focusing at the local-scale such as at the farm or basin scales. That is why, some authors (Hawkins et al., 2012; Kum et al., 2014; Gumindoga et al., 2016; Grillakis et al., 2017) have recommended the use of bias correction methods to eliminate or reduce bias to produce reliable climate change scenarios for impact assessment purposes.

The main objective of this study is to evaluate the performance of the Coordinated Regional climate Downscaling Experiment (CORDEX) models and the three (3) bias correction methods commonly used (Linear Scaling, Variance Scaling and Distribution Mapping) to simulate present and future temperature in the Lake of Guiers.

METHODOLOGY

Study area

The study area is the Lake of Guiers (Figure 1) which is the main reserve of surface freshwater in Senegal. It is located in northern Senegal, in the upper delta of the Senegal river basin, between longitude 15°40'-16° West and between latitude 16°-16°30' North. It extends between the south of city of Richard Toll (near the border with the Mauritania) and and Louga regions (toward K M SARR) (Figure 1). The minimum and maximum daily air temperatures in this city range between 22 and 36°C, respectively, while the mean annual rainfall is about 403 mm (Niang, 2011; Diédhiou et al., 2019). The main activities carried out in the semi-desert areas surrounding the lake are breeding, fishing, rice and sugar cane cultivation. The lake water is also used as a drinking water resource for the urban centers (165,000 m3/day for a population of 5 million inhabitants) (Sambou et al., 2019).

Table 1. Description of the regional climate models.

Name	GCM forcing	Institution	References
CCLM4	CNRM-CM5	CLM-community	Baldauf et al. (2011)
RACMO22T	EC-EARTH	KNMI, The Netherlands	Meijgaard et al. (2008)
RCA4	CNRM-CM5	SMHI, Sweden	Samuelsson et al. (2011)
HIRHAM5	EC-EARTH	DMI, Denmark	Christensen et al. (2006)
REMO	EC-EARTH	MPI, Germany	Jacob et al. (2007)

Datasets

This study uses daily maximum and minimum temperature data from CORDEX RCMs. They are CCLM4, RCA4, HIRHAM, REMO and RACMO. The model institutions, the regional climate models and their reference are presented in Table 1. The spatial resolution of CORDEX RCMs is 0.44° (approximately 50 km). They cover the period 1976-2005 for the historical and 2006-2100 for future. The RCMs outputs are available from this website: https://www.cordex.org/output.html.

These models are described in detail by Giorgi et al. (2009). Two periods are considered in this study: the reference period (1979 - 2005) and the future period (2006 - 2100). The RCMs RACMO, HIRHAM and REMO are forced by the outputs of the GCM EC-EARTH; while models RCA4 and CCLM4 are forced by the outputs of the GCM CNRM-CM5. The climate projections are obtained by forcing the regional climate models by the outputs of the global climate models under the greenhouse gas scenarios RCP4.5 and RCP8.5 which, respectively correspond to radiative forcing of 4.5 and 8.5 W/m² at the horizon 2100. To evaluate the performance of bias correction methods, the Water and Global Change (WATCH) Forcing Data methodology eas applied to ERA-Interim reanalysis data (WFDEI) (Weedon et al., 2014). The WFDEI data are availbable from 1979 to 2012. Two periods are considered in this study: the reference period (1979- 2005), which is the common period between RCMs data and WFDEI data and the future period (2006-2100).

Bias correction methods

In this study, three bias correction temperature methods commonly used namely linear scaling (LS), variance scaling (VS) and distribution mapping (DM) are considered. The period of calibration of this bias correction method is 1979-1993 and the period of validation is 1994-2005.

Linear scaling

The Linear Scaling (LS) method (Lenderink et al., 2007) corrects the outputs of the climate model by using the difference in the mean variability between the observations and climate model.

$$T_{\mathrm{cor,m,d}} = T_{\mathrm{raw,m,d}} + \left(\overline{T_{\mathrm{obs,m}}} - \overline{T_{\mathrm{ref,m}}}\right) \quad (1)$$

where $T_{\mathrm{cor,m,d}}$ are the corrected minimum or maximum temperature on the dth day of mth month; $T_{\mathrm{raw,m,d}}$ are the uncorrected minimum or maximum temperature on the dth day of mth month; $\overline{T_{\mathrm{obs,m}}}$ and $\overline{T_{\mathrm{ref,m}}}$ are the mean values of observed and simulated minimum or maximum temperature at the given month.

Variance scaling

For the linear scaling method, the biases in variance are not corrected. That is why the Variance Scaling (VS) method was implemented to bias correct the temperature time series (Terink et al., 2010). It is given by Equation (3):

$$T_{\mathrm{cor},m,d} = \overline{T_{\mathrm{obs},m}} + \left[T_{\mathrm{raw},m,d} - \overline{T_{\mathrm{ref},m}}\right] \times \frac{\sigma(T_{\mathrm{obs},m})}{\sigma(T_{\mathrm{raw},m})} \quad (2)$$

where $\sigma(T_{\mathrm{raw},m})$ and $\sigma(T_{\mathrm{obs},m})$ represent, respectively the standards deviation of the monthly RCMs outputs and observations during the reference period.

Distribution mapping

The Distribution Mapping (DM) method was used to correct the distribution function of the raw data (Piani et al., 2010). It is used to adjust mean, standard deviation and quantiles. The Gaussian distribution (or normal distribution) with the parameters μ (mean) and σ (standard deviation) is usually considered to adjust the temperature probability distribution (Teutschbein and Seibert, 2012):

$$F_N(x|\mu,\sigma) = \frac{1}{\sigma\times\sqrt{2\pi}} \times e^{\frac{-(x-\mu)^2}{2\sigma^2}}, x\epsilon R \quad (3)$$

The corrected temperature expressed in terms of Gaussian CDF (F_N) and its inverse (F^{-1}_N) and is given by:

$$T_{cor,m,d} = F_N^{-1}\left(F_N\left(T_{raw,m,d}|\mu_{raw,m},\sigma_{raw,m}\right)|\mu_{obs,m},\sigma_{obs,m}\right) \quad (4)$$

where F_N and F_N^{-1} represent, respectively the gamma cumulative distribution and its inverse, $T_{raw,m,d}$ is the uncorrected minimum or maximum temperature during the month m and the day d of reference period, $\mu_{raw,m}$ and $\sigma_{raw,m}$ represent, respectively the mean and standard deviation of the uncorrected temperature during the month m and $\mu_{obs,m}$ and $\mu_{obs,m}$ are, respectively the mean and the standard deviation of the observed temperature.

Performance of statistical method

To evaluate the performance of the bias correction methods, some

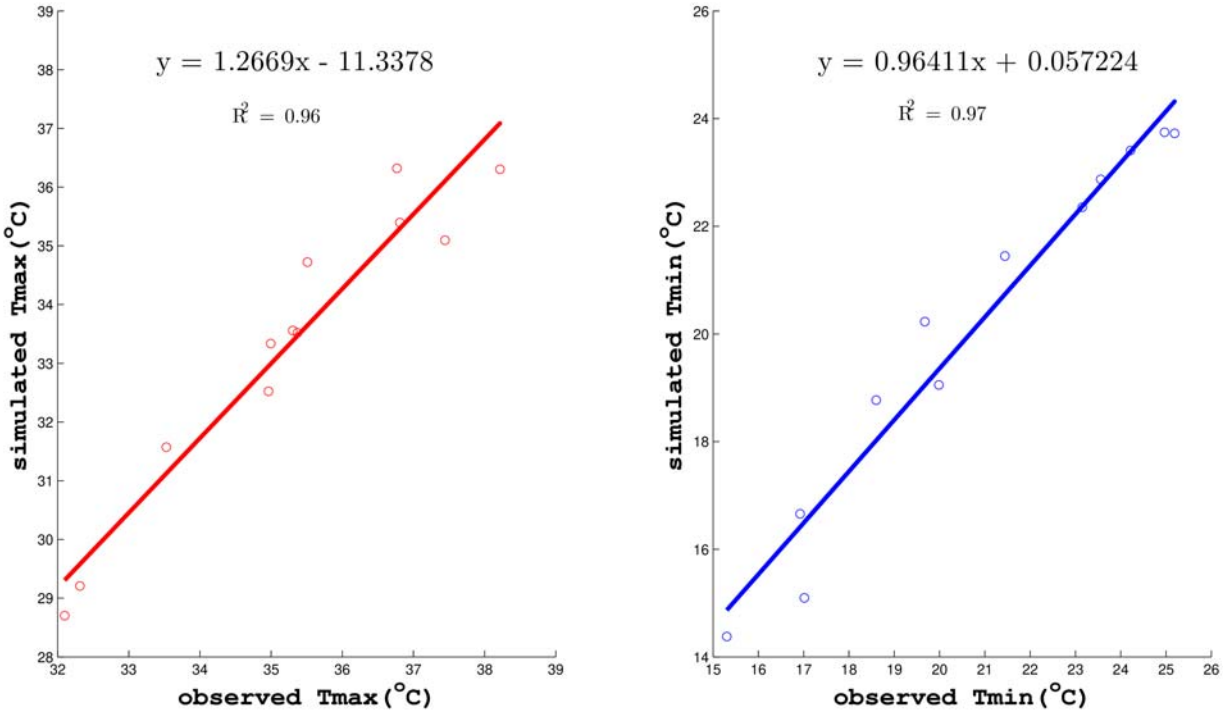

Figure 1. Scatter plots of the simulated and the WFDEI monthly maximum temperature (left panel) and monthly minimum temperature (right panel) averaged from 1979 to 2005.

statistical parameters such as the absolute bias (MB), the root mean square error (RMSE) and the Nash-Sutcliffe efficiency (NSE) were calculated.

The mean bias gives an indication of the sign of errors (underestimation or overestimation):

$$MB = \frac{\sum_{i=1}^{n}\left(T_{sim_i} - T_{obs_i}\right)}{n} \quad (5)$$

The root mean square error (RMSE) measures the amplitude of errors committed by models.

$$RMSE = \sqrt{\frac{\sum_{i=1}^{n}\left(T_{sim_i} - T_{obs_i}\right)^2}{n}} \quad (6)$$

The Nash-Sutcliffe efficiency (NSE) gives the relative magnitude of variance of residues compared to the observed variance. It is between -∞ and 1 with 1 the optimal value. The NSE values less than 0 are considered unacceptable while those between 0 and 1 are considered acceptable.

$$NSE = 1 - \frac{\sum_{i=1}^{n}\left(T_{sim_i} - T_{obs_i}\right)^2}{\sum_{i=1}^{n}\left(T_{obs_i} - \overline{T_{obs_i}}\right)^2} \quad (7)$$

where n is the number of time steps; T_{sim_i} and T_{obs_i} are, respectively the time series of the simulated and the observed (WFDEI) temperature.

RESULTS

Performance of the multi-model ensemble

Figure 2 shows the monthly maximum and minimum temperature simulated by the five CORDEX RCMs present in the ensemble-mean compared to WFDEI data from 1979 to 2005. The ensemble mean of the model was considered because numerous studies (Kim et al., 2014; Gbobaniyi et al., 2014) pointed that it better reproduces the spatial distribution of the surface temperature. WFDEI data show the lowest minimum and maximum temperature (around 16 and 32°C, respectively) in the Lake of Guiers between December and February. The highest minimum and maximum temperature (around 24 and 38°C, respectively) are recorded from April to June and from July to September, respectively. WFDEI data shows also a decrease of maximum temperature between the end of June and September corresponding to the rainy season in Senegal. The ensemble-mean of the models generally reproduces well the pattern of the monthly maximum and minimum temperature observed in the Lake. Also, the monthly maximum and minimum temperature simulated are closer to that observed, as shown in Figure 3 with a coefficient of determination of 0.96 and 0.97, respectively. It should also be noted that the ensemble mean of the models reproduces quite well the minimum temperature observed. This is confirmed by

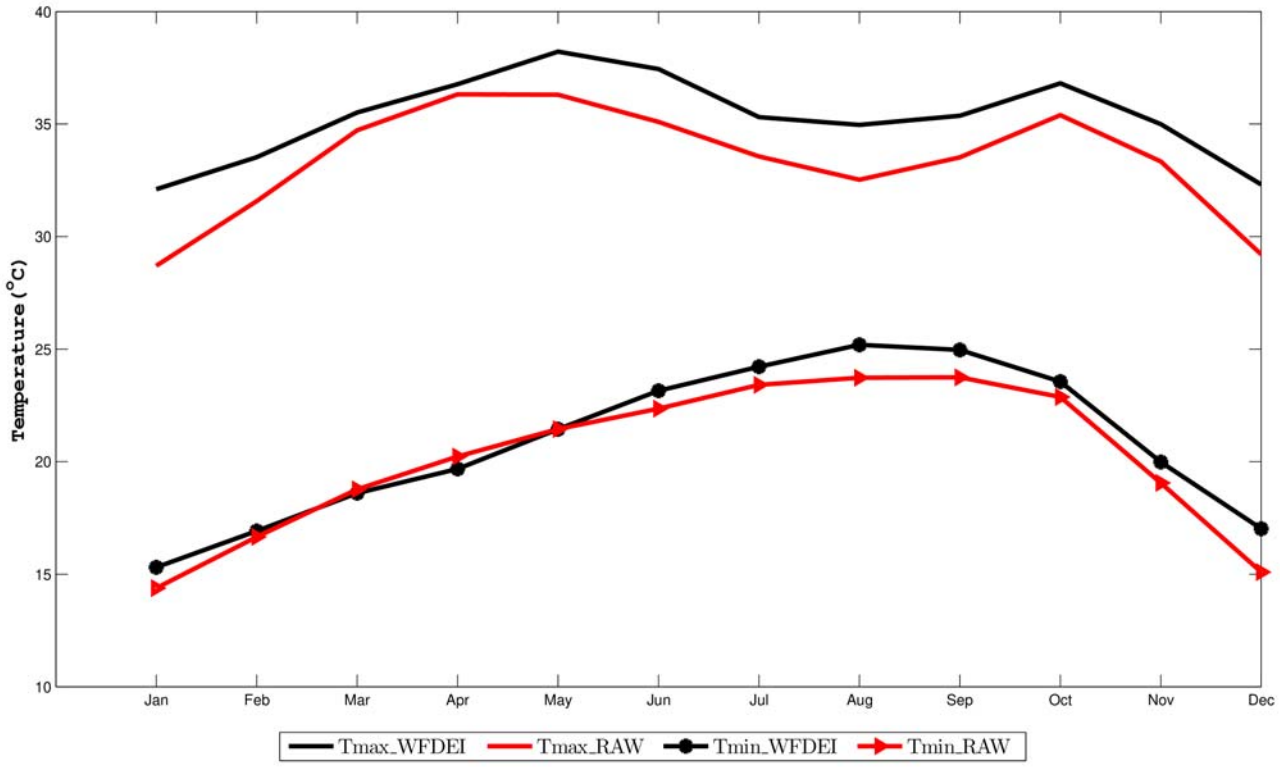

Figure 2. Monthly maximum and minimum temperature averaged from 1979 to 2005 of WFDEI data and the ensemble mean of the models. Tmax_WFDEI and Tmin_WFDEI represents respectively the maximum and the minimum temperature of WFDEI and Tmax_RAW and Tmin_RAW represent respectively the raw minimum and maximum temperature simulated by the multi-model ensemble.

Table 2. Performance measures of the raw multi-model ensemble during the period 1979-2005.

T_{max}				T_{min}			
MB	**RMSE**	**NSE**	**R**	**MB**	**RMSE**	**NSE**	**R**
-1.92	2.02	-0.30	0.95	-0.69	1.08	0.91	0.97

the results obtained in Table 2. Nevertheless, the simulated temperature is always biased. In fact, it presents an overestimation of the maximum temperature for all months with mean bias of -1.92. For the minimum temperature, it overestimates the observed values only between March and May. Thus, the performance of outputs of the multi-model ensemble can be increased by bias correction methods.

Figure 4 shows the comparison of the monthly maximum and minimum temperature from the WFDEI data, raw multi-model ensemble and bias-corrected respectively during the calibration period (1979-1993) and validation period (1994-2005). The results show that the bias in ensemble mean of the models temperature is remarkably reduced. All the three bias correction methods improve satisfactory the outputs of the ensemble mean of the models. There are very slight differences between the WFDEI data and the bias-corrected multi-model ensemble compared to raw data during the calibration data. But some contrasts exist between the three bias corrected multi-model ensemble mean and theirs performances with respect to both parameters. In fact, results show that Linear Scaling (LS) method is closer to the observed temperature followed by Distribution mapping (DM) method. The statistical performance measures of bias-corrected temperature during the calibration and the validation periods are presented in Table 3. The statistical indicators values reflect the good performances of the three bias correction methods during the calibration and validation periods. During the calibration period the mean bias is less than 0.01 excepted VS method for the monthly maximum

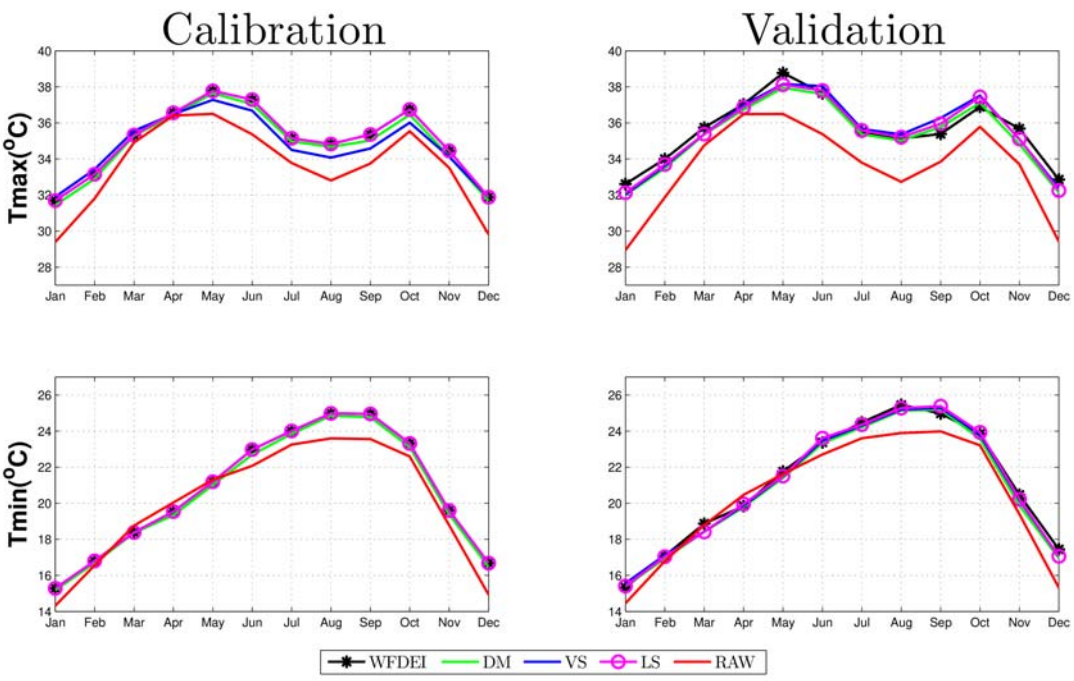

Figure 3. Monthly maximum and minimum for the calibration period (left panel) and for the validation period (right panel).

Table 3. Performance measures of the bias-corrected monthly maximum and minimum temperature during the calibration and validation periods.

Parameter	Methods	Calibration period				Validation period			
		MB	RMSE	NSE	R	MB	RMSE	NSE	R
Tmax	RAW	-1.38	1.57	0.21	0.84	-2.00	2.09	-0.48	0.83
	LS	< -0.01	0.87	0.73	0.86	-0.14	0.85	0.68	0.84
	VS	-0.30	1.02	0.65	0.85	-0.06	0.92	0.67	0.84
	DM	< 0.01	0.88	0.72	0.86	-0.10	0.88	0.67	0.84
Tmin	RAW	-0.66	1.08	0.85	0.94	-0.72	1.08	0.85	0.94
	LS	< 0.01	0.69	0.93	0.97	-0.06	0.69	0.93	0.97
	VS	< 0.01	0.66	0.94	0.97	-0.09	0.68	0.93	0.96
	DM	< 0.01	0.69	0.93	0.97	-0.05	0.70	0.93	0.97

temperature. On the other hand, VS method better corrects the mean bias of the monthly maximum temperature during the validation period. The good results obtained with the statistical parameters (RMSE < 1, NSE and R values close to 1) during both periods highlight the ability of bias correction to improve the simulated monthly maximum and minimum temperature. We also note that the ability of the three bias correction methods to better correct the minimum temperature. This might be due to fairly good capacity of the five models present in the ensemble mean to better simulate the minimum temperature. Therefore, the minimum temperature become easier to bias-corrected.

To see the performance of bias correction methods at the daily time scale, Figure 5 shows the 7-day mean of the maximum and minimum temperature from the WFDEI data, raw multi-model ensemble and bias-corrected, respectively during the calibration period (1979-1993) and validation period (1994-2005). Table 4 shows the statistical performance measures of daily maximum and minimum temperature. The results show that all bias correction methods improve also the daily maximum and minimum temperature during the calibration and the validation period. As for monthly time scale, LS and DM methods better improve the quality of daily maximum and minimum temperature simulated by multi-model

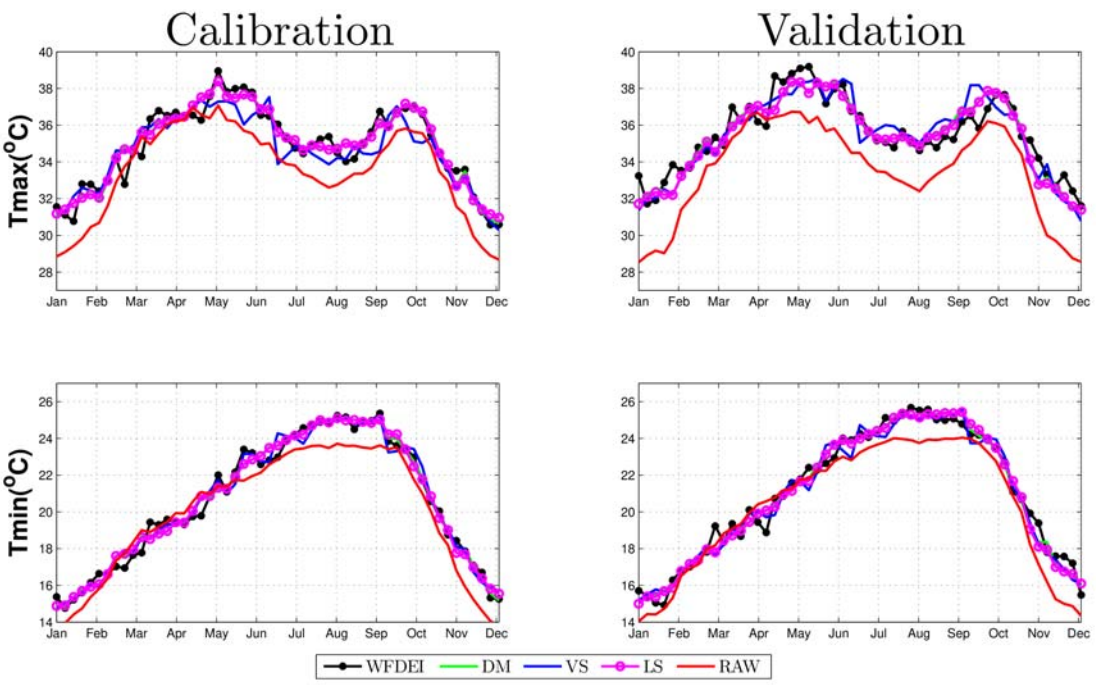

Figure 4. Daily mean maximum and minimum after smooth with the 7-day moving average method for the calibration period (left panel) and for the validation period (right panel).

Table 4. Performance measures of the bias-corrected daily maximum and minimum temperature during the calibration and validation periods.

Parameter	Methods	Calibration period				Validation period			
		MB	RMSE	NSE	R	MB	RMSE	NSE	R
Tmax	RAW	-1.38	2.78	0.02	0.50	-2.00	3.05	-0.28	0.45
	LS	< -0.01	2.44	0.21	0.57	-0.14	2.41	0.13	0.46
	VS	-0.30	2.53	0.16	0.53	-0.06	2.43	0.13	0.47
	DM	< -0.01	2.46	0.20	0.52	-0.10	2.44	0.11	0.46
Tmin	RAW	-0.66	1.89	0.61	0.80	-0.73	1.85	0.62	0.81
	LS	< -0.01	1.69	0.67	0.82	-0.06	1.63	0.68	0.83
	VS	< -0.01	1.71	0.66	0.82	-0.10	1.69	0.66	0.82
	DM	< -0.01	1.68	0.67	0.82	-0.06	1.64	0.68	0.83

ensemble. Moreover, slight differences are noted when the performance of both methods was considered. That is to say, both bias correction methods show similar performances. The results obtained in Table 4 confirm the good performances of bias correction methods. In fact, low mean bias are recorded (MB < 0.01°C) for the daily temperature values except the VS method for daily maximum temperature as in monthly scale during the calibration period. However, when we compare the statistical parameters, results show that bias correction methods perform better on the monthly scale over the daily. The results obtained during the validation period show that VS method is more suitable for daily and monthly maximum temperature. Moreover, the DM method is better suitable to bias correct the daily minimum temperature. For monthly minimum temperature, DM and LS method seem to give the best bias-correction. Globally, the three temperature bias correction methods improve the performance of the ensemble mean of the models. The ability of bias correction methods to improve the performance of the ensemble mean of the models strengthens our confidence in the future temperature

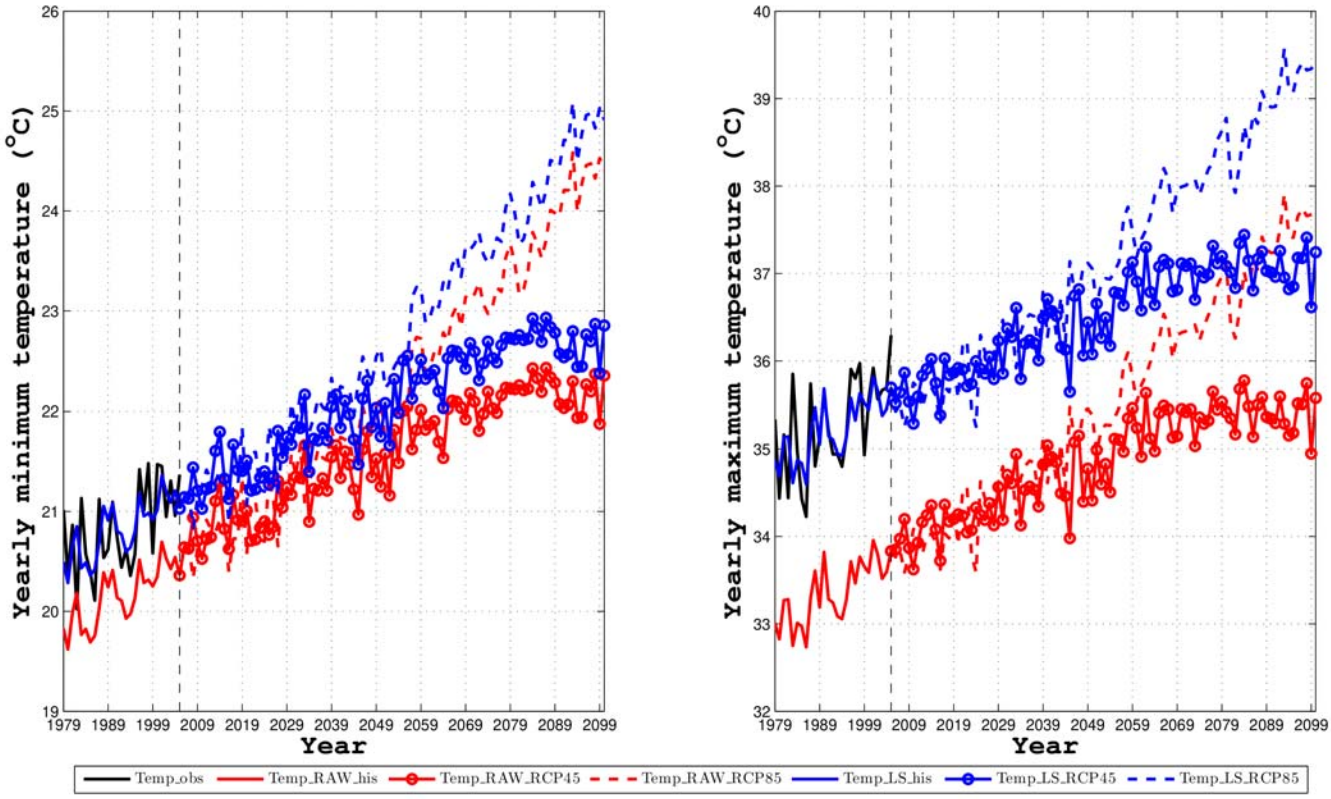

Figure 5. Impact of the LS bias correction method on projected yearly minimum and maximum temperature (left panel and right panel respectively). Temp_obs represents the observed minimum or maximum temperature, Temp_RAW_his is the raw minimum or maximum temperature during the historical period, Temp_RAW_RCP45 and Temp_RAW_RCP85 represent respectively the raw minimum or maximum temperature during the future under the scenarios RCP4.5 and RCP8.5, Temp_LS_his represents the historical minimum or maximum temperature corrected by LS method and Temp_LS_RCP4.5 and Temp_LS_RCP8.5 are respectively the future minimum or maximum temperature corrected by LS method.

projections in the Lake of Guiers.

Projection of future temperature

After evaluating the bias correction methods, the temporal evolution of annual maximum and minimum temperature from 1979 to 2100 was studied. Figures 6, 7, and 8 illustrate the impact of the LS, VS, and DM bias correction methods on the projected annual minimum and maximum temperatures, respectively. The results show that the correted data reproduce well the WFDEI data during the reference period (1979-2005) compared to raw data. However, it was found out that the corrected data by DM method (Figure 8) shows the highest performance in simulated annual temperature (MB=0.04°C/ <0.01°C, NSE=0.39/0.36 for yearly maximum/minimum temperature, respectively) compared to VS method (Figure 8) (MB=-0.04°C/-0.01°C, NSE=0.34/0.30 for yearly maximum/minimum temperature) and LS method (Figure 7) (MB=-0.05°C/ <-0.01°C, NSE=0.39/0.30 for maximum/minimum temperature). It was also noted that the multi-model mean corrected by the three methods considered shows an upward trend in temperatures compared to that uncorrected almost over the entire period in both scenarios (RCP4.5 and RCP8.5). This overall increase is greater in the pessimistic scenario (RCP8.5) than in the medium scenario (RCP4.5). The magnitude of the difference between the corrected and uncorrected multi-model mean is much greater when considering the maximum temperature. But the sign of the change signal in raw data is not modified in those bias-corrected. Globally, important increases are observed in future maximum and minimum temperature when the raw ensemble of the models and bias-corrected under both scenarios were considered. This is in agreement with several results obtained on the Sahel (IPCC, 2013; Ly et al., 2013; Sylla et al., 2016). This increase is greater from 2060 especially under the RCP8.5 scenario. In fact, an increase of 0.8 to 0.15°C per decade and of 0.5 to 0.53°C per decade is predicted, respectively under the RCP4.5 and RCP8.5 scenarios for the mean annual minimum temperature. For the mean annual maximum temperature, the increase range

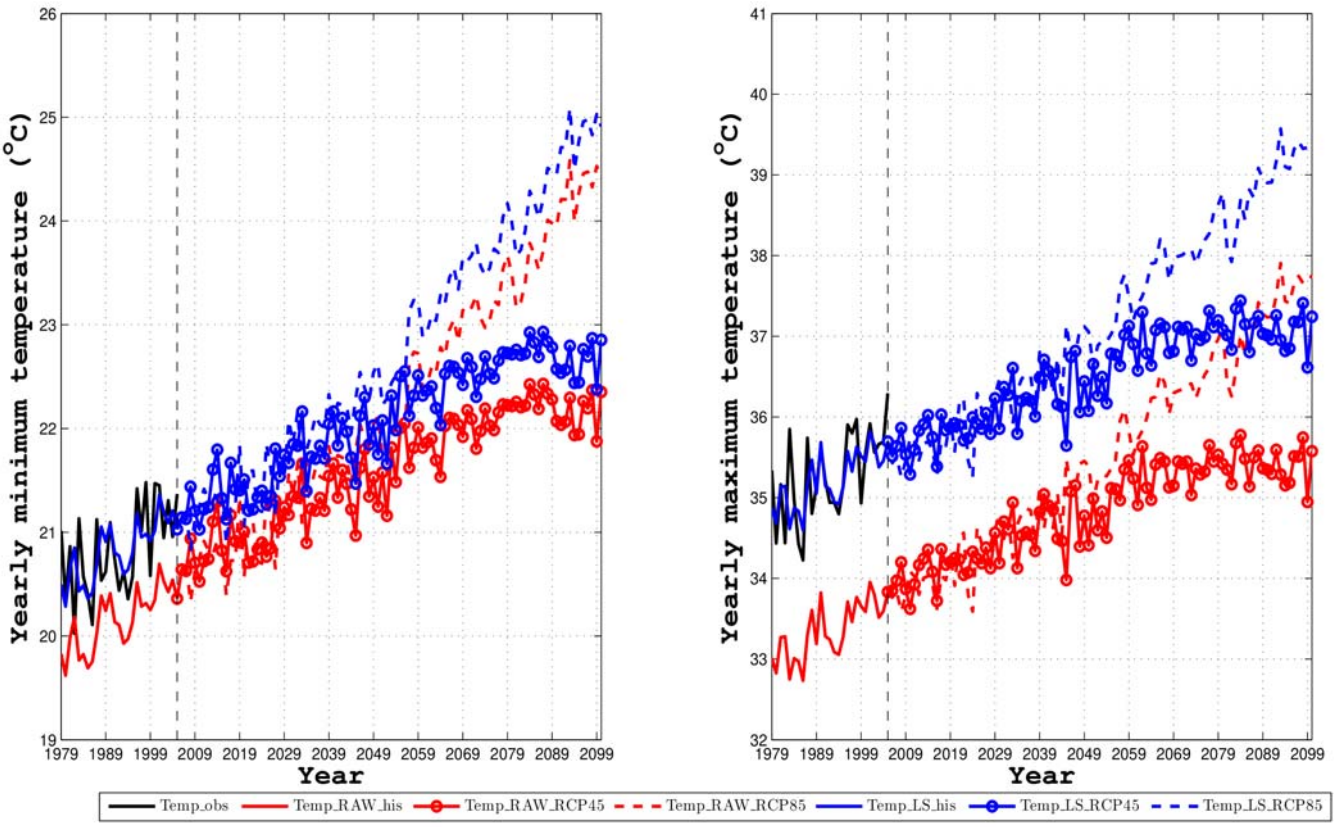

Figure 6. Impact of the VS bias correction method on projected yearly minimum and maximum temperature (left panel and right panel respectively). Temp_obs represents the observed minimum or maximum temperature, Temp_RAW_his is the raw minimum or maximum temperature during the historical period, Temp_RAW_RCP45 and Temp_RAW_RCP85 represent respectively the raw minimum or maximum temperature during the future under the scenarios RCP4.5 and RCP8.5, Temp_VS_his represents the historical minimum or maximum temperature corrected by VS method and Temp_VS_RCP4.5 and Temp_VS_RCP8.5 are respectively the future minimum or maximum temperature corrected by VS method.

between 0.08 and 0.22°C per decade and 0.55 to 0.66°C per decade, respectively under RCP4.5 and RCP8.5 scenarios. The lowest increases in minimum and maximum temperature were obtained with raw multi-model mean and the highest increases in minimum and maximum temperature were obtained with multi-model mean bias-corrected by DM (Figure 8) and VS methods (Figure 7), respectively.

DISCUSSION

This study evaluates the performance of the ensemble-mean of five (5) CORDEX regional climate models (RCMs) models and the three (3) bias correction methods commonly used (Linear Scaling, Variance Scaling and Distribuiton Mapping) to better simulate present and future temperature in the Lake of Guiers which plays an important role in the socio-economic development of Senegal (Sambou et al., 2019; Diedhiou et al., 2019). The results show that the ensemble-mean of model simulates well the observed minimum and maximum temperature. However, it still contains some bias. According to Luo et al. (2018), these biases come from to the forcing of Global Climate models (GCMs) or produced by a systematic error of the model. Therefore, it is very important to bias-correct the RCMs data before studying the climate change (Chen et al., 2013; Ajaaj et al., 2015). The results show that all methods used can improve the original RCMs outputs with few differences. The simplest bias correction method is the Linear Scaling (LS) which corrects the outputs of the climate model by using the difference in the mean variability between the observations and climate model. Thus, the biases in variance are not corrected. However, it was found that for the daily and monthly minimum temperature during the validation period LS method gives the best results. Thus, the uncorrected minimum temperature might not be biased in variance. Of the three bias correction methods used, the DM method is the most advanced. It is used to adjust the mean, the standard deviation and the quantile. This method better corrects the minimum temperature at

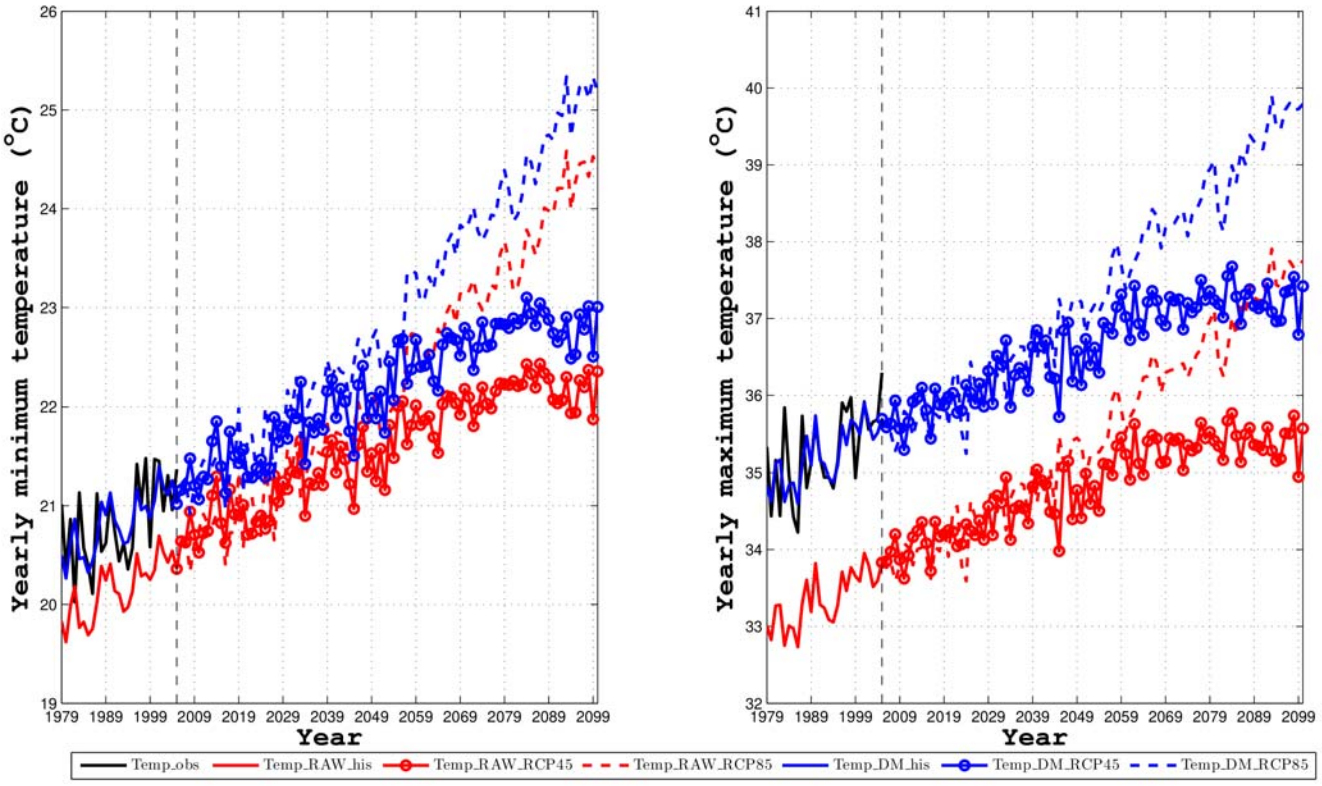

Figure 7. Impact of the DM bias correction method on projected yearly minimum and maximum temperature (left panel and right panel, respectively). Temp_obs represents the observed minimum or maximum temperature, Temp_RAW_his is the raw minimum or maximum temperature during the historical period, Temp_RAW_RCP45 and Temp_RAW_RCP85 represent respectively the raw minimum or maximum temperature during the future under the scenarios RCP4.5 and RCP8.5, Temp_DM_his represents the historical minimum or maximum temperature corrected by DM method and Temp_DM_RCP4.5 and Temp_DM_RCP8.5 are respectively the future minimum or maximum temperature corrected by DM method.

daily and monthly scale compared to others methods during the validation period. However, it seems be more suitable when we want to bias correct the extreme events (McGinnis et al., 2015; Luo et al., 2018).

After evaluation, the evolution of the future minimum and maximum temperature corrected and uncorrected under scenarios RCP4.5 and RCP8.5 from 1979-2100 was diagnosed. The multi-model mean simulated a strong rise in minimum and maximum temperature which is more important under the RCP8.5 scenario. These results are in agreement with those obtained by Giorgi et al. (2014) and Sylla et al. (2016) in Western Sahel. After correction, the trends are not so modified but the magnitude of climate change signal is amplified in the multi-model mean bias-corrected. This is in agreement with Mbaye et al. (2015) results over Senegal river basin.

The large increase of both temperature and minimum temperature could lead to an increase in evapotranspiration phenomena in Lake of Guiers (Tall et al., 2016) and a decrease in the water content of the soil located at the edge of the lake. This could lead to problems of availability of resources because this lake is the largest reservoir of freshwater in Senegal (Sambou et al., 2018). This situation could also be detrimental for agricultural yields. In fact, strong temperature increase can affect the grain weight and the duration of grain growth (Sarr and Camara, 2018).

Conclusion

In this work, the ensemble mean of 5 CORDEX RCMs was considered to analyze the evolution of future temperature in the Lake of Guiers. The performances of the ensemble mean of the models to reproduce the minimum and maximum temperature are first assessed. Results show that the multi-model ensemble mean reproduces globally well the observed data. However, it presents some biases which can be reduced by bias correction methods. After bias correction, the agreement between the multi-model ensemble mean and the WFDEI data has considerably increased.

Results show an increase of annual minimum and maximum temperature in the lake. Moreover, the

magnitude of this increase is more important in the multi-model ensemble mean bias-corrected compared to that raw, but the degree of frequency in raw data is not affected.

This future increase in temperature predicted by the uncorrected and corrected ensemble mean of the models can have harmful consequences for the local populations due to the increase of evapotranspiration and water demand. Therefore, it would be important to better quantify the future climate change impact on the hydrological cycle in the Lake of Guiers.

CONFLICT OF INTERESTS

The author has not declared any conflict of interests.

REFERENCES

Ajaaj AA, Mishra, AK, Khan AA (2015). Comparison of bias correction techniques for GPCC rainfall data in semi-arid climate. Stochastic Environmental Research and Risk Assessment 30(6):1659-1675.

Akinsanola AA, Ogunjobi KO (2017). Evaluation of present-day rainfall simulations over West Africa in CORDEX regional climate models. Environmental Earth Sciences 76(10):366.

Baguis P, Roulin E, Willems P, Ntegeka V (2010). Climate change scenarios for precipitation 25 and potential evapotranspiration over central Belgium. Theoretical and Applied Climatology 99(3):273-286.

Baldauf M, Seifert A, Förstner J, Majewski D, Raschendorfer M, Reinhardt T (2011). Operational convective-scale numerical weather prediction with the COSMO model: description and sensitivies. Monthly Weather Review doi: 10.1175/MWR.-D-10-05013.1

Chen J, Brissette FP, Chaumont D, Braun M (2013). Finding appropriate bias correction methods in downscaling precipitation for hydrologic impact studies over North America. Water Resources Research 49(7):4187-205.

Christensen JH, Carter TR, Rummukainen M, Amanatidis G (2007). Evaluating the performance and utility of regional climate models: the PRUDENCE project.

Déqué M, Somot S, Sanchez-Gomez E, Goodess CM, Jacob D, Lenderink G, Christensen OB (2012). The spread amongst ENSEMBLES regional scenarios: regional climate models, driving general circulation models and interannual variability. Climate Dynamics 38(5):951-964.

Diédhiou C, Diop S, Faye G, Moshod T, Wade S (2019) Study on the Applicability of Landsat-8 Images as a Tool for Monitoring the Trophic State of Lake Guiers (Senegal). Journal of Water Resource and Protection 11(4):434-447. https://doi.org/10.4236/jwarp.2019.114026

Gbobaniyi E, Sarr A, Sylla MB, Diallo I, Lennard C, Dosio A, Lamptey B (2014). Climatology, annual cycle and interannual variability of precipitation and temperature in CORDEX simulations over West Africa. International Journal of Climatology 34:2241-2257. http://dx.doi.org/10.1002/joc.3834.

Gelata CD, Gobosho L (2018). Climate Change Induced Temperature Prediction and Bias Correction in Finchaa Watershed. American-

Eurasian Journal of Agriculture and Environmental Sciences 18(6):324-337.

Giorgi F, Jones C, Asrar G (2009). Addressing climate information needs at the regional level. The CORDEX framework. WMO Bulletin, July 2009 issue.

Giorgi F, Coppola E, Raffael F, Diro GT, Fuentes-Franco R, Giuliani G, Mamgain A, Llopart MP, Mariotti L, Torma C (2014). Changes in extremes and hydroclimate regimes in the CREMA ensemble projections, Abdus Salam International Centre for Theoretical Physics, Trieste. Italy. Climate Change doi 10.1007/s10584-014- 1117-0.

Grillakis MG, Koutroulis AG, Daliakopoulos IN, Tsanis IK (2017). A method to preserve trends in quantile mapping bias correction of climate modeled temperature. Earth System Dynamics 8:889-900.

Gumindoga W, Rientjes THM, Haile AT, Makurira H, Reggiani P (2016). Bias correction schemes for CMORPH satellite rainfall estimates in the Zambezi River Basin. Hydrology and Earth System Sciences Discussions doi:10.5194/hess-2016-33.

Hawkins E, Ho CK, Osborne T, Challinor AJ (2012). Calibration and bias correction of climate projections for crop modelling: an idealised case study over Europe. Agricultural and Forest Meteorology doi: 10.1016/j.agrformet.2012.04.007.

IPCC (2013). Climate Change (2013): The Physical Science Basis. In T. F. Stocker, D. Qin, G. -K. Plattner, M. Tignor, S.K. Allen, J. Boschung, A. Nauels, Y. Xia, V. Bex and P.M. Midgley (Eds.), Contribution of Working Group I to the Fifth Assessment Report of the Intergovernmental Panel on Climate Change (p. 1535). Cambridge, United Kingdom and New York, NY, U.

Jacob D, Barring L, Christensen OB, Christensen JH, Hagemann S, Hirschi M, Kjellström E, Lenderink G, Rockel B, Schar C, Seneviratne SI, Somot S, van Ulden A, van den Hurk B (2007). An Inter-Comparison of Regional Climate Models for Europe: Design of the Experiments and Model Performance. Climate Change 81:31-52. http://dx.doi.org/10.1007/s10584-006-9213-4

Kim J, Waliser DE, Mattmann CA, Goodale CE, Hart AF, Zimdars PA, Favre A (2014). Evaluation of the CORDEX-Africa multi-RCM hindcast: systematic model errors. Climate Dynamics 42(5):1189-1202.

Klutse NAB, Sylla MB, Diallo I, Sarr A, Dosio A, Diedhiou A, Kamga A, Lamptey B, Ali A, Gbobaniyi EO, Awuso K, Lennard C, Hewitson B, Nikulin G, Panitz HJ, Büchner M (2015). Daily characteristics of West African summer monsoon precipitation in CORDEX simulations. Theoretical and Applied Climatology DOI 10.1007/s00704-014-1352-3

Kum D, Lim KJ, Jang CH, Ryu J, Yang JE, Kim SJ, Kong DS, Jung Y (2014). Projecting Future Climate Change Scenarios Using Three Bias- Correction Methods. Advances in Meteorology. Volume 2014, Article ID 704151, 12 pages. http://dx.doi.org/10.1155/2014/704151

Lenderink G, Buishand A, van Deursen W (2007). Estimates of future discharges of the river Rhine using two scenario methodologies: direct versus delta approach. Hydrology and Earth System Sciences 11(3):1145-1159.

Luo M, Liu T, Meng F, Duan Y, Frankl A, Bao A, De Maeyer P (2018). Comparing Bias Correction Methods Used in Downscaling Precipitation and Temperature from Regional Climate Models: A Case Study from the Kaidu River Basin in Western China. Water 10(8):1046. doi:10.3390/w10081046

Ly M, SB, Traoré A, Alhassane, Sarr B (2013). Evolution of Some Observed Climate Extremes in the west African Sahel. Weather and Climate Extreme 1:19-25. doi.org/10.1016/j.

Mbaye ML, Faye B, Sambou D, Gaye AT (2018). Potential effect of bias correction on extreme precipitation and temperature changes over Senegal River Basin (West Africa). Science de la vie, de la terre et agronomie 6(2). ISSN 2424-7235.

McGinnis S, Nychka D, Mearns LO (2015). A new distribution mapping technique for climate model bias correction. In Machine Learning and Data Mining Approaches to Climate Science: Proceedings of the Fourth International Workshop on Climate Informatics; Lakshmanan, V, Gilleland, E, McGovern, A, Tingley, M, Eds.; Springer: Boulder, CO, USA.

Meijgaard E, van Ulft LH, van den Berg WJ, Bosveld F, van den Hurk B, Lenderink G, Siebesma AP (2008). The KNMI Regional Atmospheric Climate Model RACMO, Version 2.1. KNMI Technical Report 302:43.

Niang A (2011). Aménagement du lac de Guiers de 1824 à l'avénement des grands barrages du fleuve Sénégal: Prospective géographique. Climat et Développement.

Nikulin G, Jones C, Giorgi F, Asrar G, Büchner M, Cerezo-Mota R, Christensen OB, Déqué M, Fernandez J, Hänsler A, van Meijgaard E, Samuelsson P, Sylla MB, Sushama L (2012). Precipitation climatology in an ensemble of CORDEX-Africa regional climate simulations. Journal of Climate 25(18):6057-6078.

Paeth H, Hall NM, Gaertner MA, Alonso MD, Moumouni S, Polcher J, Ruti PM, Fink AH, Gosset M, Lebel T, Gaye AT, Rowell DP, Moufouma-Okia W, Jacob D, Rockel B, Giorgi F, Rummukainen M (2011). Progress in regional downscaling of West African precipitation. Atmospheric Science Letters 12(1):75-82.

Piani C, Haerter JO, Coppola E (2010). Statistical bias correction for daily precipitation in regional climate models over Europe. Theoretical and Applied Climatology 99(1):187-192.

Salack S, Muller B, Gaye AT (2011). Rain-based factors of high agricultural impacts over Senegal. Part I: integration of local to sub- regional trends and variability. Theoretical and Applied Climatology 106(1):1-22.

Sambou D, Diekkrüger B, Dina W, Verah H (2018). Water availability and demand under climate change and population growth in Lake Guiers, Senegal. 17th World Lake Conference, Lake Kasumigaura, Ibaraki, Japan, 2018.

Sambou D, Diekkrüger B, Mbaye ML (2019). Trends and projections of climate change over the basin of Lake Guiers, Senegal. Conference: EGU General Assembly 2019.

Samuelsson P, Jones CG, Willén U, Ullerstig A, Gollvik S, Hansson U, Jansson C, Kjellström E, Nikulin G, Wyser K (2011). The Rossby Centre Regional Climate Model RCA3: Model Description and Performance. Tellus A 63(1):4-23. http://dx.doi.org/10.1111/j.1600-0870.2010.00478.x.

Sarr AB, Camara M (2018). Simulation of the impact of climate change on peanut yield in Senegal. International Journal of Physical Sciences 13(5):79-89.

Sylla MB, Nikiema PM, Gibba P, Kebe I, Klutse NAB (2016). Climate Change over West Africa: Recent trends and future projections. J.A. Yaro and J. Hesselberg (eds.). Adaptation to Climate Change and Variability in Rural west Africa doi:10.1007/978-3-319-31499-0_3.

Tall M, Sylla MB, Diallo I, Pal JS, Faye A, Mbaye ML, Gaye AT (2016). Projected impact of climate change in the hydroclimatology of Senegal with a focus over the Lake of Guiers for the twenty-first century. Theoretical and Applied Climatology doi:10.1007/s00704- 016-1805-y

Terink W, Hurkmans RTWL, Torfs PJJF, Uijlenhoet R (2010). Evaluation of a bias correction method applied to downscaled precipitation and temperature reanalysis data for the Rhine basin. Hydrol. Earth System Science 14(4):687-703.

Teutschbein C, Seiber J (2012). Bias correction of regional climate model simulations for hydrological climate-change impact studies: Review and evaluation of different methods. Journal of Hydrology 456:12-29. doi: 10.1016/j.jhydrol.2012.05.052.

Weedon GP, Balsamo G, Bellouin N, Gomes S, Best MJ, Viterbo P (2014). The WFDEI meteorological forcing data set: WATCH forcing data methodology applied to ERA-interim reanalysis data. Water Resources Research 50(9):7505-7514.

Related Journals: